8-2017

Characterization of Nanoparticles Using Solid State Nanopores

Santoshi Nandivada
University of Arkansas, Fayetteville

Characterization of Nanoparticles Using
Solid State Nanopores

A dissertation submitted in partial fulfillment
of the requirements for the degree of
Doctor of Philosophy in Physics

by

Santoshi Nandivada
Osmania University
Bachelor of Science in Physics, 2005
Osmania University
Master of Science in Physics, 2007
University of Arkansas
Master of Science in Physics, 2014

August 2017
University of Arkansas

This dissertation is approved for recommendation to the Graduate Council

_____

Dr. Jiali Li
Dissertation Director

_____   _____

Dr. William Oliver III   Dr. Julia Kennefick
Committee Member   Committee Member

_____   _____

Dr. Reeta Vyas   Dr. David McNabb
Committee Member   Committee Member

Abstract

Solid state nanopores are widely used in detection of highly charged biomolecules like DNA and proteins. In this study, we use a solid state nanopore based device to characterize spherical nanoparticles to estimate their size and electrical charge using the principle of resistive pulse technique. The principle of resistive pulse technique is the method of counting and sizing particles suspended in a fluid medium, which are electrophoretically driven through a channel and produce current blockage signals due to giving rise to a change in its initial current. This change in current is denoted as a current blockage or as a resistive pulse. The information from these current blockage signals in case of nanopore devices and spherical nanoparticles helps us to look at the properties of each individual nanoparticles such as size, electrical charge and electrophoretic mobility. In this thesis, two spherical nanoparticles of different sizes and different surface charge groups are used: Negatively charged 25 nm iron oxide nanoparticle with $-COOH$ surface group and positively charged 53 nm polystyrene nanoparticle with $-NH_2$ surface group. Nanopores used in these studies are about twice the nanoparticle size. These nanopores were fabricated by various fabrication techniques such as, Focused ion beam milling and ion beam sculpting method. The current blockage events produced by these two nanoparticles were measured as a function of applied voltage. The parameters extracted from the current blockage events, such as the current drop amplitudes and event duration are analyzed to estimate the size and electrical charge of the nanoparticles. Estimation of drift velocity of the nanoparticle and diffusion coefficient are also discussed. The estimated size is then compared to the nanoparticle size obtained from dynamic light scattering technique. Stable nanoparticles are widely used in biological and pharmacological studies and understanding the behavior of these nanoparticles in a nanopore environment would make a significant contribution to the studies at the nanoscale.

Acknowledgments

I want to start by thanking my advisor Dr. Jiali Li for providing the resources, guidance and expertise to conduct this project. I also want to thank all of my committee members for suggesting and motivating me to improve my skills over the years.

I want to thank Dr. Jiali Li, Dr. Reeta Vyas, Dr. Surendra Singh and Ms. Tamara Snyder for helping me to be a better student, mentoring me in various stages of graduate school and encouraging me to be a better physics teacher.

I want to thank Richard Penhallegon for teaching me how to fix broken things in lab and in life- No matter how broken they are, they would be up and running. Jessica and Ryan, thank you for sharing your knowledge of physics with me. Thank you for your love, support, friendship, and belief in me. Y'all are incredible and I am extremely happy that you and your families are a part of our life. I also want to thank my previous and current labmates for their support and companionship. A big thank you hug to all the friends that I met at 825 West Dickson Street that made my life through graduate school easier, happier and memorable.

I want to thank Anne and Jim for their love support and encouragement. Finally to my husband Kevin, thank you for standing by my side and holding me up when things seem to be dark.

Contents

List of Figures

List of Tables

Chapter 1

Introduction

1.1   General introduction

>There's plenty of room at the bottom-Feynman 1959

This famous quote is from the lecture given by Richard Feynman in 1959 at an American Physical Society meeting in Cal tech. This lecture presented Feynman's ideas about exploring the world of material science and biology with devices that could manipulate atoms and achieve a resolution to look at the base pairs of a DNA molecule. This lecture is regarded as one of the foundations for this futuristic new field of science called nanotechnology and Feynman is considered the spiritual father of this field.

The field of nanotechnology that emerged in the 90's has its roots in this lecture given in 1959. The invention of different material characterization techniques like scanning tunneling microscopy [1] in 1981 and atomic force microscopy [2] in 1986, and their ability to manipulate atoms made a significant contribution to the field. The capability to achieve nanometer resolution using a transmission electron microscope (TEM) gave the opportunity to look at materials and biomolecules at nanoscale. This was followed by the improvement in techniques which allowed the fabrication of nanoscale devices using electron beams [3] and ion beams [4].

The scale of biomolecules in the area of interest range from 2-1000 nm and these include molecules like DNA [4], RNA [5], antibodies [6], viruses [7] and bacterial phages [8]. Nanoscale devices such as nanopores [9] and nanotubes [10] are used to detect these biomolecules and study their physical and chemical properties. The information obtained from these nanoscale sensors has given scientists the power to sequence the genomes of numerous biomolecules and viruses.

1.2 Nanopores - What are they, and what is their significance?

A nanopore [9] is a nanometer sized hole in a nanometer thick membrane. Combined with the experimental setup, it serves as an electrical sensor to detect various biomolecules and obtain information about their physical and chemical characteristics. A nanopore can be viewed as a Coulter counter at nanoscale. Nanopores of different sizes [9, 11, 12] are used to detect various biomolecules ranging from 2-1000 nm in size.

A typical experimental setup [13] consists of a nanopore tightly sealed between two microfluidic chambers, each equipped with a thin electrode. Such a setup is shown in Fig. 1.1. The microfluidic chambers consist of an ionic solution, and the nanopore serves as the only channel connecting them. When an electric potential is applied across the nanopore membrane, the negative ions in the ionic solution constitute the current through the nanopore. When a biomolecule, like a charged nanoparticle or a DNA molecule [13], is introduced into one of the microfluidic chambers and then due to the applied voltage it is electrophoretically driven through the nanopore into the other microfluidic chamber. This process of a biomolecule passing through the nanopore is known as translocation, and every translocation results in a change in the current through the nanopore. This change in current that is observed for a very small duration of time is an indication that the passing biomolecule is displacing electrolyte ions and it is known as an event. Each event can be characterized by two parameters: a change in current and the time duration for the passage of the nanoparticle. These two parameters can be related to the size and charge [10] of the biomolecule. Other properties of the biomolecules such as velocity and electrophoretic mobility [14] can be derived by studying its event dynamics using a nanopore.

Nanopores are mostly used in studying the properties of DNA-like molecules [15]. Apart from DNA, they have also been used to detect single molecules like ssDNA [13], RNA [5], different kinds of proteins [16, 17], and charged nanoparticles of different shapes and sizes [11, 18]. They have also been used to trap and identify single nanoparticles greater than
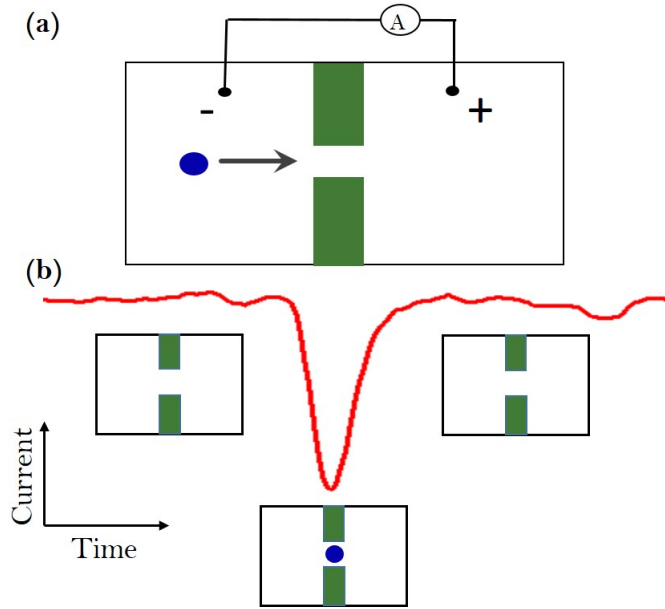
Figure 1.1: (a) Schematic illustration of nanopore setup, with a nanoparticle. (b) Schematic illustration of a current trace with an event produced by a single nanoparticle passing through the nanopore.

the pore diameter [19], in synthesis of nanoparticles [20] and single molecule selective multi-detection [21]. Nanopores present themselves to be a versatile sensor with a varied number of applications and they can be easily integrated into "lab on chip" systems [22].

1.3   Principle of detection - Coulter counter

The detection principle of a nanopore sensor is based on the principle of the Coulter counter [23]. Invented in the 1950s, the Coulter counter is a device used to detect and size particles suspended in a fluid medium. It was popular for its ability to study red and white blood cells, contributing significantly to the field of hematology [24]. The method of counting and measuring the size of the particles suspended in a fluid medium is called the resistive pulse technique [25].

A typical Coulter counter consists of two reservoirs filled with an ionic solution separated by a thin channel as shown in Fig. 1.2 [26]. Also shown in Fig. 1.2 are the other components. Each of these reservoirs is equipped with an electrode; a counter that is connected to a voltage
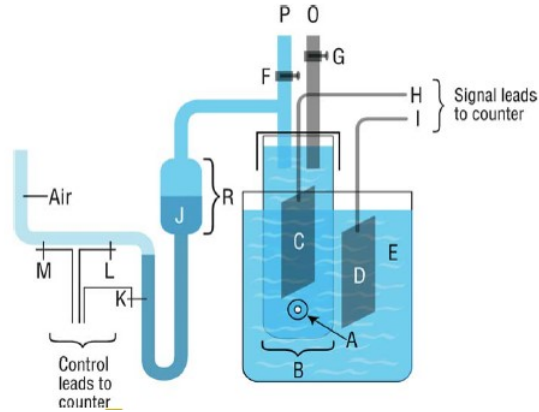
Figure 1.2: Functional schematic of the Coulter counter showing all the components. Listed below are some of the important components Aperture (A)- 100 μm was used to count the colloidal suspension. This was enclosed in a fluid reservoir with electrodes C & D. Also included, the mercury reservoir, R, and vaccum pump, P, used to drive the colloids through the aperture using the pressure difference [26].

source, reservoirs that are driven by a vaccum pump and a detection circuit containing a current detector and other electronics like a pulse counter and an oscilloscope. When a potential difference is applied across the reservoirs, a current is detected through the channel due the negative ions of the ionic solution flowing through the channel. Using Ohm's law and the dimensions of the channel, the initial resistance of the channel can be calculated. The particles are suspended in the same fluid medium as the ionic solution are introduced into one of the reservoirs. Due to the applied pressure difference generated using the vaccum pump, these particles are driven through the channel resulting a change in the initial resistance of the channel. This change in resistance is due to the exclusion of negative ions from the channel proportional to the volume of the particle and it is detected in the form of a pulse in the signal readout. This change in resistance that is observed for a small duration of time is known as a resistive pulse [25]. This technique was initially used to measure and count the particles suspended in a fluid medium and is now the foundation for commercially available cell counters that are used in various medical and biological laboratories [27] and resistive pulse sensors like nanopores.
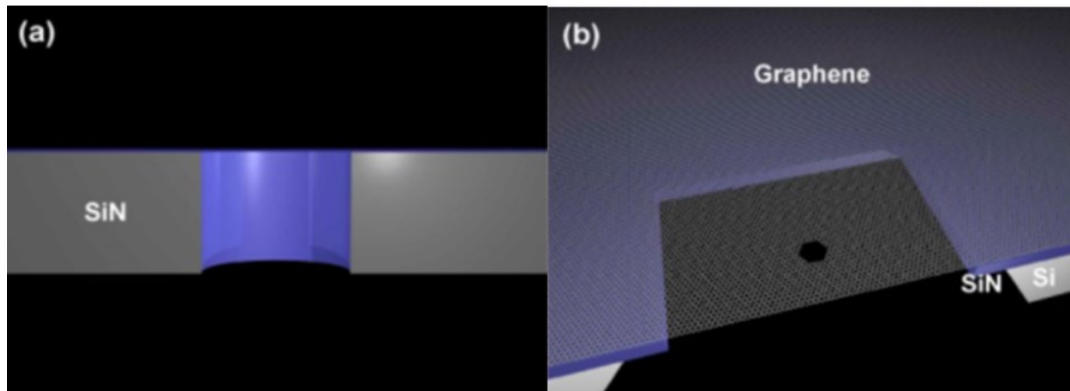
Figure 1.3: (a) Schematic illustration of a nanopore formed in silicon nitride (SiN), several tens of nanometers in thickness. The dimensions of the nanopore (diameter, length) can be tailored to the size of the biomolecule. (b) Schematic illustration of a nanopore in a graphene membrane, few nanometers thick supported on a SiN substrate [30].

1.4   Evolution of nanoscale Coulter counter

Since the original Coulter counter was patented in the 1950's, a lot of progress has been made in the field of nanotechnology. Researchers have been able to shrink the Coulter counter from micron scale to nanoscale. Different types of fabrication techniques and different types of materials have made it possible to miniaturize the Coulter counter by a 1000 times. The 100 μm glass channel in Coulters initial patent [23] has been reduced to a merely 5 nm graphene channel in graphene nanopores [28]. Fig. 1.3 shows two types of nanopores used in the field of single molecule detection. Solid state nanopores with several tens of nm in thickness [13] fabricated in silicon nitride provide the ability of customization in the geometry of the nanopore that makes it versatile sensor to study a number of biomolecules and nanoparticles. Graphene nanopores with only a few nm in thickness [28] are a more recent addition to the field that offer precision over solid state nanopores especially to study the base pair resolution of DNA molecule. Improvements in high bandwidth electronics have made it possible to detect signals on the order of few microseconds [29]. This facilitated the conversion of the Coulter counter to be a resistive pulse sensor at nanoscale and allowed the study of biomolecules such as DNA, RNA, proteins and viruses [4, 5, 7, 29].

1.4.1 Detection of biomolecules

Solid state nanopores were fabricated to study long, highly charged molecules such as DNA with a goal to sequence DNA and hence contribute to the genome sequencing project [31]. The dimensions of the nanopore played an important role in sensitivity and detection. Solid state nanopores offered both robustness and customizable dimensions that biological nanopores [5] did not offer. This made solid state nanopores more appealing to the nanopore community.

Resistive pulse technology has also been applied to detect and study the properties of low charge to mass ratio molecules like viruses. Most virions studied are in the range of 30-500 nm and consist of an insulated outer shell with the genetic material inside. Charged spherical nanoparticles of similar sizes are used to structurally represent virions in nanopore studies [11].

To study biomolecules in this size range, the resistive pulse sensor went through a size shrink. This included improvements in areas of material selection in which the sensor was fabricated as well as development of specific fabrication techniques [32]. The resistive pulse sensor evolved from counting micron range cells in Coulter's patent to a platform studying nanoparticles and viruses [33].

1.4.2 Early studies to impact the field of resistive pulse technology

Initially the Coulter counter was made with glass channels to study the particle suspensions. These glass channels were limited to 100 μm in width and to study particle suspensions smaller than 100 μm, channels of smaller dimension were required. This made Coulter electronics to look at sapphire washers and ceramic gaskets which allowed them to solve the glass fusing problems with Coulter counters and helped them to design 30 μm channels. This led to studying a variety of particle suspensions such as oils, emulsions, blood cells, latex particles $\sim$ all of the order of several micro-meter(μm), compared to the channel width. The requirement to study the particle emulsions was that the width of the particle/analyte under

consideration was smaller than the channel width and hence would be detectable [26].

In the year 1970, two researchers from GE R& D took the principle of the Coulter counter and applied it to counting and sizing latex particles in the sub-micron range using electric field instead of pressure gradients. This was done using a single submicron pore that was isolated from an array of pores made by irradiating 10 μm plastic sheets with the radioactive metallic element Californium 252 (^{252}Cf). They studied insulated polystyrene particles of different sizes ranging from 0.09 μm to 0.35 μm using track etched pores of dimensions 0.4 μm to 0.5 μm. This study also included two theoretical models explaining that the magnitude of each resistive pulse observed could be related to the geometry of the pore and the particle [25].

This study presents two theoretical models that support the experimental data. The magnitude of resistive pulses caused by an insulated spherical particle electrophoretically driven through the conducting cylinder is related to the volume of the particle. This insulated particle also causes a change in resistance of the channel by displacing ions through the channel. Several models are discussed to estimate the change in resistance of the conducting cylinder by the inserted insulated sphere.

Maxwell's solution for considering the volume fraction to calculate the change in resistance takes both the volume of the sphere and the cylinder into consideration [34]. It also relates the change in resistance directly to the cube of the diameter of the sphere and inversely proportional to the 4th power of the diameter of the channel. This solution is valid when $d \ll D$, where d is the diameter of the insulated spherical particle and D is the diameter of the cylindrical channel.

To accommodate for a broader range of pore and particle dimensions, a solution to Laplace's equation is presented by solving for the potential using spherical harmonics. The tubular stream line current is calculated at the boundary conditions and then the change in resistance is calculated. This solution still yields the above mentioned Maxwellian value in the smaller limits but also incorporates the specific considerations for different pore and

particle dimensions.

This study is considered to be one of the foundations of resistive pulse technology as it was able to achieve a detection limit of 60 nm without using a pressure gradient in the 70's. Hence, surpassing the commercially available Coulter counter by an order of magnitude and opening frontiers to detect spherical viruses and nanoscale contaminants. With its theoretical model and analytical expressions, one can size the particle or explore the dimensions of the pore. It extended the power of the resistive pulse technique into the nanoscale colloidal range.

This sub-micron particle detector was further developed into an analyzer called 'Nanopar' that was used to study several types of Type 2 Oncornaviruses in 1977. This study measured several properties of these viruses (100-140 nm) using a (400 nm diameter, 3.8 μm length) pore. These measurements include size, electrophoretic mobility and concentration of these viruses in their native environment [35].

1.4.3   Recent studies

The concept of change in resistance when a particle is passing through the channel has been applied to many later studies for detection of biomolecules. Some of the significant studies are listed below.

In 2001 Saleh and Sohn published an article about a micro-chip coulter counter that was used to study nanoscale colloids [22]. The micro-chip coulter counter was fabricated on a quartz substrate using electron beam lithography (EBL). The dimensions of this device were 0.2-0.6 μm^2 in cross sectional area and $\sim$10 μm in length. Using the theory of Deblois and Bean [25], the relative change in resistance was calculated and compared experimentally when a particle of given size was driven through using a voltage bias. This study was also able to distinguish between particles of different sizes based on the pulse height and width. The resolution achieved by this study was to detect a 87 nm negatively charged nanoparticle using a 220 nm in diameter, and 8.3 μm in length micro-chip coulter counter.

At the same time, Crook's group in Texas was studying the concept of the resistive pulse technique using a single carbon multi walled nanotube(CMWNT) [36]. They were successfully able to demonstrate the characterization of 60 nm negatively charged nanoparticles using a 132 nm in diameter, 900 nm in length single carbon multi walled nanotube mounted on a supporting Polydimethylsiloxane(PDMS) structure. Their study included calculating the size, surface charge, electrophoretic mobility from the resistive pulse heights and resistive pulse widths [10, 14]. The measurement of size and electrophoretic mobility of the negatively charged nanoparticles were then compared to the measurements obtained from transmission electron microscopy (TEM) and dynamic light scattering (DLS) techniques.

In 2008, a group from Arizona were the first to fabricate a nanoscale Coulter counter with silicon on an insulator substrate using electron bean lithography (EBL) [37]. In this study pores of varying diameter were fabricated and their conductance was characterized at different electrolyte concentrations. Later, three differently sized nanoparticles 60, 100, 130 nm were characterised using a 240 nm diameter pore. The theoretical current drop was calculated from the theory Deblois and Bean, which was in agreement with the experimental observations.

In recent years, solid state nanopores have been used as a platform to study separation of biomolecules. In one study conducted the M.J. Kim group at Drexel university [38] the nanopore surface was chemically modified to increase the event frequency and electrically discriminate two differently sized spherical nanoparticles. A 150 nm diameter nanopore was fabricated in 50 nm thick free standing silicon nitride using focused ion beam (FIB) and was chemically modified using APTES to characterise 28 nm and 55 nm negatively charged nanoparticles. This was the first study of its kind to explore the pore surface charge properties using a multi ion model [39]. The chemical surface modification of the nanopore resulted in an increase in event frequency for both the nanoparticles.

Solid state nanopores have also been used to study the dynamics of electrically charged colloids at nanoscale [40]. This study, was conducted by Bacri et.al looked at various translo-

cation dynamics caused by the colloid as a function of voltage using a 85 nm Silica nanoparticle in a 175 nm diameter fabricated in a 50 nm thick silicon nitride membrane. The authors also distinguish different type of events based on the different translocation times. Each average time depicts a particular type of interaction between the pore-particle surface.

Henry White's group at Utah studied the translocation dynamics of two differently sized negatively charged nanoparticles 160 nm, 80 nm in diameter using conical nanopores [41]. These nanopores are formed within glass nanopore membranes with a diameter of 250 nm and a length of 25 μm. Due to the different geometry of the nanopore, the resistive pulses observed have a unique assymetric triangular shape. Geometry also contributes to a different magnitude of electric field along the length of the pore. This in turn affects the translocation rate of the nanoparticle through the pore. This group also studied the effect of pressure on translocation rate [42].

Siwy's group at UC Irvine studied the particle transport through polymer nanopores (PET) and silicon nitride nanopores. In one study, two differently sized silica nanoparticles 55 nm, 110 nm in diameter were characterised using 200-300 nm diameter pores fabricated in silicon nitride membranes of different thicknesses 50 nm, 100 nm and 500 nm [11]. This study covered both low aspect and high aspect ratio cylindrical pores and discussed the effect of a geometrically dependent electric field on nanoparticle translocation rate.

The studies listed above present some of the important contributions to the field of nanoparticle detection using nanopore in terms of theoretical model development, nanopore fabrication techniques and novel experimental findings. Most of these studies use negatively charged spherical nanoparticle, which could be modeled as a spherical virus in biological systems.
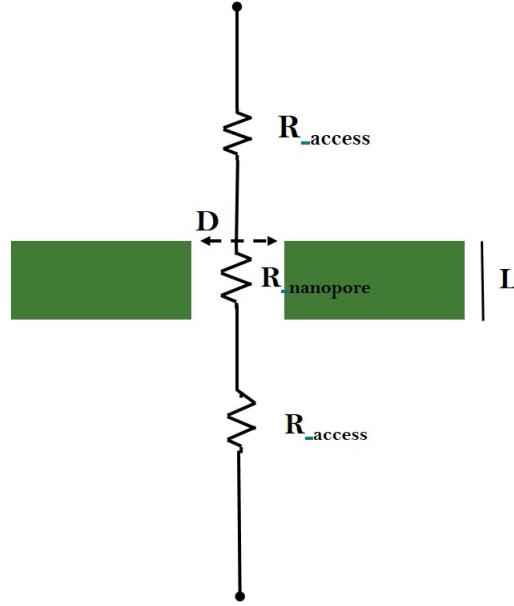
Figure 1.4: Electrical equivalent of a nanopore of thickness L nm and Diameter D nm.

1.5 Nanopore - nanoparticle event parameters

1.5.1 Event amplitude

The electrical equivalent of a nanopore can be represented as a collection of three resistors in series. Such an arrangement is shown in Fig. 1.4 [43]. The resistors on either ends contribute to the access resistance and the resistor in the middle is analogous to pore resistance. The total resistance of the nanopore is the sum of the total access resistance and the pore resistance.

Consider a nanopore of length (L) and diameter (D) filled with an electrolyte of conductivity $\sigma_{electrolyte}$ under an applied voltage (V). Using Ohms law we calculate the current through the nanopore.

$$V = I_0 R \tag{1.1}$$

In equation 1.1, I_0 is the open pore current detected through the nanopore when a potential difference (V) is applied. The applied voltage causes the negative ions in the

11

electrolyte to migrate towards the positive electrode.

The total resistance R of the nanopore is the sum of pore resistance and total access resistance contributed by the ends of the pore. Assuming the nanopore geometry to be a cylinder, we can write the mathematical equations representing the resistance.

$$R_{nanopore} = \frac{4L}{\pi D^2 \sigma_{elec}} \tag{1.2}$$

The access resistance is given by the Hall resistance [44]

$$R_{access} = \frac{2}{2\sigma_{elec}D} = \frac{1}{\sigma_{elec}D} \tag{1.3}$$

The total resistance of the nanopore is the sum of $R_{nanopore}$ and R_{access} from equations (1.2) and (1.3)

$$R = \frac{4(L + 0.8D)}{\pi \sigma_{elec} D^2} \tag{1.4}$$

Substituting R in Ohm's law to find I_0, we find

$$I_0 = V \left(\frac{\pi \sigma_{elec} D^2}{4(L + 0.8D)} \right) \tag{1.5}$$

Consider a spherical nanoparticle of diameter d is inserted in the nanopore. This nanoparticle will exclude negative ions equal to its volume when it is being electrophoretically driven through the channel. This will cause a drop in the open pore current for a small amount of time until the particle completes its passage through the pore. This momentary drop in nanopore's open pore current is called the blockade current (I_b). The change in current amplitude caused by the nanoparticle translocating through the nanopore is the difference between the open pore current and the blockade current.

$$\Delta I = |I_0 - I_b| \tag{1.6}$$

$$\Delta I \sim \Delta R \tag{1.7}$$

$$\Delta R = |R - R_b| \tag{1.8}$$

$$\frac{\Delta I}{I_0} = S(D, d) \left(\frac{d^3}{L + 0.8D} D^2 \right) \tag{1.9}$$

From equation (1.9) $\Delta I/I_0$, is the relative change in current drop and it is directly proportional to the cube of the diameter of the nanoparticle and inversely proportional to the square of the diameter of the nanopore. $S(D, d)$ is the correction factor extracted from the Deblois and Bean theory [25]. The diameter d of the nanoparticle can be estimated from the experimental average current drop. The length of the nanopore can also be estimated if using a nanoparticle with known diameter.

1.5.2 Event duration

The event duration of the nanoparticle is defined as the time it spends in the sensing zone of the nanopore during an event. The length of the sensing zone depends on the geometry and the electric field distribution of the nanopore. The event duration is also inversely dependent on the applied voltage.

The event duration is inversely proportional to the average velocity of the nanoparticle. This average velocity is dictated by different forces acting on the nanoparticle inside the nanopore. The main contribution is from two types of forces. The first is the electrophoretic force which is due to the applied voltage and the second is the electroosmotic force which arises due to a net charge on the nanopore walls and the ions in the surrounding electrolyte.

The electrophoretic velocity of the nanoparticle can be related to its zeta potential using Graham's equation [45]. The electrophoretic mobility of the nanoparticle is directly proportional to the zeta potential and is given by the following equation

$$\mu_e = \frac{A\varepsilon_r\varepsilon_0\zeta}{\eta} = \frac{v_{electrophoretic}}{E} \qquad (1.10)$$

Here μ_e is the electrophoretic mobility of the nanoparticle, and A is the correction factor dependent on the ratio of diameter of the nanoparticle and it's Debye length κ^{-1}.

$$d\kappa \gg 1; A = 1$$

$$d\kappa \ll 1; A = 2/3$$

The Debye length of a nanoparticle [46] is given by the following equation:

$$\kappa^{-1}(nm) = \frac{3.04}{\sqrt{I(M)}} \qquad (1.11)$$

where $I(M)$ is the molar concentration of the electrolyte.

1.6 Motivation for this dissertation

Studying nanometer sized particles is very important because these nanoscale particles are a part of everyday commercial products such as toothpastes, make-up, detergent and pharmaceuticals. The intrinsic properties like shape, size, charge and concentration dictate the behavior of these nanometer sized particles in their colloids [47].

Also, a nanometer sized particle with a charge is very similar in structure to a virion. Understanding the behavior of these particles in various sub-micron environments would make a significant contribution to the study of viruses in plants, animals and humans at a cellular level [48].

These particles are usually studied for average size using ensemble techniques like Dynamic light Scattering(DLS). DLS measurements usually represent an average value of the sample with a high error [49]. It also requires a significant amount of sample volume around

1 ml, which might not always be possible. Studying differently shaped nanoparticles is difficult with a DLS setup because all the theoretical models are applied to spherical nanoparticles.

On the other hand, techniques like Transmission electron microscopy(TEM) and Scanning electron microscopy (SEM) can be used to study nano meter sized particles. All these measurements involve extensive sample preparation and are not cost effective. These measurements are performed under high vacuum, which collapses the electric double layer of the nanoparticle and true information about the size of the nanoparticle in its native environment is not obtained [50].

With the concept of resistive pulse technique,nanopores can determine the properties of the nanoparticle like shape [51, 52], size [53], charge [10, 18], and concentration [14] in their native environment using a very small sample volume ∼40 μl without altering the electric double layer around it. All these parameters have been studied using proteins in nanopores [54] thus making the nanopore sensor as a promising device for detecting and characterizing nanoparticles.

Nanopores fabricated using the Ion beam sculpting method in which the nanopore of desired dimensions is sculpted inside a ∼100 nm FIB hole using high energy noble gas ions have been extensively used to study various DNA and protein translocations [55–59]. This technique results in a nanopore with unique geometry that is small in diameter and thin in length. This type of nanopores are suitable to study DNA translocations due to their small dimensions. The DNA is captured at the entrance of the nanopore and is pulled through due to its high effective negative charge. The length of the DNA molecule allows it to pass through in different configurations and the thickness of the nanopore [60] contributes to the event amplitude. The thinner the nanopore [61, 62], better the resolution between the electrical signature produced by the base pairs is achieved.

In this dissertation, we use the same IBS fabricated nanopores to study spherical nanoparticles. Due to their geometry, spherical nanoparticles exhibit a different behavior in the
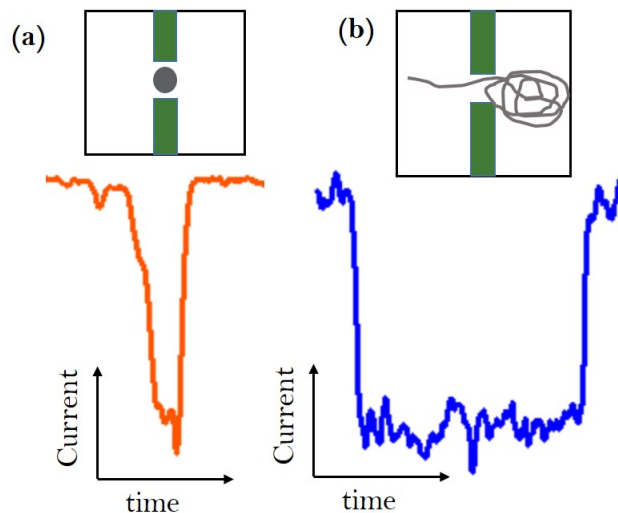
Figure 1.5: Illustration of a single nanoparticle passing through a IBS fabricated silicon nitride pore. Shape of the nanoparticle event does not have a square bottom. Event duration (∼ few hundreds of microseconds), recreated using real data. (b) Illustration of a λ-DNA molecule passing through a IBS fabricated silicon nitride pore. Shape of the event has a well defined square bottom (∼ few milliseconds) due to the shape and high negative charge of the molecule, that allows it to translocate in different configurations, recreated using real data.

nanopore environment. This is clearly depicted in all the translocation parameters that can be measured using a nanopore. Two different sized particles 25 nm, 53 nm in diameter with different surface charge groups and nanopores under 100 nm in diameter have been used in this study and their translocation behavior is discussed extensively. The smaller nanopores have been fabricated using Ion beam sculpting method, contributing to their different geometry. The bigger nanopore was milled using a Focussed ion beam. The event amplitude and event duration is studied as a function of voltage, and pH of the electrolyte.

In some recent studies, the surface of the nanopore was chemically modified to increase the nanoparticle event frequency [38, 63] while using a negatively charged nanoparticle. In this study, we present the translocation dynamics of both positively and negatively charged nanoparticles with the same surface charge nanopore and without any additional chemical modification to its surface charge. From Fig. 1.5 we can see the two different types of events generated by a spherical nanoparticle with dimensions smaller than both the diameter and

thickness of the nanopore and by a λ-DNA molecule that is long and highly charged and can pass through the nanopores in different configurations. These two events were distinguished based on the event amplitude and event duration and the shape of the event. Studying nanoparticles with diameter d<60nm using a Ion beam sculpted nanopore is challenging in terms of experimental design specifications and data analysis,but it also adds versatility in the type of molecules studied by this particular type of nanopore.

Chapter 2

Experimental methods

2.1 Nanopore fabrication

Fabrication of the free standing membrane: Solid state nanopores are considered to be a robust and more dependable alternative to the biological nanopores existing in lipid bilayer membranes. They also offer the flexibility of custom pore diameters by incorporating fabrication techniques at the nanoscale [64]. The successful translocation of DNA molecules through nanopores was first demonstrated by the Harvard group in 2003 [9]. These nanopores were fabricated from a silicon nitride membrane supported by a Si substrate using a feedback controlled ion beam sculpting system [4, 65]. Silicon nitride is a well-studied semiconductor material that is highly compatible with nanoscale fabrication procedures. The inherent properties of silicon nitride, such as high tensile strength, high chemical resistance, high electrical resistivity, as well as the ability to serve as an effective barrier to diffusion of water and sodium makes it an ideal candidate for the fabrication of nanopores [66].

In recent years, nanopores have been fabricated in a variety of materials like graphene [67–69], molybdenum disulfide [70, 71] and boron nitride [72] using various fabrication techniques. These materials and methods contribute to different geometries and surface properties for the nanopores made in them but high throughput from these pores is still under review. So far, silicon nitride stands as the most suitable material for the fabrication of nanopores. Over the past decade the nanopore community has made a lot of progress in making this stable semiconductor membrane thinner ($\sim$3 nm) in order to achieve near base pair resolution when studying DNA molecules. [73, 74].

We fabricated our nanopores using the same feedback controlled mechanism used by the Harvard nanopore lab. The initial step in making solid state nanopores is to create a stable free standing silicon nitride membrane. This is done by coating an 8-inch diameter wafer containing 380 μm Si with 275 nm thick Si_3N_4 on both sides using low pressure

chemcical vapor deposition (LPCVD). This wafer is then modified on one side using standard photolithography techniques where it is coated with a photoresist and a mask is imprinted on it. Later this wafer is etched with high energy ions using reactive ion etch through the top layer of silicon nitride and through the silicon. As a last step, a traditional wet bench KOH etch is performed along the (111) plane to yield a pit through every imprinted photo lithography square 3 mm × 3 mm pattern containing a free standing 275 nm thick silicon nitride. The detailed procedure for fabricating the free standing membrane is discussed here [75].

2.2   Ion beam sculpting and post-close annealing

A brief overview of the fabrication process includes the fabrication of ∼275 nm thick stable free standing membrane in silicon nitride with a Si substrate using conventional photolithograpy, reactive ion etching and chemical etching technique on an 8-inch wafer. Initially a ∼100 nm hole is created in each 3 mm × 3 mm window housing the free standing silicon nitride membrane using a powerful 50 keV focused Ga^+ ion beam. This process is carried out by an FEI/Micrion 9500 focused ion beam setup at Harvard. FIB systems are popular for their ability to investigate nanoscale structures using a highly energetic and focused ion beam, but in this case they are used to mill ∼100 nm nanopores across each 3 mm × 3 mm window in a 8-inch wafer. This FIB setup has a spot size of 5 nm and is operated at a current of 20 nA giving the user ability to mill FIB holes up to 60 nm in diameter [65].

The wafer containing several hundreds of 3 mm × 3 mm windows, each with a milled FIB hole is further fabricated one chip at a time in a high vaccum setup with feedback controlled ion beam sculpting mechanism using 3 keV noble gas ions. The ion beam sculpting process can be summarized as follows: the chip containing ∼100 nm FIB hole is sputtered by a high energy electron beam to maintain charge neutrality on the surface and then exposed to very narrow several hundred micron diameter noble gas ion beam. The noble gas ions interact with the silicon nitride atoms and cause them move along the length of the FIB hole due to

19

the process of surface adatom deposition [4, 76]. This process results in formation of a thin silicon nitride membrane and a shrinkage of diameter of the ∼100 nm FIB hole. This entire process can be closely monitored by quantitatively observing the parameters like type of ion beam, ion beam flux F (ions nm^{-1}s^{-1}), area of the FIB hole (nm^2) before being exposed to the ion flux, ion count rate ($\frac{ions}{nm^2}$), area (nm^2) of the desired nanopore [77]. This monitoring and precision is possible due to the various inbuilt parts of the vaccum system consisting of electromagnetic lenses, deflection plates, channeltron detector and labview program. The important steps in the fabrication of nanopores using IBS are shown in Fig 2.1. The details of design and specifications of the ion beam sculpting apparatus is described in the following references [75]. This process allows the user to fabricate nanopores of any desired diameter less than 100 nm and is very well known for fabricating thin and small ∼5 nm diameter nanopores widely used to study highly charged molecules like DNA.

Post close annealing is the post ion beam process done on each individual chip containing a nanopore. The annealing process includes baking of the chip at 800-850°C in a furnace. This process is carried out on all the samples to ensure a decreased etch rate under experimental conditions. The study conducted by Rollings et.al [78] shows a significant decrease in etch rate of IBS nanopores when they are post close annealed. This is due to reduction of dangling bonds on the surface of silicon nitride left over as a side effect of IBS fabrication.

2.3   TEM drilling of IBS closed samples

Using a high energy TEM beam to drill a nanopore in a free-standing silicon nitride membrane is one of the popular methods of fabricating nanopores. The focused high energy TEM drilling method yields nanopores in sub ∼10 nm range [3]. In this section, we briefly talk about using the same technique to drill a nanopore in completely closed samples from th ion beam sculpting process. From Sec 2.2, we know that the high energy noble gas ions impinge on the silicon nitride atoms and cause them to laterally transport and form a thin membrane at the top causing the ∼100 nm hole to shrink into a nanopore of desired dimension [78, 79].
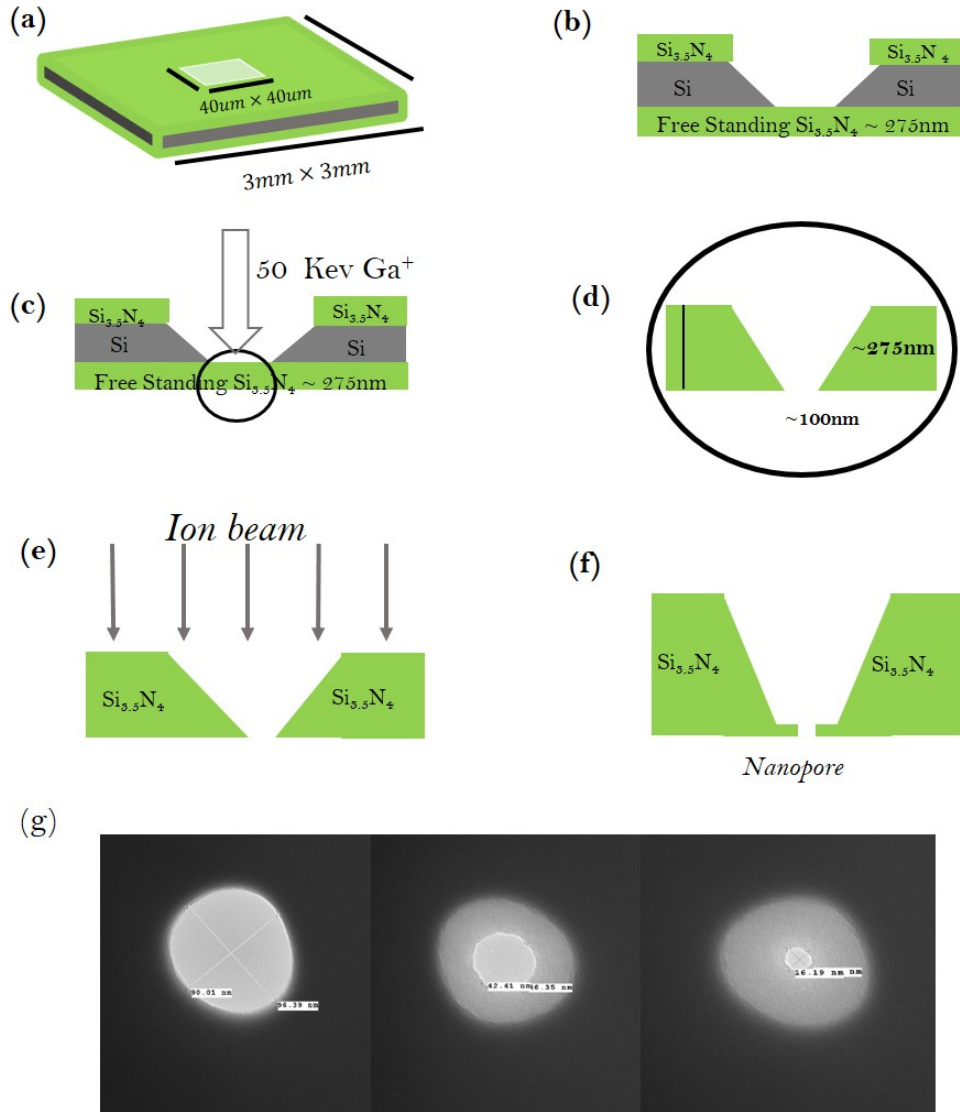
Figure 2.1: Schematic illustration of nanopore fabrication process using the ion beam sculpting method. (a) Planar view of the 3 mm × 3 mm chip with a 40 μm window etched in the center containing the freestanding Si_3N_4 membrane. (b) Schematic illustration of the cross section of the chip containing 380 μm thick Si surrounded by Si_3N_4 on both sides, cross section of the 40 μm etched window containing the freestanding Si_3N_4 shown. (c) Schematic illustration of focused ion beam milling (FIB) using 50 keV Ga ion beam that mills a ~100 nm diameter hole in the membrane. (d) Cross-section of the milled FIB hole. (e) Illustration of noble gas ion beam imparted on the FIB hole causing it to sculpt into a nanopore. (f) Illustration of a completely formed nanopore from the ion beam sculpting process in a FIB hole. (g) TEM images of FIB with 90 nm diameter, 40 nm diameter nanopore fabricated within a FIB, 16 nm diameter smaller nanopore fabricated in the FIB showing the customization in pore sizes.

Sometimes, this process results in a closed membrane. These samples are suitable for TEM drilling due to the thin membrane on the top. When using a 200 keV Technai column, drilling nanopores is possible when the membrane thickness is greater than 90 nm. From EFTEM thickness maps it is known that IBS nanopores meet this thickness requirement [61], so an IBS closed sample makes an ideal candidate for TEM drilling. The drilling is done in nanoprobe mode under high magnification and the TEM beam is condensed and focused at the center of the closed membrane. Both the objective lens astigmatism and condenser lens stigmatism need to be corrected to obtain a focused beam. The beam current (nA) and dose rate ($\sim 10^5$) $\frac{electrons}{nm^2 s}$) can be monitored on the screen by the user during the process. The drilling time can be upto a minute under these specific conditions.

Illustration of an IBS closed sample and TEM drilling is shown in Fig 2.2. Also shown in the figure are TEM images of the closed membrane and the corresponding TEM drilled nanopore in 2.2(c). In 2.2(d) is the TEM image of the nanopore taken under high magnification. This entire process was carried out using a 200 keV Technai TEM at Arkansas Bio and Nano Material Characterization Facility.

2.4 E-beam lithography nanopores

The process of fabricating nanopores using a freestanding silicon nitride membrane and e-beam lithography is briefly discussed below and shown in Fig 2.3. It consists of coating a sample consisting of several 3 mm × 3 mm chips containing ~275 nm thick free standing Si_3N_4. This sample was coated with an e-beam resist and subjected to the process of e-beam lithography where the pattern containing an array of 2 μm diameter circles were written on the membrane. After the process of lithography, the sample was subjected to reactive ion etch (RIE) using high energy ions in RIE plasma. This process reduced the thickness of the membrane containing 2 μm diameter pattern to less than 90 nm making it suitable to be drilled under TEM. Later, the sample was cleaned and a nanopore was drilled using high energy TEM beam inside one of the selected 2 μm diameter circular pattern. The goal of
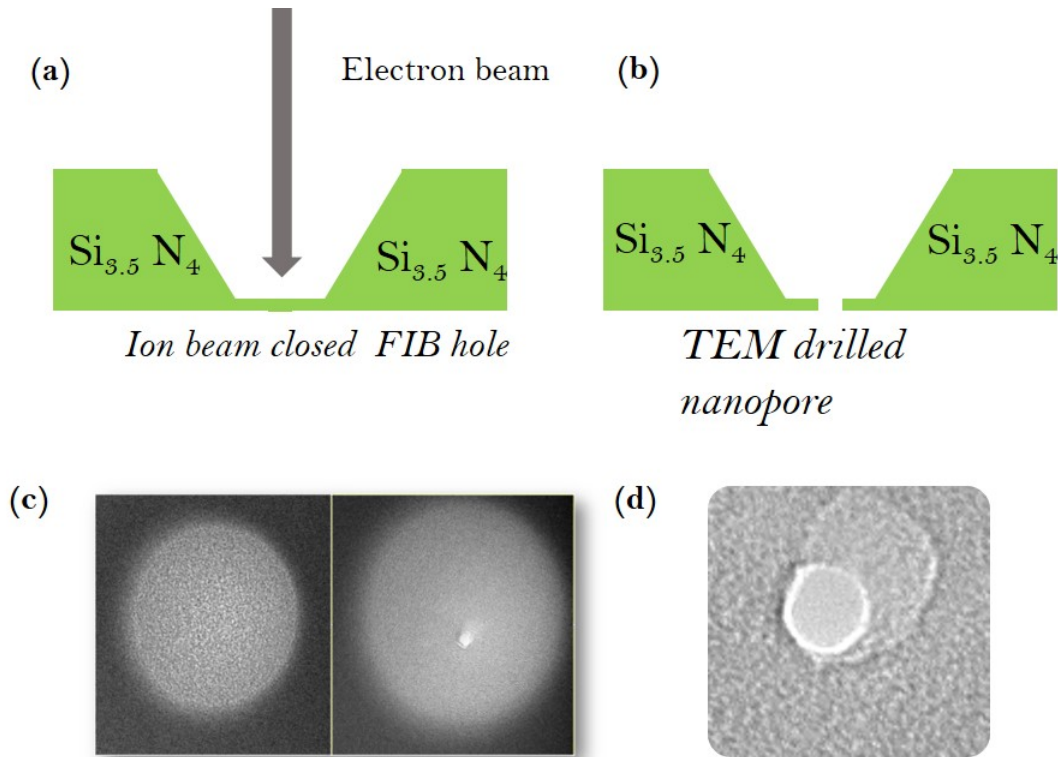
Figure 2.2: Schematic illustration of fabricating nanopores in IBS closed membranes by TEM drilling. (a) Illustration of a 300 keV TEM beam drilling through the closed membrane. This closed membrane was formed in the IBS system and has a membrane thickness of less than 90 nm making it suitable for TEM drilling. (b) Illustration of the nanopore formed by TEM drilling, this is suitable to drill small nanopores less than 10 nm in diameter as the TEM beam can be condensed and focused to small beam diameter. (c) TEM image of a closed membrane followed by TEM image of the same membrane with a TEM drilled nanopore. (d) Magnified TEM image of the nanopore drilled using TEM.

the project was to create nanopores with varying thickness using this procedure.

2.5 Experimental setup

2.5.1 Fluidic system

The fluidic system in which nanoparticle translocation experiments are conducted is shown above in Fig. 2.4. The same fluidic setup has been extensively used for all DNA and some protein translocation studies conducted by our research group [55–59]. The fluidic system consists of a custom machined aluminum cell with a slot to fit polydimethylsiloxane (PDMS) chambers. The two half cells with their respective PDMS chambers and the nanopore sandwiched in between them is tightened using screws. The nanopore serves as the only channel between the PDMS chambers in the top and bottom cells. The PDMS chambers are fabricated in such a way that the side that is in contact with the nanopore forms an airtight seal around it. This provides the nanopore chip with a PDMS gasket-like structure on the top and bottom. The three channels fabricated inside each PDMS chamber serve as an inlet, outlet and electrode facilitators. These inbuilt channels for inlet and outlet are further extended outside the aluminum cell using sterile plastic tubing and sterile broad gauge syringe needles. These connections are connected to sterile (3 ml-5 ml) syringes that serve as the fluid inlet and outlet for each PDMS chamber. The channel used for the Ag/AgCl electrodes provides a slot that is fitted so that the electrodes are close to the nanopore surface. The electrode on the -cis side is connected to ground and the electrode on trans side is connected to the axopatch head stage with a 1 mm axopatch connecter. The fluidic setup is housed in a smaller Faraday cage which is placed in a bigger faraday cage placed on a vibration isolation table to minimize the effect of noise on sensitive measurements.

The PDMS chambers are fabricated for every translocation experiment and are not reused due to contamination problems. The tubing and syringes can be reused, but only after thorough cleaning and the electrodes are bleached using chlorine for each translocation experiment [80].

(a) *Electron beam exposure*

(b) *Etch by High energy ions in RIE plasma @17nm/min(Ar,CF$_4$,O$_2$)*

3% PMMA ~ 300nm

Free standing Si$_{3.5}$N$_4$~275nm

Si

Si

Si$_{3.5}$N$_4$

Si$_{3.5}$N$_4$

40um window

E-beam pattern

Si$_{3.5}$N$_4$~ 80nm

Si

Si

Si$_{3.5}$N$_4$

Si$_{3.5}$N$_4$

40um window

(c)

(d)

(e)
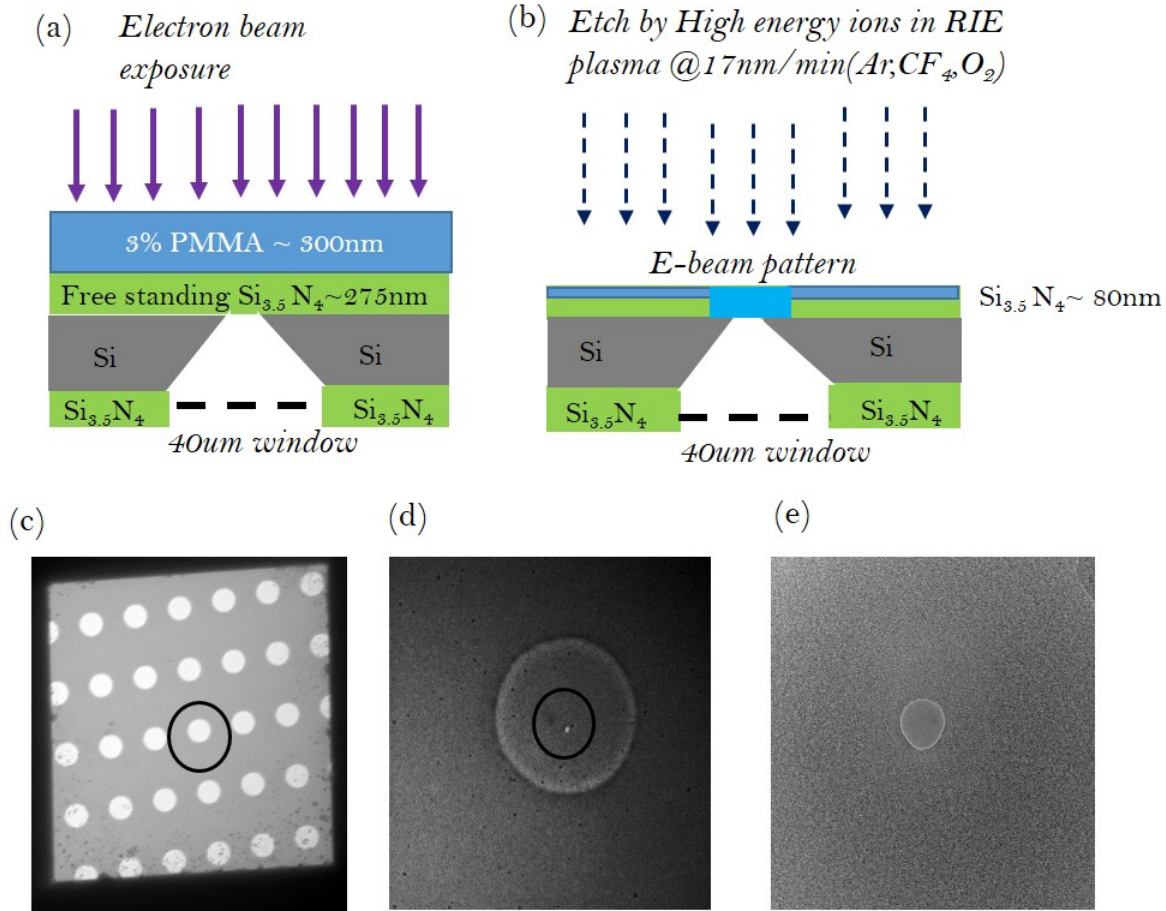
Figure 2.3: Schematic illustration and TEM images of nanopores fabricated by E-beam lithography (EBL). (a) Illustration showing the process of e-beam lithography on a chip containing 275 nm thick free standing Si$_3$N$_4$ coated with a 300 nm e-beam resist. The chip is further processed to remove the resist. (b) Illustration showing the process of reactive ion etch (RIE) using high energy ions to decrease the thickness of Si$_3$N$_4$ with the e-beam pattern etched in it. The thickness was decreased to 80 nm to make it suitable for TEM drilling. (c) Low magnification TEM image showing the 40 μm $\times$ 40 μm free standing Si$_3$N$_4$ of thickness 80 nm with e-beam pattern of 2 μm circles. (d) TEM image of one of the 2 μm circles that was selected to drill a nanopore. The little dot enclosed in a black circle is the TEM drilled nanopore. (e) TEM image of a 10 nm nanopore drilled by TEM. This is a part of 2 μm circular pattern that was made by EBL and thinned down by RIE.
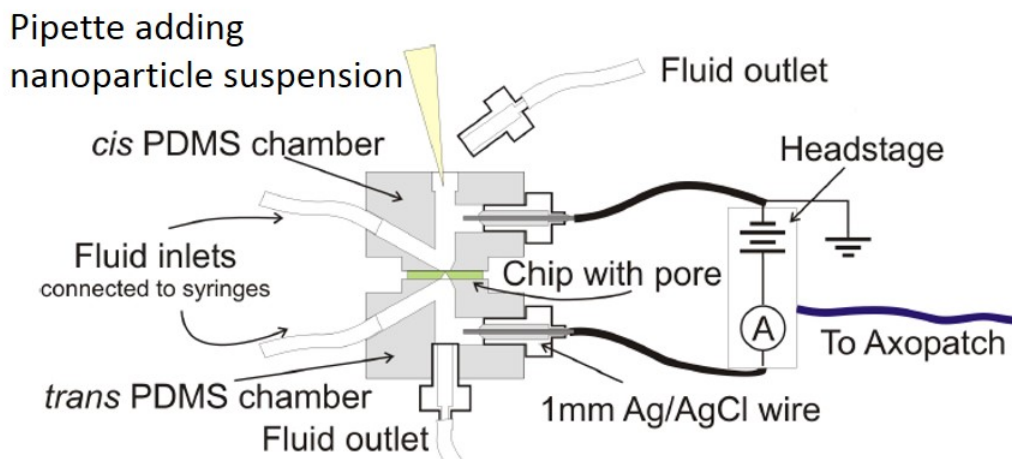
Figure 2.4: Schematic illustration of the fluidic setup in which nanopore experiments are conducted. Borrowed from Rollings *et al* [80]. The setup shows polydimethylsiloxane (PDMS) chambers with channels for fluid inlets, fluid outlet and the Ag/AgCl electrodes. The chip containing nanopore secured between the two PDMS chambers. The setup is connected to the Axopatch head stage and ground using the Ag/AgCl electrodes [80].

2.6 Processing data files

Event data files are collected using a variable length protocol in Clampex. The recorded data, consisting of hundreds of thousands of data points that include information about the header file, pre and post trigger points, events and baseline data as a function of time and sampling frequency are stored in an axon batch file with a .abf extension. This .abf file can be viewed in Clampfit and is usually referred to as raw data as it contains all the data points for an event trace including baseline fluctuations and noise. To extract the information we need about different types of events, the raw data has to be pre-processed to remove any baseline fluctuations, reverse polarity in case of positively charged nanoparticles. After the pre-processing, the base corrected file is further analyzed using DNA7, a homebuilt Matlab software to extract event duration and event depth [55–58, 81, 82] from current blockage events. This extracted data is transferred into a plotting software like Igor or Python to make various plots. These include scatter plots, distributions for current drop and event duration which further give us the average values of current drop and event duration for

each voltage.

2.6.1 Preprocessing raw data

The raw data containing current blockage events is stored as an integer type .abf file. This data is collected using a variable length protocol. The variable length acquisition mode allows the user to set the trigger either above or below the baseline current and collect data as events in real time when the baseline drops below the set trigger level. A voltage clamp is used for this experiment, it allows the user to apply voltage across the nanopore membrane connected to the Axopatch electronics. The data is collected at a sampling frequency of 250 KHz. The data is also filtered using a low-pass filter at 10 kHz, which allows signals until the cut-off frequency and blocks all higher frequencies.

(a) Polarity reversal

Event traces have a steady adjusted baseline at +1000 pA and all the events that drop from the baseline have a positive polarity. However, in case of events with positively charged nanoparticles, the adjusted baseline is at -1000 pA and events have a negative polarity. The detected events cause an increase in the baseline current instead of reduction due to the positive charge on the nanoparticle.

In order to get the data ready for further processing using Matlab, one would have to reverse the polarity of event drops and the baseline. This is to ensure that the threshold levels detect the decrease in current from the baseline as an event and collect its amplitude and duration information. This step can either be carried out in Clampfit or in the Matlab routine of Base Adjust 4.1 [82]. In Clampfit it is done by changing the polarity of the scale factor of the signal. This option is inbuilt in the Clampfit software under signal parameters.

In Base Adjust 4.1, this can be done by choosing the option of positive polarity. The output .abf file which is base corrected will have a reversed polarity of all the events that are captured using variable length protocol.

(b) Baseline correction

Event traces consist of segments where baseline current fluctuates due to the presence of charged particles on the surface of the pore and noise contributions from the instrumentation and inherent nanopore surface charge fluctuations. It is hard to get all the event information from a noisy, fluctuating baseline. Baseline correction/adjustment is required to get a stable baseline by removing fluctuations caused by the particle- pore interaction. This is done by using one of the inbuilt features in Clampfit. It is found under the analysis option. This feature lets you adjust baseline shift manually by clicking on the baseline in a selected section of the trace. This feature cannot be used for abrupt shifts in baseline. These abrupt shifts are caused by falling baselines, indicating impending blockages that can usually be reversed by switching the applied voltage bias. Baseline correction can also be done using the Matlab based program Base Adjust 4.1 [82, 83] which is a part of the DNA7 software used for further analysis.

Figure 2.5 shows an example of pre-processing routines applied to the raw data. The routines applied to this raw data trace are discussed above. This is a part of the event trace that was recorded at 120 mV when positively charged 53 nm positively charged nanoparticles were translocating through a 100 nm FIB hole. The original trace obtained captured events with positive polarity and consists of a rapidly fluctuating baseline as shown in Fig 2.5(a). Both the Pre-processing routines were applied to the entire event trace. The polarity of the events were reversed as well as the baseline was corrected to +1000 pA using Clampfit.

2.6.2 Data analysis with DNA 7

DNA7 is a Matlab based program that has been routinely used by our lab to analyze various DNA translocation data [55–58, 80, 81]. It was developed by Dr. Jiali Li and John Wang. Several updates have been added to this software by Dr. Jim Uplinger [82] and by Dr. Ryan Rollings [83].

DNA7 consists of a core program with Matlab sub routines that identify and characterize
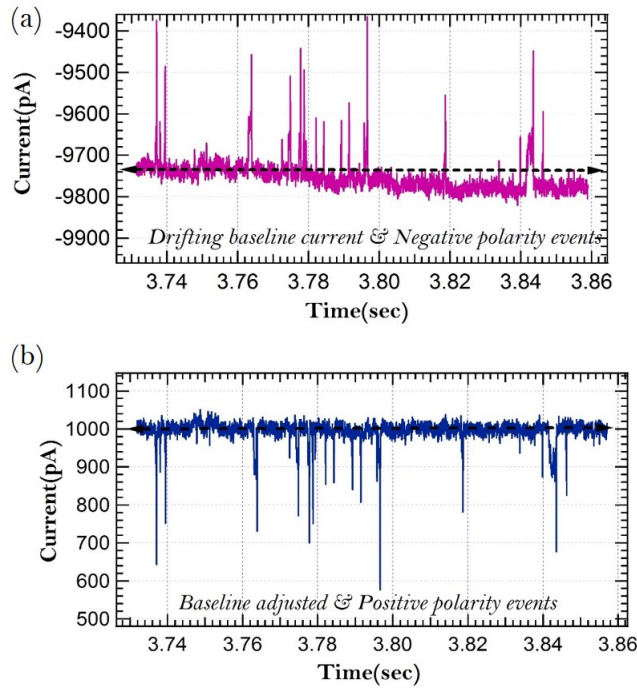
Figure 2.5: Pre-processing the raw data. (a) Current vs time trace showing an event trace with a drifting baseline at -9700 pA and negative polarity events at 120 mV. (b) Current vs Time trace showing the same event trace as in (a) but with a baseline adjustment that minimizes the baseline drift and positive polarity events.
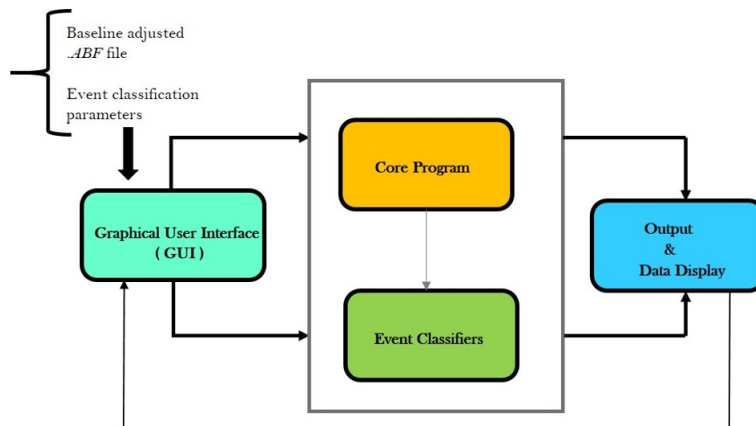
Figure 2.6: Block diagram for DNA 7 showing the four main components. Each component consists of various Matlab sub-routines that take the user input base adjusted .abf file and event classification parameters and analyse the events. This information is then directed to the output and data display component which can be accessed by the user using the main GUI to visually represent the analyzed data.
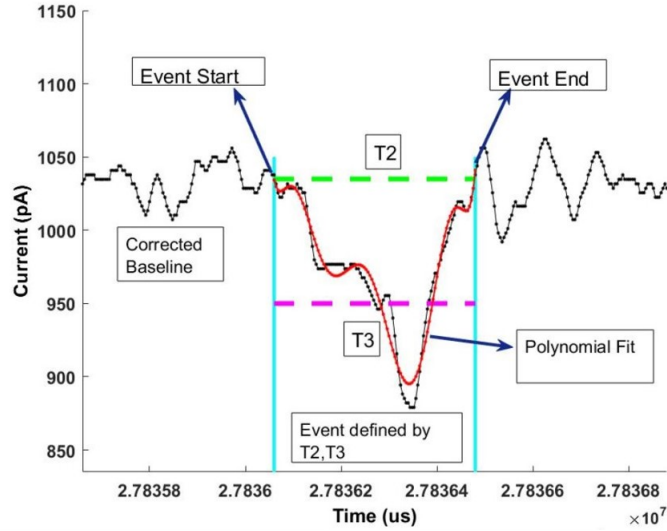
Figure 2.7: Matlab figure of DNA 7 processing an event. This event was part of the event trace obtained from 53 nm positively charged polystyrene nanoparticles in a 100 nm nanopore at 60 mV. This trace was polarity reversed and base corrected before DNA 7. In DNA 7, this current drop shown in figure is recognized as an event defined by passing through $T2$ and $T3$. $T2$ and $T3$ are threshold values set by the user, a part of event classification parameters.

events based on the given event classification parameters. A block diagram of DNA7 is shown in 2.6. Please refer to the following reference for an in-detail call diagram of the matlab routines [83]. DNA7 analysis is the next step in data analysis after the .abf file is base adjusted either using Base Adjust or Clampfit. The user has to input the base adjusted .abf file and the event classification parameters to the DNA7 graphical user interface (GUI). All the Matlab subroutines are accessed by the GUI and these event sub-routines direct Matlab based functions to define and characterize each event in a given file by looking at the user defined classification parameters. Once all the events are identified, the data display which is also a part of the GUI highlights giving users access to generate scatter plots and different types of histograms.

Fig. 2.7 presents an example of detection of events by DNA7 based on the given classification parameters. An event is defined if the baseline falls below two threshold levels $T2$ and $T3$. In the above figure, the event is both preceded and followed by baseline fluctuations that

30

fall below $T2$ but not $T3$ and DNA7 clearly does not recognize these fluctuations as events. It is clear that DNA7 follows the sub-routines, helping the user visualize to look at all the characterized events. Thresholds $T2$ and $T3$ determine the event depth and event duration of each event. The event depth is measured by the amplitude of the average current drop below the threshold $T2$ and the event duration is measured by threshold $T3$ by calculating the full width half maximum (FWHM) of an event.

The event plot feature of DNA7 allows user to look through every individual event in the given base corrected file and get an estimate of the chosen event classification parameters. All the data that has been presented in this work has been analyzed by using DNA7 and all its sub-routines. Users interested in learning more about the software can access it at *ssn.uark.edu*.

2.7   Experimental protocols

2.7.1   Pre wetting of the nanopore chip after TEM imaging

After TEM imaging, each nanopore chip is enclosed in a 1 cm $\times$ 1 cm gel box. This box is updated with information about the size of the nanopore, as well as any specific features observed on the membrane under TEM and the TEM image number. These gel boxes are placed in a dry box and information about the images is updated in the TEM notebook.

Before using the selected nanopores to do a translocation experiment,the nanopores are pre-wetted. This step marks the transition of the nanopore chip from the dry side (fabrication, characterization) to the wet-side (translocation experiment). This step is emphasized by the authors cited in reference [80] mentioned under footnote 6. This step is essential to be carried out with especially with nanopores sculpted with ion beam sculpting apparatus (IBSA) to ensure that the pore surface is appropriately wet enough. The pre wetting process facilitates the measurement of the predicted open pore current and low rms noise and making the nanopore suitable for nanoparticle translocation experiments. Nanopores that have not been pre wetted usually do not show the predicted open pore current and have high rms

noise. In such cases KOH can be used as a wetting agent but using KOH causes the pore membrane to etch open rapidly and become a 100 nm diamter FIB hole in which they are sculpted [78]. Using KOH does not guarantee a low rms noise pore.

The pre wetting protocol is listed below:

1. Choose the required pore of suitable size for the translocation experiment after TEM imaging. Note the additional notes provided about the condition of the membrane from the TEM imaging.

2. Pour 10 ml of ACS grade Acetone into a clean, unused 20ml glass vial. Place the chip carefully with flat side up using tweezers. Cap the vial and wait for 10 minutes. Acetone is a highly flammable solvent, proper protection should be used while handling it. Acetone also serves as a solvent and cleans the nanopore chip by dissolving any remnants from the fabrication or imaging process. After 10 minutes, carefully pour the acetone out of the vial into the used acetone container.

3. Next, carefully pour 5 ml of ACS grade IPA into the vial and rinse the chip. This is to ensure that all the acetone has been removed from the vial. Following the rinse, pour 10 ml of ACS grade IPA and let the chip soak in it for 10 minutes. Later,carefully pour the IPA out of the vial into the used IPA container.

4. Using 200 nm filtered 50% high purity ethanol, pour 10ml of 50% ethanol into the vial and rinse the chip. This is to ensure that all the IPA has been removed from the vial. This step is repeated for two exchanges. The pore is finally stored in 50% ethanol with the soak date included on it. This information along with the pore size and TEM image number can be written on the cap of the glass vial or by using a little sticker on the bottle.

5. The pore remains in its bottle containing 50% ethanol for several days until the day of the translocation experiment. All the 100 nm FIN holes used in this study are pre wetted using the same procedure and are stored in 50% ethanol.

2.7.2 PDMS chamber fabrication

Polydimethylsiloxane (PDMS) is a clear, chemically inert polymer used to make the microfluidic chambers that constitute the cis and trans chambers to the nanopore chip. Each chamber consists of three fabricated channels on each side using an aluminum mold serve as inlets and outlets carrying electrolyte to the nanopore chip and a channel to insert the Ag/Agcl electrodes, thereby facilitating the application of electric field across the nanopore membrane.

Apart from providing the path for the electrolyte and electric field, PDMS chambers seal the nanopore membrane with a small PDMS gasket around it such that low rms noise single molecule measurements are possible [10, 84]. Nano bubbles are the main cause for noise and pore conduction problem [85]. It is very important that the fabricated PDMS chambers do not have any air bubbles inside the channel. This is due to the fact when pressure is applied to flow the solution, bubbles in the channel can cause the channel to rupture and break the free standing membrane.

Two PDMS chambers are required for every translocation experiment. The fabrication protocol is listed below and PDMS chambers are not re-used after adding nanoparticles due to contamination. Aluminum molds designed in the machine shop with Mcmaster-carr pins of specific dimensions are used to fabricate the PDMS chambers.

1. To fabricate PDMS chambers we use the Sylgard 184 elastomer kit that consists of PDMS and a bottle of hardener. To handle PDMS, proper protective gear should be worn.

2. Mix the PDMS and the hardener in 10:1 ratio in a clean plastic disposable cup. Place the cup on a scale and add the required amount of PDMS using a clean 5 ml syringe. Then add the correct amount of hardener using a micropipetter.

3. Mix the gel thoroughly in the cup using a clean spatula.

4. Degas the gel using a degasser and bell jar for at least 30 minutes. The degassing time depends on the amount of gel being used. The air bubbles should completely disappear after degassing.

5. While the gel is degassing, clean the aluminum mold and pins using acetone and sonicate for 15 minutes followed by IPA treatment and sonication for 15 minutes. Then the molds and pins are blow dried with N2.

6. To fabricate the chambers,use a clean petri dish as the base in which the bottom mold and its two pins are placed and the de-gassed PDMS is carefully poured. Then place the top mold and its pin such that all the pins connect and the top and bottom pieces fit together. The pin arrangement can be viewed from the bottom of the petri dish.

7. This petri dish containing the mold filled with PDMS and aligned with its pins is placed on a hot plate at 70°C for 6 hrs. The PDMS chambers are formed within the mold and are now ready to be used.

2.7.3   Ag/AgCl electrode fabrication

Ag/AgCl electrodes are widely used in electrophysiological measurements based on the patch-clamp technique. They are used in single molecule measurements using an electrolyte with chloride ions. The main purpose of the Ag/AgCl electrode is to apply electric field in the bulk of the solution and produce a current through the nanopore by forming a gigaseal around the membrane. It consists of a silver wire connected to an electrical wire. The silver end of the wire is coated with chlorine by the process of bleaching. Chlorine in combination with silver gives rise to silver chloride coating on the electrode. When an electric field is applied, electrons flow through the copper wire and then into the silver wire causing a chemical reaction with silver chloride coating resulting in silver ions and chloride ions.

$$AgCl + e^- \leftrightarrow Ag^+ + Cl^- \tag{2.1}$$

For nanopore experiments, two Ag/AgCl electrodes are needed to form a complete circuit. One electrode is grounded and the other is connected to a potential V. Listed below is the protocol to fabricate these electrodes.

1. Start with 3 cm of Ag wire and clean luer valves. Both the products are purchased from Small Parts Inc.

2. Insert the Ag wire into the luer valve and seal the bottom end using gorilla glue.This makes the leur valve with silver wire suitable for PDMS filling.

3. 24 hours later, fill the bottom sealed leur valves with PDMS gel such that it makes a concave shape on the top enclosing the pin using a micro pippeter. The PDMS should be thoroughly degassed such that air bubbles are not trapped inside the leur valve around the silver wire.

4. The filled pins are baked overnight in the furnace at 75°C. Later, the sealed pins are attached to an electrical wire containing the corresponding attachments for the experimental setup.

5. The electrodes are sanded and bleached in chlorine bleach for 30 min every time they are used in experiments.

2.7.4 Solution preparation

The electrolyte solution that flows through the nanopore membrane plays the most important role in establishing various pore conduction parameters. These parameters reveal information about the pore geometry and rms noise. Hence it is required that the electrolyte should not contain any contaminants.

The electrolyte solution used for all our nanopore experiments is potassium chloride (KCl) in various molar concentrations and at different pH's adjusted using a buffer. It is purchased from Sigma Aldrich. All the solutions being introduced to the pore membrane

are dual filtered using VWR 200 nm filters and a Whatman 20 nm syringe filter. All the solutions after filtering are transferred into a 45 ml centrifuge tubes and then degassed using a rough vacuum pump while being sonicated at 40°C. The conductivity of all the solutions is measured and recorded before used in the experiments.

1 M KCl (pH 7) solutions are made from diluting the 3 M KCl stock solution with 18 MΩ DI water. The pH value of KCl is changed using buffers. These buffers are also diluted from their stock solution and the calculated amount of the buffer is added to the diluted KCl solution. For experiments using smaller concentration of KCl, the solutions are made from 1 M KCl stock solution, calculated amount of buffer solution and 18 MΩ DI water.

2.7.5   Nanoparticle sample preparation

Nanoparticle sample preparation is another key parts of the translocation experiment. Proper steps are to be taken to ensure that nanoparticle sample is stable and contaminant free.

The nanoparticles used in this study : 25 nm iron oxide with $-COOH$ group suspended in DI water with an initial concentration of 5 mg/ml. These particles were purchased from Ocean Nanotech. The 53 nm polystyrene with $-NH_2$ group suspended in DI water with an initial concentration of 1.2×10^{15} particle/ml. These particles were purchased from Bangs Laboratories.

To prepare the 10 nm iron oxide with $-COOH$ group nanoparticle sample, given protocol was followed:

1. The base electrolyte used for the suspension of iron nanoparticles samples was 1 M KCl + 10 mM TE. It was made from diluting the stock solutions of 3 M KCl , 10X TE in calculated volume. All the chemicals were purchased from Sigma-Aldrich.

2. For the nanoparticle dilution to the required concentration, a stock solution containing 10^{15} particles/ml is made using 20 nm filtered DI water. A final concentration of 10^{14} particles/ml was obtained by diluting the stock solution using the base electrolyte.

3. The nanoparticle solution is stored at 4° C. The sample was moved to room temperature 30 minutes before the translocation experiment. The solution is also sonicated for 10 min before being introduced to the nanopore membrane.

To prepare the polystrene with $-NH_2$ nanoparticle sample, given protocol was followed:

1. The base electrolyte used for the suspension of Polystyrene nanoparticles samples was 0.2 M KCl + 20 mM CHES+ 0.01 %(V/V) Triton X-100. It was made from diluting the stock solutions of 1 M KCl ,0.2 M CHES and 1 %(V/V) Triton X-100) in calculated volume. All the chemicals were purchased from Sigma-Aldrich.

2. The surfactant 0.01 %(V/V) Triton x-100 was diluted from stock solution 1 % Triton x-100. It was then added to the base electrolyte. The solution was placed on a stirring plate and a Teflon stirrer was used to stir the solution. This step was to ensure that the surfactant completely dissolved in the base electrolyte.

3. For the nanoparticle dilution to the required concentration, a stock solution containing 10^{15} particles/ml is made using 20 nm filtered DI. A final concentration of 10^{14} particles/ml was obtained by diluting the stock solution using the surfactant added base electrolyte.

4. The nanoparticle solution is refrigerated in a fridge at 4° C and it is placed at room temperature 30 minutes before the translocation experiment. The solution is also sonicated for 10min before being introduced to the nanopore membrane.

2.7.6 Pore conduction protocols

Listed below are the pore opening protocols that are carried out during a translocation experiment. These protocols involve a pre wetted nanopore sample,a clean set of PDMS chambers, bleached Ag/AgCl electrodes, 20 nm filtered solutions and the required nanoparticle solution.

2.7.7   P-cleaning of the pre wetted sample

A pre-wetted nanopore chip is P-cleaned before setup for a translocation experiment. The process of P-cleaning has shown to make the nanopore surface hydrophilic. The process of P-cleaning is listed below

1. Mix ACS grade sulphuric acid and 30% hydrogen peroxide in a 3:1 ratio in a clean 10 ml glass beaker. Mix the solution thoroughly and place the beaker on a hot plate at 90° C. All protective measures must be well ensured before carrying out this step.

2. Using a clean tweezer, carefully place the pre wetted nanopore chip such that the flat side of the chip is facing up. The nanopore chip should be P-cleaned for 15 min.

3. After 15 min, carefully move the chip to a 15 ml clean glass beaker containing degassed 20 nm filtered DI-Water. Rinse the chip with DI water a couple of times.

4. Dispose the P-cleaning solution as per the waste chemical removal guidelines.

2.7.8   Alignment of the chip and setup

The P-cleaned nanopore chip is now hydrophilic and it is placed on the clean PDMS chamber with the flat side facing up using an optical microscope and clean tweezers. This chamber is enclosed in an aluminum shell that comprises the trans chamber of the setup. The shell is milled in a way to facilitate the fluid inlets, outlets and electrodes. The experimental setup consists of two such half shells containing PDMS chambers which together make the cis and trans portions of the setup. These two halves can be tightened together using screws and hence making a tight PDMS seal across the membrane.

2.7.9   Clampfit measurements

Clampex is a data acquisition software that is a proprietary product of Axon instruments. It is the software used to record and detect various single channel measurements using the

Axopatch 200B. Clampfit is another additional program used to analyse the data using various tools.

(a) Open pore current trace

This first Clampex trace measures the open pore current through the nanopore when a voltage is applied across it. The voltage is applied using a Voltage clamp built in Axopatch 200B. This is transferred into the microfluidic chambers around the pores using the two Ag/AgCl electrodes and the Axopatch 200B electronics.

When the nanopore is completely conducting, the open pore current can be related to the geometry of the pore using the measured TEM diameter. The correct open pore current value represents a well conducting pore with low rms noise suitable to conduct nanoparticle translocation experiments.

$$I_0 = V \left(\frac{\pi \sigma_{elec} D^2}{4(L + 0.8D)} \right) \tag{2.2}$$

The open pore current is estimated using the above equation when the geometry of the nanopore is approximated to be a 1-D cylinder with diameter D and length L. While working with Ion beam sculpted nanopores, we account for the thickness of the pore (t_p) measured through EFTEM measurements and thickness of the vestibule (t_v) in which the nanopore is fabricated [78, 83].

Fig 2.8(a) shows an open pore current trace recorded in Clampex. The current measured at 0 mV, +120 mV, -120 mV using a 1 M KCl solution shows an appropriate open pore current for a 12 nm diameter nanopore. The signal also shows low rms noise values. Low open pore current value usually suggests several pore conduction problems. These include incomplete wetting of the pore surface, micro or nano bubbles in the fluid or near the membrane and (or) electrode conduction problems. These conduction problems make the pore very noisy rendering it unsuitable for nanoparticle translocation experiments.

(b) Noise trace

This trace is measured at three different voltages to get an estimate of the rms value of the open pore current. These voltages are 0 mV and the applied voltages . The high rms value indicates conduction problems such as incomplete wetting and presence of nano or micro bubbles around the pore surface. Sometimes, conduction problems can be resolved by applying pressure using the fluid inlet and outlet syringes.

$$I_{rms} < 10 \ pA \tag{2.3}$$

This value of rms value indicates that the nanopore is low in noise and suitable for conducting translocation experiments as event drops can be clearly detected from the baseline current.

(c) I-V trace

This trace records the value of open pore current as a function of applied voltage. This is carried out in incremental increase in voltage values resulting and I-V measurement over 200 points. The I-V curve of a well conducting pore is a straight line passing through the origin. A straight line fit will result in the conductance of the pore. This can be related to the open pore current (I_0), Area of the pore $(A = \pi D^2)$ and conductivity of the solution (σ_{elec}). This expression results in calculating the effective length of the nanopore during the experiment. The expression to calculate the effective length of the nanopore is given by

$$L_{eff} = \frac{\pi \sigma_{elec} D^2}{4G_0} - 3.2D \tag{2.4}$$

Where G_0 : The initial conductance of the pore calculated from the I-V curve before adding any nanoparticles. An example of an I-V curve is shown in Fig 2.6(b), the conductance calculated from the slope is used to calculate the effective length of the nanopore(L_{eff}).
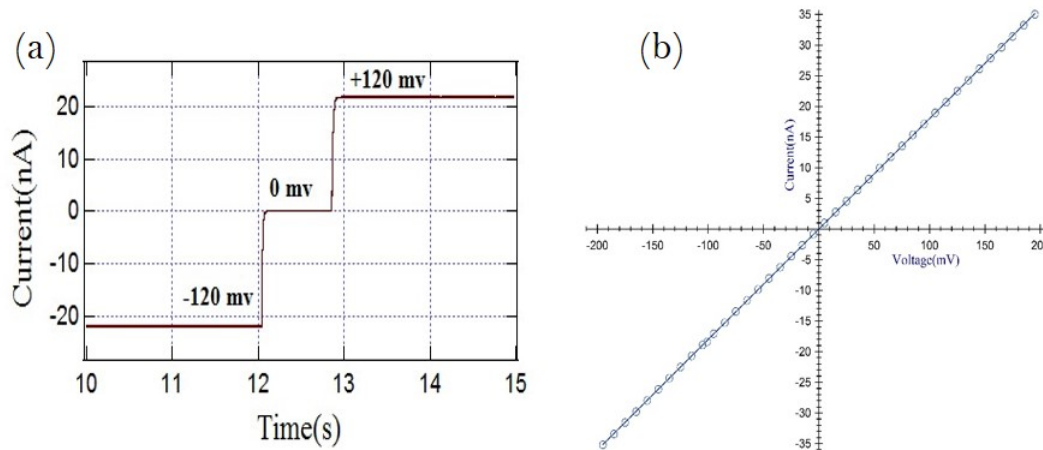
Figure 2.8: (a) Open pore traces showing the Current vs Time of a conducting nanopore at 0 mV, +120 mV , -120 mV. (b) I-V trace of the same nanopore showing a linear relationship between Current and Voltage.

(d) Adding nanoparticles and recording current blockage events

After establishing conduction through the pore, verifying that it shows the correct open pore current, low rms noise and calculating the effective length of the pore, we are now ready to introduce the nanoparticles suspended in the same electrolyte. The nanoparticles are introduced on the cis-side using a micropipetter. 40 μl of electrolyte is replaced by the same amount of nanoparticle solution in the cis-side of the microfluidic PDMS chamber. The set-up is left undisturbed at $V = 0 \ mV$ for 10 minutes for the nanoparticles to attain equilibrium and any drifts in the open pore current caused by the electro-chemical potential could be adjusted using pipette offset on Axopatch 200B [86]. When a voltage is applied across the membrane, the nanoparticles are electrophoretically driven through the membrane resulting in various types of blockage events. These events can be distinguished based on their current blockage and event duration.

(e) Event trace

Event trace or Variable length event trace is a trigger based Axopatch protocol that uses single or dual channel measurements to record current blockage events. The adjustable
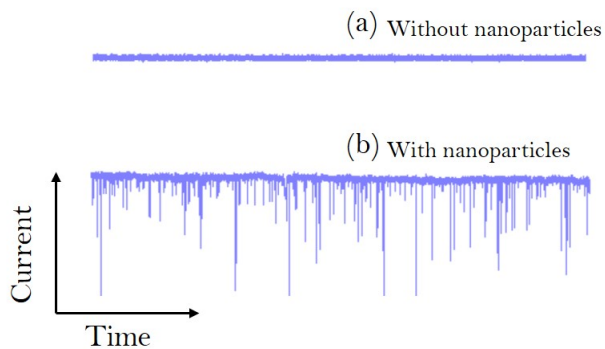
Figure 2.9: Illustration of an event trace recreated from real data. (a) Current vs Time trace without nanoparticles. (b) Current vs time trace with nanoparticles added. Both the traces are at 120 mV for a duration of one second.

trigger can be moved near the open pore current and captures the current drops/ current raises caused by the translocating particle. Fig 2.9 shows an example of the Current vs Time trace before and after adding nanoparticles. In 2.9(a), a stable baseline current is recorded for a duration of one second and in 2.9(b), the baseline current with drops caused by translocating nanoparticles is captured using an adjustable trigger for one second. Event trace is recorded as a function of voltage and lasts about 2-3 minutes until the baseline drops and sticky events are observed.

Chapter 3

Theory of nanopore physics

3.1 Introduction

Spherical nanoparticle translocations through micropores and nanopores is a well established field [10, 11, 14, 22, 25, 36–38, 40, 41]. The important parameters to gain an insight into this complicated translocation process include the pore surface chemistry, particle surface chemistry and their behavior in the enclosed system with an electrolyte consisting of million's of ionic charges. This insight is composed of various smaller parts and for a better understanding of the nanopore system is approached terms of these ionic charges.

For this study, approximately 10^{14} particles/ml, all with similar charge, were suspended in an electrolyte and introduced into a very small volume near the silicon nitride nanopore. When an electric field was applied, these nanoparticles were driven to the positive electrode, giving rise to a change in a current drop by recording a translocation event. From this current drop generated by the nanoparticles, the size of the nanoparticle could be estimated. Apart from the estimation of size, the translocation dynamics such as the interaction of the nanopore with one single nanoparticle, the blockages caused by several nanoparticles could all be understood in terms of the surface charge properties of pore and particles.

This chapter tries to bring these well-known concepts about nanopore-nanoparticles and their interaction with an aim to provide a background to the theoretical concepts that cannot be ignored while studying this sub-field. All these derivations are borrowed from literature gathered here to deepen the understanding of this small world of nanopores and nanoparticles governed by the laws and concepts of physics and chemistry.

3.2 Resistance of a nanopore

A nanopore of length L and diameter D can be considered geometrically as a cylinder connecting two microliter volume reservoirs. The nanopore serves as the only connection

between them. These reservoirs and the nanopore are filled with a uniform electrolyte solution of conductivity (σ_s). When an electric field is applied across the nanopore, all the anions in the electrolyte are driven to the anode and all the cations are driven to the cathode. The total current density through the nanopore is due to the ion fluxes contributed by the anions and cations calculated using the Nernst-Planck equation for an ion transport process. More details about the derivation described here [43].

The ion flux due to each type of ion is given by the equation

$$j_i = D_i c_i \frac{z_i F}{RT} E \tag{3.1}$$

Where j_i : Ion flux of the ith ion species; D_i : Diffusion coefficient of the ith ion species; c_i: concentration of the ith ion species; z_i: charge of the ith ion species; R : Faraday constant; T : Temperature and E : Applied electric field.

The total current density is given by

$$J = F \sum_i z_i j_i \tag{3.2}$$

The electrolyte used is monovalent$(1:1)$ KCl.

Considering $c_+ = c_- = c$ and $z_+ = z_- = z$

Where $c_+ = c(K^+)$ and $c_- = c(Cl^-)$; $z_+ = z(K^+)$ and $z_- = z(Cl^-)$

Expanding equation (3.2) to include both type of ion species and using (3.1)

$$J = F(z D_+ c \frac{zF}{RT} E + z D_- c \frac{zF}{RT} E) \tag{3.3}$$

Where D_+ and D_- are diffusion coefficients for the K^+ and Cl^- ions

$$J = \frac{z^2 F^2}{RT}(D_+ + D_-)cE \tag{3.4}$$

The above equation can be re-written using $\sigma_s = \frac{z^2 F^2}{RT}(D_+ + D_-)c$

Where σ_s: Conductivity of the solution

$$J = \sigma_s E \qquad (3.5)$$

Equation (3.5) represents the total current density through a cylindrical nanopore with a monovalent electrolyte of conductivity σ_s under the influence of an electric field E. This equation is an alternate form of Ohm's law.

Current density $J = \frac{Current}{Area} = \frac{I}{A}$

For a cylindrical nanopore of diameter D, Area $A = \frac{\pi D^2}{4}$

Rewriting the equation for Current density

$$J = \frac{4I}{\pi D^2} \qquad (3.6)$$

Equating (3.5) and (3.6) , we get

$$\sigma_s E = \frac{4I}{\pi D^2} \qquad (3.7)$$

We can also rewrite $E = \frac{V_{applied}}{L}$; Where L: Length of the nanopore membrane

Rewriting (3.7) using the expression for E, we obtain the Current (I) through the cylindrical nanopore

$$I = \sigma_s \frac{\pi D^2}{4L} V_{applied} \qquad (3.8)$$

Using Ohm's law $V = IR$, we obtain the equation for the resistance of the cylindrical nanopore

$$R_{pore} = \frac{4L}{\sigma_s \pi D^2} \qquad (3.9)$$

Conductance of the nanopore is the inverse of its resistance

$$G_{pore} = \frac{1}{R_{pore}} = \frac{\sigma_s \pi D^2}{4L} \qquad (3.10)$$

In conclusion, we derive the pore conductance (resistance) as a function of pore geometry

and electrolyte conductivity using electrostatics and the Nernst-Planck equation for ion flow. This parameter plays an important role in determination of nanoparticle diameter.

3.2.1   Access resistance contribution

In the previous section we arrived at an equation for the pore resistance R_{pore} using electrostatics and the Nernst-Planck equation for ion flow. The geometry of the nanopore was simplified to be a 1-D cylinder for all approximations which was characterized by its Diameter (D nm) and Length (L nm). When a voltage bias (V) is applied across the entire setup consisting of the reservoirs surrounding the nanopore and the pore itself, an electric field (E) is acting through the pore and it's surroundings. This electric field can be visualzed as electric field lines passing through the cylinder. Since, we already know the pore resistance R_{pore}, the convergence of these electric field lines around the ends of the nanopore adds additional contribution to the total pore resistance. This additional resistance contributed by the ends of the pore is called access resistance R_{access}. More details on access resistance contribution in nanopores can be found here [11, 43, 87–89].

The equation for access resistance was derived by Hall [44], where the hemisphere surrounding the ends of the pore is considered to have the same diameter as the pore. The resistance is calculated using the concept of equipotential lines and Ohm's law on this hemisphere. The total access resistance R_{access} is twice the resistance on one hemisphere.

$$R_{access} = \frac{1}{\sigma_s.D} \tag{3.11}$$

Where σ_s: conductivity of the electrolyte and D: nanopore diameter. Adding the contribution of access resistance (3.11) to pore resistance (3.9), we now arrive at the expression for the total resistance of the nanopore.

$$R_{Total} = R_{pore} + R_{access} \tag{3.12}$$

46

$$R_{Total} = \frac{4L}{\sigma_s \pi D^2} + \frac{1}{\sigma_s . D} \tag{3.13}$$

$$G_{Total} = \frac{\sigma_s \pi D^2}{4L + \pi D} \tag{3.14}$$

From equation (3.13), we can deduct the direct dependence of the total pore resistance to the aspect ratio ($\frac{L}{D}$). For really long pores, ($\frac{L}{D} >> 1$), the access resistance contribution can be neglected. However for solid state nanopores $L \sim D$ this is not the case. It has been shown by Hyun et. al [87] that for smaller pores the contribution of R_{access} plays a significant role in determining the total resistance of the pore.

3.3 Conductance approximation for different electrolyte concentration

In Sec 3.2, we derived the resistance of the nanopore using a simple Ohmic conduction model. From equation (3.14), we see that the total pore conductance has direct dependence on the conductivity of the electrolyte(σ_s). Since $\sigma_s \propto M$ where M is the molar concentration, we can deduce that the conductance of the pore and open pore current have a direct dependence on electrolyte concentration. M is dominated by the bulk ion concentration. This simple model also assumes the surface and the walls of the nanopore to be uncharged under the condition that the length of the Debye layer (λ_D) is much smaller than the radius of the pore ($\lambda_D << r_{pore}(nm)$).

3.3.1 Concept of electric double layer and Debye length

Let us look at the electrolyte in more detail. The electrolyte used in all experiments described in this thesis is a monovalent electrolyte (KCl). The main components of this electrolyte are water molecules, potassium (K^+) and chloride (Cl^-) free ions. On the other hand, the nanopore membrane made of silicon nitride has silanol groups on the surface and acquires a negative charge by ionization.

$$SiOH \rightarrow SiO^- + H^+ \tag{3.15}$$

The presence of a negatively charged surface in the solution causes an interaction that results in re-arrangement of free ions in the solution and in the formation of an electric double layer around the charged surface. The thickness of the electric double layer surrounding the charged surface is called the Debye length (λ_D).

The double layer, as the name suggests, is an ensemble of layers formed by the redistribution of free ions due to the presence of a charged surface. These layers can be further classified to examine the free ion distribution in detail. The presence of the negatively charged surface in the electrolyte causes the K^+ ions to move close to the surface and Cl^- ions to move away. By electrostatic attraction, the positive ions are attracted and by electrostatic repulsion, the negative ions are repelled from the charged surface. The first layer consists of positive ions that are attracted to the negatively charged surface, these ions experience very strong attraction and they constitute an immobile layer, known as the Stern layer. Adjoining this first layer is another layer of positive charges and a few negative charges that are mobile and constitute the shear plane. No slip boundary condition can be applied and the shear plane marks the boundary of the diffuse layer. After the shear plane, the ions are more free to move in the diffuse layer. The concentration of ions varies in such a way that the charge neutrality is achieved.

The surface potential of the charged surface varies exponentially as a function of distance from the charged surface. The potential at the shear plane is known as the Zeta potential (ζ) or electrokinetic potential.

Let us re-derive a well known derivation for the potential for an electric double layer and understand the concept of the Debye length numerically [46].

Consider a 1-D charged surface in the presence of an electrolyte containing free ions. The potential (ψ) on the charged surface can be related to the density of free ions (ρ_f) using the Poisson equation.

$$\epsilon \nabla^2 \psi = -\rho_f \tag{3.16}$$

$$\epsilon \frac{\partial^2 \psi}{\partial x^2} = -\rho_f \tag{3.17}$$

The re-distribution of ions causes the concentration of both the species of ions to reach an equilibrium as they are moving away from the charged surface but within the electric double layer. The Boltzmann distribution is used to describe this concentration equilibrium by relating the ionic number concentration (n_i) to the electric potential (ψ).

$$n_i = n_{i\infty} \exp\left(-\frac{z_i e \psi}{K_B T}\right) \tag{3.18}$$

Re-writing ρ_f in terms of ionic number concentrations and their corresponding valencies, we can relate the density of free ions (ρ_f) in terms of electric potential (ψ) using the Boltzmann distribution.

$$\rho_f = \sum_{i=1}^{N} z_i e n_i \tag{3.19}$$

Using equations (3.18) and (3.19), we rewrite equation (3.17)

$$\epsilon \frac{\partial^2 \psi}{\partial x^2} = -\sum_{i=1}^{N} z_i e n_{i\infty} \exp\left(\frac{-z_i e \psi}{K_B T}\right) \tag{3.20}$$

Where ϵ: dielectric permittivity of the solvent, ψ: electric potential, N: total number of ions, z_i: valence of the ith ionic species, e: electron charge; $n_{i\infty}$: ionic concentration at the neutral state with no potential; T: absolute temperature in Kelvin and K_B: Boltzmann constant. Equation (3.20) is also known as the Poisson-Boltzmann equation. This equation describes the behavior of electric potential (ψ) in the double layer surrounding the charged surface in terms of ionic concentration (n_i) and their valencies (z_i).

3.3.2 The Gouy-Chapman Theory

The Gouy-Chapman theory presents the solution for equation (3.20) for the case of a monovalent electrolyte where the valencies of anion and cation are equal.

Where $z_+ = z_- = z$. Expanding equation (3.20) for both anionic and cationic concentration for a monovalent electrolyte, we get

$$\epsilon \frac{\partial^2 \psi}{\partial x^2} = -zen_\infty \left[\exp(\frac{-ze\psi}{K_B T}) - \exp(\frac{ze\psi}{K_B T}) \right] \tag{3.21}$$

Which can be further simplified into

$$\epsilon \frac{\partial^2 \psi}{\partial x^2} = 2zen_\infty \sinh\left(\frac{ze\psi}{K_B T} \right) \tag{3.22}$$

This is a second order differential equation that is solved for electric potential of the Debye layer (ψ) using the following boundary conditions

$$At \quad x = 0 \quad \psi = \psi_s \quad ; \tag{3.23}$$

$$As \quad x \to \infty \quad \psi = 0 \tag{3.24}$$

Where ψ_s: surface potential at $x = 0$

Which yields the following solution for (3.22)

$$\Psi = 2\ln \left[\frac{1 + \exp(-\kappa x) \tanh(\frac{\Psi_s}{4})}{1 - \exp(-\kappa x) \tanh(\frac{\Psi_s}{4})} \right] \tag{3.25}$$

50

Where the dimensionless potentials Ψ and Ψ_s and κ^{-1} are defined as follows

$$\Psi = \frac{ze\psi}{K_B T} \tag{3.26}$$

$$\Psi_s = \frac{ze\psi_s}{K_B T} \tag{3.27}$$

$$\kappa^{-1} = \left(\frac{\epsilon K_B T}{2e^2 z^2 n_\infty} \right)^{\frac{1}{2}} \tag{3.28}$$

Where κ^{-1} is the Debye length. The Debye length as seen from equation (3.28) is dependent on the electrolyte properties rather than the charged surface properties. It is defined as the characteristic length from the charged surface where the surface potential drops to 0.33 of its original value. It is also inversely proportional to the ionic number concentration (n_∞) and the valence of the electrolyte (z). This suggests an inverse relationship with the molar concentration (M) of the electrolyte. The higher the electrolyte concentration, the smaller the thickness of the Debye length around a charged surface. A simplified expression for the Debye length (κ^{-1}) can be calculated by substituting all the physical constants in equation (3.28), which results in

$$\kappa^{-1} = \frac{3.04}{z\sqrt{M}} \times 10^{-10} m \tag{3.29}$$

Where M: molar concentration and z: valence of the electrolyte. For the case of a monovalent electrolyte $z = 1$ [46].

3.3.3 The Debye-Huckel approximation

The Debye-Huckel approximation is also known as the linearised version of the Poisson-Botlzmann equation (3.18). This approximation is mostly followed when the surface potential is very small. When $\psi_s \ll 0.025V$, we can approximate $\frac{ze\psi}{K_B T} \ll 1$. This simplifies equation (3.23) where $\sinh\left(\frac{ze\psi}{K_B T} \right) \approx \frac{ze\psi}{K_B T}$.

Equation (3.23) can be re-written in its simplified version

$$\epsilon \frac{\partial^2 \psi}{\partial x^2} = \frac{2e^2 z^2 n_\infty}{\epsilon K_B T} = \kappa^2 \psi \qquad (3.30)$$

Solving this differential equation at the following boundary conditions

$$At \quad x = 0 \quad \psi = \psi_s \quad ; \qquad (3.31)$$

$$As \quad x \to \infty \quad \psi = 0 \qquad (3.32)$$

yields the following solution for ψ

$$\psi = \psi_s \exp(-\kappa x) \qquad (3.33)$$

From equation (3.3), we can see that the surface potential decreases exponentially as a function of x, which is defined as the distance from the charged surface. The Debye-Huckel approximation is not only valid for small surface potential but is also a better approximation for high surface potential when compared to the exact solution presented by the Gouy-Chapman analysis in equation (3.23) [46].

3.3.4 Debye screening length as a function of electrolyte concentration for a flat charged surface

From the theoretical derivations presented above, we see that in case a flat charged surface immersed in a monovalent electrolyte such as a nanopore the electric potential in the double layer surrounding the charged surface decreases exponentially as a function of distance from the charged surface. This characteristic distance is defined as the Debye screening length. From equation (3.29), we see that Debye screening length has an inverse relation with the electrolyte concentration.

Shown below in the Figure 3.1 is a plot between Ionic concentration of an electrolyte (M) and the Debye screening length (κ^{-1}) around the planar charged surface surrounded by the electrolyte using equation (3.29). The concentration varies from 10^{-6} M to 1 M for a monovalent KCl as the electrolyte and the thickness of the double layer is calculated using equation (3.29). From the plot it is clearly visible that the higher electrolyte concentration is, the smaller is the thickness of the double layer. The thin double layer approximation is mostly considered in nanopore experiments studying highly charged and long molecules like dna and protein [54, 87]. These long molecule experiments are mostly conducted in high electrolyte concentrations so that the surface charge effects due to the nanopore surface can be neglected. The thickness of double layer at 1 M KCl is, $\kappa^{-1} = 0.3nm$. The total pore conductance in this case arises from the contribution of access resistance of the nanopore. As the molar concentration decreases, the thickness of the double layer increases and so does the effect of ion redistribution inside a nanopore. The contribution of surface charge effects is clearly dominant at or below 0.1 M KCl electrolyte concentration in nanopore experiments [90–92]. At or below this concentration, the conductance of the nanopore deviates from the behavior suggested by the simple Ohmic conduction model and has a contribution from the surface charge of the nanopore.

3.3.5 Effect of zeta potential and surface charge on pore conductance

The zeta potential (ζ) and surface charge (σ) of the charged surface inserted in an electrolyte are two important parameters that determine the electrokinetic behavior of the charged surface. Surface charge is dependent on the pH of the electrolyte and zeta potential is dependent on the electrolyte concentration. These two parameters along with the Debye length (κ^{-1}) play an important role in facilitating the translocation of nanoparticle through the nanopore.

The zeta potential as defined earlier in section 3.3.1 is the potential of the charged surface at the shear plane. The charge on the surface of the nanopore and its zeta potential can be
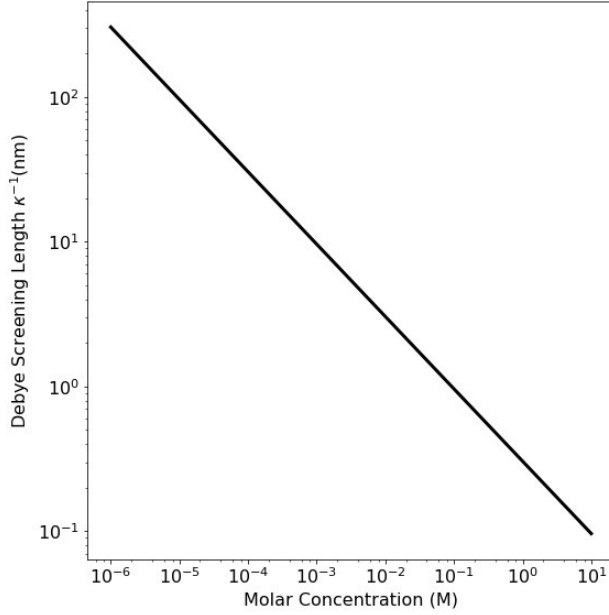
Figure 3.1: Debye screening length plotted as a function of molar concentration for KCl using equation (3.29).

related using Grahame's equation [45]. This equation is calculated from the Gouy-Chapman theory and Poisson's equation by assuming the condition of electroneutrality across the double layer.

$$\sigma = -\int_0^\infty \rho_e dx \tag{3.34}$$

Where $\int_0^\infty \rho_e dx$ is the total charge present in the double layer and ψ is the surface potential. Surface charge is related to the zeta potential by solving (3.34) resulting in the Graham's equation [45, 90, 92, 93].

$$\sigma(\zeta) = \frac{2\epsilon\epsilon_0 K_B T \kappa}{e} \sinh\left(\frac{e\zeta}{2K_B T}\right) \tag{3.35}$$

where $\epsilon\epsilon_0$ is the permittivity and κ is the Debye-Huckel parameter which is the inverse of debye length.

The above equation can be further simplified by assuming the condition for small values of

ζ, $\sinh\left(\frac{ze\zeta}{K_BT}\right) \approx \frac{ze\zeta}{K_BT}$.

$$\sigma(\zeta) = \frac{\epsilon\epsilon_0\zeta}{\kappa} \tag{3.36}$$

Re-writing the above equation for the zeta potential of the charged surface, we arrive at an equation in terms of surface charge of the pore (σ_{pore}) and the Debye length (κ^{-1}).

$$\zeta_{pore} = \frac{\kappa^{-1}\sigma_{pore}}{\epsilon\epsilon_0} \tag{3.37}$$

Where κ^{-1} : Debye length and σ_{pore}: surface charge of the nanopore. Measuring ζ_{pore} requires streaming potential measurements using a very specific setup that includes the potential to be measured as a function of applied pressure. However qualitative measurements of zeta potential are presented by these authors [92–94] and they include relating the surface charge of the nanopore to either salt concentration or the Debye length of the electrolyte. Readers interested in learning about the full derivation to the expressions shown below are requested to look here [92, 93]. From references [93] and [92]

$$\sigma_{pore} = -\frac{\epsilon\epsilon_0\zeta_F}{\kappa_F^{-1}} \tag{3.38}$$

Where ζ_F and κ_F are the zeta potential and Debye length from the following reference [94]. Substituting equation (3.38) in (3.37), we get

$$\zeta_{pore} = -\frac{\kappa^{-1}\zeta_F}{\kappa_F^{-1}} \tag{3.39}$$

Equation (3.39), can be used to estimate the zeta potential of the pore assuming that the nanopore experiments are conducted using the same electrolyte conditions as Firnkes et.al [94]. Another suggested approach is given by [90, 92] using the Graham equation and Behren's and Grier relationship to express zeta potential as a function of electrolyte concentration.

55

$$\zeta(M) = 30 \log(M) \tag{3.40}$$

The zeta potential and surface charge play an important role in determining the electrokinetics of the translocation process. Their values contribute to electroosmosis inside the nanopore walls and this process influences the translocation rate. These parameters are especially important when studying proteins and nanoparticles and their translocations when dominated by electroosmosis instead of electrophoresis [92, 94]. The modified expression for conductance now includes contributions from both the nanopore geometry and nanopore surface charge. It is given by the equation (3.44). Further details on derivation can be found here [90, 92].

$$G_{Total} = G_{pore} + G_{poresurface} \tag{3.41}$$

$$G_{pore} = \frac{\sigma_s \pi D^2}{4L} = \frac{\pi D^2}{4L}(\mu_k + \mu_{cl})n_{Kcl}e \tag{3.42}$$

Where,

$$G_{poresurface} = \frac{\mu_k \pi D}{L}\sigma_{pore} \tag{3.43}$$

$$G_{Total} = \frac{\pi D^2}{4L}(\mu_k + \mu_{cl})n_{KCL}e + \frac{\mu_k \pi D}{L}\sigma_{pore} \tag{3.44}$$

From the above equation, we observe that the total conductance of the pore depends both on geometry and surface charge of the pore. The contributions from surface charge play a dominant role when studying low charge to mass ratio particles like spherical nanoparticles.

3.4 Theoretical considerations for determination of particle diameter

Over the years, many theoretical models have been developed to understand the concept of resistive pulse technique. These theoretical models have been refined, as there has been more in depth studies on the pore-particle interaction. The fundamental concept in all these models resonates with the concept of the Coulter counter. The change in resistance caused by the translocating particle can be related to the size of the particle. The geometry and

charge of the nanopore used in the nanoscale Coulter counter plays an important role in precisely determining the size of the nanoparticle passing through it. These models also highlight the theoretical considerations to be included when studying nanoparticles using nanopores, supported by experimental evidence. The two most important parameters to consider are

1. Choosing the appropriate molar concentration of the electrolyte so that the nanoparticles do not aggregate and the surface charge effects of the nanopore membrane are not dominant. This is discussed in 3.2 of this chapter.

2. Choosing an optimum ratio of $\frac{D_{pore}}{D_{particle}}$ to conduct experiments.

3.4.1 Optimum ratio of $\frac{D_{pore}}{D_{particle}}$

The 3D nanopore geometry is determined by measuring the effective diameter of the nanopore and the effective length of the nanopore under experimental conditions. Most nanopores are elliptical and hence the effective diameter is the geometric mean of the measured diameters. This is possible by imaging nanopores after fabrication using transmission electron microscopy(TEM). This is particularly significant when using smaller nanopores $10-100\,nm$ [18, 38]. Nanopores larger than $100\,nm$ can be easily imaged using a scanning electron microscope [41].

The length or thickness of the nanopore immediately after fabrication can be approximated to the thickness of the membrane in which the nanopore has been fabricated. This is also very dependent on the fabrication procedure used. Some nanopores are fabricated within a cavity. This cavity is present in the membrane and the nanopore is fabricated using high energy ion or electron beams [4]. Energy filtered TEM is used to characterize the thickness of these nanopores [61, 78]. Since resistive pulse experiments are done when a nanopore is tightly sealed in between two microfluidic chambers with a monovalent electrolyte flowing through the nanopore. The effective length of the nanopore is determined by taking several

I-V measurements across the nanopore [10, 14] and it is calculated from the slope of the I-V curve.

The thickness to diameter ratio for a nanopore defines another parameter called the aspect ratio. Nanopores are sometimes distinguished for selective single molecule detection based on this parameter. Nanopores with an aspect ratio of $\frac{L}{D} < 1$ are known as low aspect ratio nanopores and with $\frac{L}{D} \geq 1$ are called high aspect ratio nanopores.

When we consider the total resistance of a nanopore based on the aspect ratio, we see that in the case of high aspect ratio pores, the access resistance and the pore resistance have the same magnitude with pore resistance dominating the total resistance. For low aspect ratio nanopores, the access resistance contribution dominates the total resistance. The open pore current is directly dependent on the electrolyte conductivity and diameter of the pore and inversely proportional to the length of the pore. This puts emphasis on choosing an optimum pore with appropriate diameter and suitable length so that the single molecule can be studied using the resistive pulse technique. The geometrical shape of the nanopore plays an important role in the behavior of the nanopore when used as a single molecule sensor. Most nanopores are either cylindrical or conical in shape [10, 11, 41, 95].

A quick geometrical comparison shows that the cylindrical nanopores offer longer sensing zones which increases the translocation time for a particle passing through it. This gives a better time resolution when it comes to sensing nanoparticles. The drawbacks include, the slow capture and slower translocation rate which is attributed to the electric field distribution being weak at the entrance of the pore [11]. On the other hand, conical nanopores show an improvement in capture of the nanoparticle and increased translocation rate [41]. This is due to the presence of a strong electric field near the entrance of the pore, but fabricating smaller conical pores is difficult and minimizing noise effects under experimental conditions is hard. The smaller conical nanopores are suitable to study long highly charged molecules like DNA but not to study spherical nanoparticles considering the optimum ratio and electrolyte selection.

DNA molecule experiments are conducted in nanopores with a high aspect ratio. The diameter of the pore is very close to the diameter of the DNA molecule. The experiment is conducted at high salt concentration to see a higher open pore current through the pore that is easily distinguishable from noise and the pores with small thickness are chosen to yield maximum current drop to distinguish the signature of base pairs as the DNA molecule passes through them [13, 62].

Nanoparticles of various sizes can be studied using both high aspect ratio and low aspect ratio nanopores [11, 40]. The important geometrical parameter to consider is the ratio of pore diameter to particle diameter $\frac{D_{pore}}{d_{particle}}$ as the current drop produced by the translocating particle is proportional to $\frac{d^3}{D^3}$ and is not particularly length dependent [25]. If the pore diameter is very close to the particle diameter ($D_{pore} \sim d_{particle}$), due to low charge to mass ratio of nanoparticles, and due to experiemnts being conducted at low salt concentrations results in the Debye layer of the nanopore to occupy a significant part of the pore diameter. This would overlap with the Debye layer of the nanoparticle and give rise to conductive spikes instead of resistive pulses [86].

3.4.2 Negatively charged 30 nm polystyrene nanoparticle with -COOH surface group data

Presented below are some interesting results observed when 30 nm negatively charged polystyrene nanoparticle with $-COOH$ was translocated through a 42 nm IBS nanopore. This experiment was conducted at a salt concentration of 0.1 M KCl + 20 mM CHES at pH 9. The nanopores were fabricated using the IBS system and fabrication procedure discussed in Chapter 2. All the conduction protocols discussed in Chapter 2 were followed to establish conduction through the nanopore. All the nanoparticle samples were prepared and stored according to the protocols discussed in Chapter 2.

In Fig 3.2, event traces captured at different voltages are shown. From these traces we can see that resistive pulses were observed at 120mv and then conductive spikes were
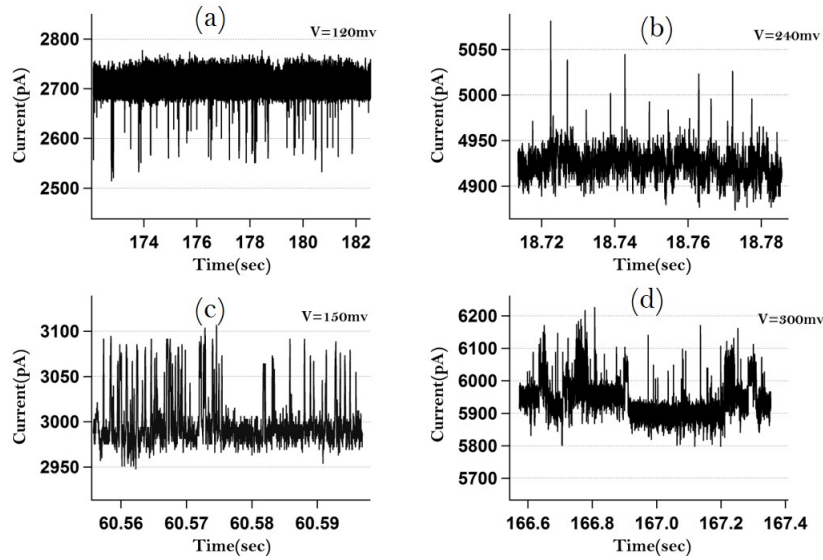
Figure 3.2: Event traces recorded using 30 nm negatively charged polystyrene nanoparticles in a 42 nm nanopore at four different voltages. (a) Resistive pulses recorded at 120 mV. (b) Conductive spikes recorded at 240 mV. (c) Conductive spikes recorded at 150 mV. (d) Conductive spikes recorded at 300 mV.
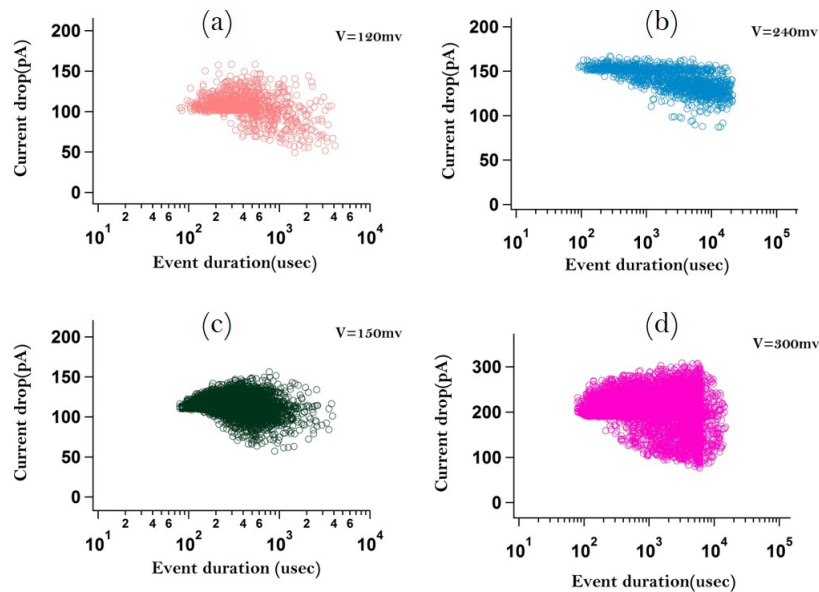
Figure 3.3: Scatter plots showing Current drop(pA) vs Event duration(us) for events produced by 30 nm negatively charged polystyrene nanoparticles in a 42 nm nanopore at four different voltages. (a) 120 mV. (b) 240 mV. (c) 150 mV. (d) 300 mV.
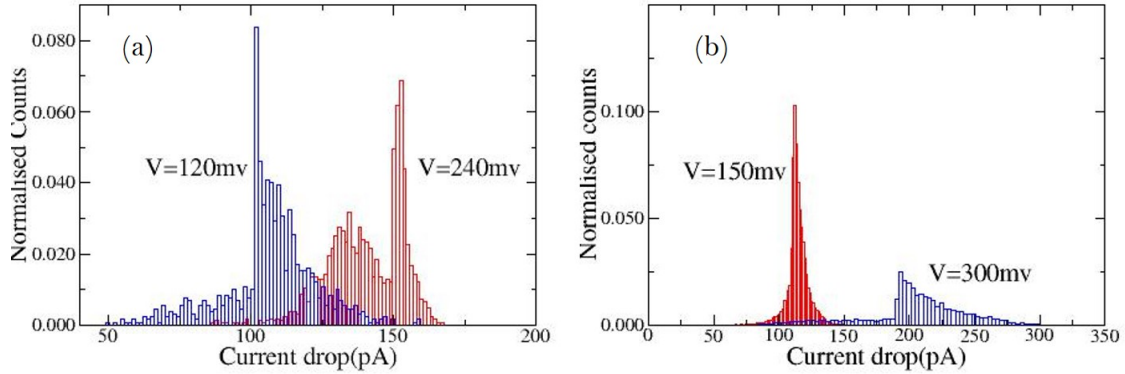
Figure 3.4: Current drop distributions of events recorded using 30 nm polytsrene nanoparticles in a 42 nm nanopore at four different voltages. (a) Normalised currrent distribution for 120 mV and 240 mV. (b) Normalised currrent distribution for 150 mV and 300 mV.

observed from 150 mV onwards. The pore still had conduction and at higher voltages it showed the appropriate open pore current. If the particles would have clogged the surface of the pore, it would not have any conduction. Voltage dependence translocation were recorded and further analysed by using DNA7. We assume the conductive spikes to be an effect of choosing $\frac{D_{pore}}{D_{particle}} < 1.5$ and conducting this experiment at 0.1 M KCl where the conductance of the nanopore starts deviating from its predicted behavior due to dominant surface charge effects [92]. This is supported by similar observations in the following references [18, 86, 96].

In Fig 3.3, scatter plots of analyzed translocation events at different voltages are plotted followed by current drop distributions for each voltage in Fig 3.4. From the scatter plots we can see that the number of events are increasing as the voltage is increasing, indicating that more number of particles are driven through the pore. Another important observation is the average event duration increases with voltage, this is atypical behavior of nanoparticle translocations. From the histograms representing the current drop distributions, we see that the average current drop increases as the voltage increases which is in agreement with the expected behavior. As the focus of this dissertation was to estimate the size of the nanoparticle from the translocation experiments, we use this experimental evidence to support the

optimum ratio for $1.5 < \frac{D_{pore}}{D_{particle}} < 2$ and move onto studying a bigger nanoparticle with the 100 nm FIB nanopore with a salt concentration higher than 0.1 M.

Chapter 4

Characterization of nanoparticles using solid state nanopores

4.1   Introduction

Solid state nanopores have been widely used for detection of biomolecules such as DNA and protein [9, 54] since 2000. Fabrication and integration at nanoscale have facilitated researchers to fine tune the features of the soild state nanopores to make them a more efficient detector of biomolecules. The hybrid nanopores promise the sequencing goals that the nanopore community has been pursuing since 2000. On the other hand, nanopores are gaining popularity in studying nanoparticles. Nanoparticles of different shape, size and charge are a widespread aspect of all scientific fields from engineering to medicine. Nanopores based on the concept of resistive pulse technique serve as a versatile sensor to study these molecules. With the advancement in fabrication techniques, researchers can now customize the size of the nanopore to study a particular nanoparticle. The interaction of the nanoparticle with the nanopore is enhanced by the surface charge effect contributions arising from the pore surface. This interaction contributes to different types of translocation events and translocation dynamics while studying nanoparticles.

The interest in studying nanoparticles using a pore sensor originates from the concept of the Coulter counter. With tremendous progress in the field of nanotechnology, pore sensors can now be fabricated at a nano scale and particles of the size of virions can be studied. Most of the recent studies in this subfield include studying the spherical nanoparticle translocations with nanopores that have low aspect ratio and with size specifications limited to 100 nm. In this work, we present the translocation behavior of two different types of nanoparticles using a high aspect ratio sub 100 nm nanopore. The nanopores used in this study have been fabricated by a combination of focused ion and high energy noble gas ions. The nanoparticles used in this study are include of negatively charged iron oxide with a $-COOH$ surface group as well as positively charged polystyrene with -NH_2 surface group. Both these nanoparticles

are under 60 nm in diameter. We present a detailed description of the translocation behavior exhibited by these nanoparticles in silicon nitride nanopores.

4.2 Experimental methods

4.2.1 Nanopore fabrication & characterization

For studying the translocation dynamics of iron nanoparticles with a $-COOH$ surface group, nanopores fabricated using a Xe^+ beam in a feedback controlled ion beam sculpting system were used. For studying the translocation dynamics of polystyrene nanoparticles with $-NH_2$, focused ion beam (FIB) holes, nanopores 100 nm in diameter made by a 50 KeV Ga^+ ion beam were used. These bigger nanopores generally referred as FIB holes are used to fabricate smaller nanopores by the ion beam sculpting process. Both the nanopores and FIB holes are fabricated in free-standing 275 nm thick silicon nitride.

A detailed description of the fabrication of nanopores using the ion beam sculpting system is discussed in Chapter 2 and can also be found here [4, 65, 75]. A brief overview of the fabrication process includes the fabrication of a 275 nm thick stable free standing membrane in silicon nitride with a Si substrate using conventional photolithograpy, reactive ion etching and a chemical etching technique. Initially a 100 nm hole is created in each 3 mm × 3 mm window housing the free standing silicon nitride membrane using a powerful 50 KeV focused Ga^+ ion beam. This process is carried out by a FEI/Micrion 9500 Focused ion beam setup at Harvard. FIB systems are popular for their ability to investigate nanoscale structures using a highly energetic and focussed ion beam but in this case they are used to mill 100 nm nanopores across each 3 mm × 3 mm window in a 8-inch wafer. This FIB setup has a spot size of 5 nm and is operated at a current of 20 nA giving the user ability to mill FIB holes up to 60 nm in diameter [65].

The wafer containing several hundreds of 3 mm × 3 mm windows, each with a milled FIB hole is further fabricated into a nanopore one chip at a time in a high vacuum setup with a feedback controlled ion beam sculpting mechanism using 3 keV noble gas ions. The

ion beam sculpting process can be summarized as follows- the chip containing 100 nm FIB hole is sputtered by a high energy electron beam to maintain charge neutrality on the surface and then exposed to a very narrow several hundred micron diameter noble gas ion beam. The noble gas ions interact with the silicon nitride atoms and cause them to move along the length of the FIB hole due to the process of surface adatom deposition. This process results in formation of a thin silicon nitride membrane and a shrinkage of diameter of the 100 nm FIB hole. This entire process can be closely monitored by looking at the parameters such as ion beam flux F (ions nm^{-1}s^{-1}), area of the FIB hole(nm^2) before being exposed to the ion flux, ion count rate ($\frac{ions}{nm^2}$), and area (nm^2) of the desired nanopore. This monitoring and precision is possible due to the various inbuilt parts of the system consisting of electromagnetic lenses, deflection plates, channeltron detector and labview program. This process allows the user to fabricate nanopores of any desired diameter less than 100 nm and is very well known for fabricating thin and small 5 nm nanopores widely used to study highly charged molecules like DNA.

Transmission electron microscopy(TEM) imaging was used to measure the dimensions (d_1 $nm\times$ d_2 nm) of the FIB milled 100 nm nanopores and smaller ion beam sculpted nanopores. JEOL $JEM-1100$ and FEI-TECHNAI were simultaneously used to measure the dimensions of the FIB and nanopore. JEOL with a 100 kV electron beam provided an easy way to simply measure the dimension of the FIB and the nanopore, whereas TECHNAI with a 200 kV electron beam and additional electron optics provided imaging with EFTEM that helped in looking at the 3-D structure of the nanopore [78]. Once the nanopore size was determined using TEM measurements, the nanopore chosen for each translocation experiment was roughly twice the size of the average nanoparticle size.

4.2.2 Nanoparticle characterization

Both of the nanoparticles used for this study are commercially available and were purchased from specific nanoparticle suppliers. Nanoparticles composed of iron oxide with $-COOH$

surface group were purchased from Ocean Nanotech, California and polystyrene with $-NH_2$ nanoparticles were purchased from Bangs Laboratories, Indiana. Both of these nanoparticles were suspended in DI water.

The manufacturer's dimension of the iron nanoparticles suspended in DI water was estimated to be at 25 ± 2 nm with an initial concentration of 5 $\frac{mg}{ml}$. Ocean nanotech strongly suggests that these nanoparticles are stable in high salt concentrations but does not guarantee the same estimated size. This agrees with our observation; when suspended in 1 M KCl + 10 mM TE at a concentration of 5×10^{14} $\frac{particles}{ml}$ the average size of the suspension was found to be 45 nm with a polydispersity index of 0.3 suggesting that these nanoparticles are highly polydisperse. These measurements were carried out using dynamic light scattering (DLS). All experiments were conducted at this high salt concentration of 1 M KCl +10 mM TE, resembling DNA translocation experiments. Nanoparticle samples were sonicated for 10 minutes to prevent aggregation and several runs for DLS measurement were conducted.

The nanoparticle suspension was stored in a refrigerator at 4°C and before each translocation experiment, moved to room temperature for 20 minutes and then sonicated in a water bath at room temperature for 10 minutes before being used in the experiment. Nanoparticle suspensions were freshly made 24 hours before the experiment using 20 nm filtered 1 M KCl + 10 mM TE in an uncontaminated environment. DLS measurements were immediately conducted to ensure the size and quality of the nanoparticle sample.

The manufacturer's diameter of polystyrene nanoparticles with $-NH_2$ were estimated to be at $53 \pm 10 nm$. These nanoparticles were suspended in DI water with an initial particle concentration of 1.2×10^{15} $\frac{particles}{ml}$. For nanoparticle experiments, the original nanoparticle solution was diluted to make a stock solution of 10^{15} $\frac{particles}{ml}$ with 20 nm filtered DI water. Further dilutions with the electrolyte 20 nm filtered 0.2 M KCl+20 mM CHES was used for the experiments. The final concentration of nanoparticles used for the experiment was 5×10^{14} $\frac{particles}{ml}$ in the above mentioned electrolyte. Surfactant Triton-X 100 was also added to the nanoparticle-containing electrolyte at 0.01% ($\frac{V}{V}$) to prevent aggregation [72, 86].

These electrolyte solutions with nanoparticles were characterized for size using DLS and an estimated size of 56 ± 12 nm for the nanoparticles was obtained. Each sample was sonicated for 10 minutes prior to the DLS measurement. 0.2 M KCl was chosen to be the electrolyte for conducting these experiments for two reasons. One, the concentration was high enough that a simple Ohmic conduction model of nanopores was still applicable without considering surface charge effects caused by the pore. This was supported by some experiments conducted at a 0.1 M KCl electrolyte concentration with polystyrene nanoparticles with $-COOH$ sized at 33 nm and a 50 nm IBS nanopore, where conductive spikes instead of resistive spikes were clearly observed. Two, the nanoparticle solution seemed to be stable and monodisperse at this salt concentration buffered at a pH of 9. This allowed us to look at the stability of the nanoparticles at pH 10 with the same electrolyte and the size estimate using DLS were similar. The nanoparticle samples were stored in a refrigerator at 4°C and similar to iron nanoparticle samples mentioned above. They were moved to room temperature for 20 minutes before being used in the experiment and sonicated in a water bath at room temperature for 10 minutes. Translocation experiments were conducted using both the samples at pH 9 and pH 10 and the electrolyte buffered to the same pH was used in each case.

4.2.3 Nanoparticle event measurements

To conduct nanopore-nanoparticle experiments, the nanopores were subjected to the pre-wetting process. This step was carried out to ensure that the nanopore membranes were residue free from fabrication and characterization procedures and to facilitate the process of wetting. Prior to being used in a translocation experiment, the nanopore chip was P-cleaned for 15 minutes at 90°C using H_2SO_4 and H_2O_2 at a 3 : 1 ratio and then rinsed with 20 nm filtered and degassed DI water several times. The nanopore chip was then carefully transferred to the custom made aluminum cells containing unused and clean PDMS chambers. These aluminum cells are tightly sealed enclosing the nanopore and the surrounding PDMS chambers. These PDMS chambers surrounding the nanopore have a pre-fabricated inlet and

outlet channels to facilitate electrolyte flow through the nanopore chip. Another channel was included to hold Ag/AgCl electrodes on both sides of the chip to apply electric voltage across the membrane. This aluminum cell is enclosed by a Faraday cage. This setup is connected to a headstage which is a part of Axopatch 200B and Digidata 1440A. The system facilitates nanoscale measurements by providing a voltage clamp and detecting the current through the nanopore.

Once the pore-conduction protocol was carried out and the pore shows the expected open pore current and noise values, the nanoparticle suspended in the same electrolyte solution were introduced into the *cis*-side of the setup. After introducing nanoparticle suspension to the nanopore environment, the setup was left undisturbed for 10 minutes and then any offset in the open pore current values was adjusted using the drift offset feature on Axopatch 200B. Event measurements were performed at selectively increasing voltages in the range of $-1V$ to $+1V$, and all the event data was recorded at a sampling rate of 250 kHz with a 10 kHz low pass bessel filter using Axopatch proprietary software pCLAMP 9.

The nanopore conduction traces were anlaysed using Clapmfit and the current blockage data was analysed using a custom Matlab software DNA7. The processed data was plotted using Igor and Python.

4.3 Results & Discussion: Iron nanoparticles with -COOH surface group

Motivation

Iron nanoparticles are widely used in a number of biomedical applications. These include research based application using iron nanoparticles for targeted drug delivery and in magnetic resonance imaging. All these biomedical applications require precise information on the size, surface charge and stability of these nanoparticles so they can be modified for various applications [97]. Nanopores because of their unique ability to characterize individual particles based on the size and charge can be used as a sensor to detect more information about these nanoparticles and their behavior at nanoscale.

Determining the nanopore geometry

In Fig 4.1(a), the effective length l_{eff} of the nanopore under experimental conditions was calculated using the slope of the I-V curve. This measurement was obtained using an episodic file in clampex by applying voltage in increments of 20 mV from -200 mV to +200 mV and measuring the corresponding current through the nanopore. The two I-V curves illustrate this measurement during two different times while the experiment was being conducted.

The 2-D geometry of the nanopore used in this experiment was obtained using HR-TEM images. The chip was heat cleaned at 750°C followed by closing into a nanopore using 3keV Xenon ion beam. The nanopore was then imaged with Technai(200 kV) at a regular magnification of 10 KX and the average diameter of the nanopore was measured to be 42.5 nm.

Fig 4.1(b) describes the 2D geometry of another ion beam sculpted nanopore used to study iron nanoparticles. This image was taken after the experiment was conducted. The spherical nanoparticles are clearly visible on the surface of the free standing membrane. The nanopore was stored in its gel box after the experiment and blow dried with N_2 before imaging in TEM. This image was taken using Technai at 10 KX magnification.

Fig 4.1(c), 4.1(d) and 4.1(e) are schematic illustrations of single events recreated from real data. The voltages for these events were recorded are 120 mV, 60 mV and 40 mV respectively.

Several tens of experiments were conducted with this nanoparticle and nanopores ranging in diameter from 20-100 nm. For this section only one set of results are included. This set describes the complete translocation behavior with voltage dependence. The translocation experiment was carried out with a pore of diameter 42.5 nm at a salt concentration 1 M KCl + 10 mM TE and the nanoparticles were suspended in the same solution at a concentration of 5×10^{14} particles/ml. In case of the IBS pore, I-V curves contain a significant amount of information about the nanopore etching open into an FIB under experimental conditions. This process changes the geometry of the nanopore during the experiment by causing the
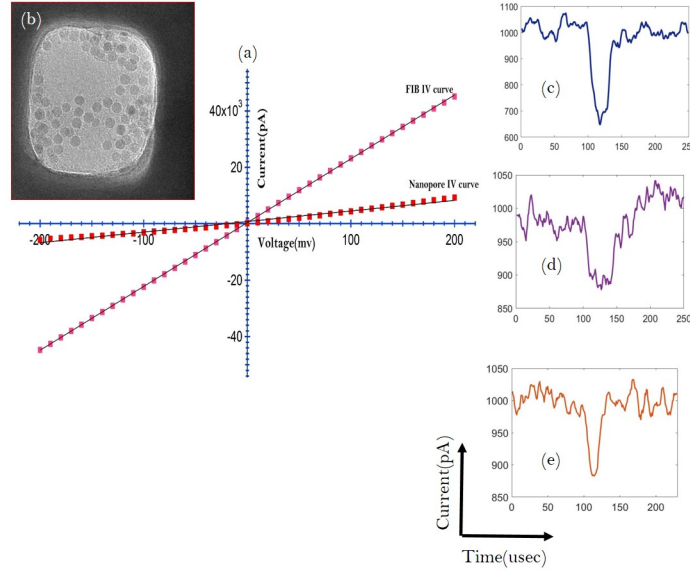
Figure 4.1: (a) I-V curves of the nanopore used in the experiment. It shows two linear I-V curves with different slope, one for a nanopore and the other when it has etched open into an FIB. (b) TEM image of the nanopore after the translocation experiment with iron nanoparticles on its surface. (c, d, e) Schematic illustration of events recorded at 120 mV, 60 mV, 40 mV

.

thin nanopore to etch open and retain the geometry of the FIB hole in which it was originally fabricated. This is clearly indicated by the increase in the value of the open pore current during the experiment and also by the slope of the I-V curve. IBS nanopores have been shown experimentally to have laterally etched open by Rollings et.al, [78]. From 4.1(b) we can calculate the slope for two I-V curves and they were found to be 37.6 nS for the red I-V curve, 226 nS for the pink I-V curve. The change in slope of these I-V curves indicates a change in the effective length of the nanopore and this difference in geometry is supported by the open pore current recorded at different times during the experiment. As the nanoparticle translocations are observed after the pink I-V curve, we assume that the nanopore has etched open into an FIB and hence we use the effective length calculated from the pink I-V curve which was $l_{eff} = 198$ nm for all further calculations. The diameter of the nanopore was estimated to be around 90 nm at this point in time.

From the TEM image 4.1(b) we can clearly identify the spherical nanoparticles sticking on

the surface of the nanopore. This confirms the possibility that the nanoparticles have actually translocated through the pore. This assumption is also supported by the translocation events that were only observed after the nanoparticles were added. This TEM image represents another nanopore used in this set of experiments. Data from this nanopore is not presented here as it did not successfully show voltage dependence. However, this image supports the lateral etching of nanopore as studied by Rollings et.al, and clearly indicated by the open pore current and I-V curve measurements.

Fig 4.1(c), 4.1(d) and 4.1(e) each show a schematic of a single event recorded at different voltages during the experiment. The variable length event-traces were recorded after the nanoparticles suspended in the same electrolyte solution as the pore were introduced into the - *cis* side of the setup. When a potential of 120 mV, 60 mV and 40 mV was applied, the negatively charged nanoparticles were electrophoretically driven through the pore and resulted in translocation events. It is clearly visible from each single event that the amplitude of current drop caused by a translocating particle changes with the applied voltage.

Voltage dependent translocation behavior

As the geometry of the nanopore has been discussed in detail, we move forward to inferring the behavior of the nanoparticle translocations as a function of applied voltage. The translocation data was analyzed using the matlab-based program DNA 7 and the processed data was further plotted using Python. Fig 4.2 consists of five subplots that summarize the voltage dependence. Fig 4.2(a), 4.2(b) and 4.2(c) are scatter plots of the extracted events at 40 mV, 60 mV and 120 mV respectively. These scatter plots consist of current drop *(pA)* on the y-axis and translocation time *(μs)* on the x-axis. Each dot represents a translocation event that was analyzed. Fig 4.2(d) is a plot showing the behavior of the average current drop as a function of applied voltage. Fig 4.2(e) is a plot showing the behavior of the average translocation time as a function of applied voltage.

The initial data was collected in Clampex using a variable length event detection file and
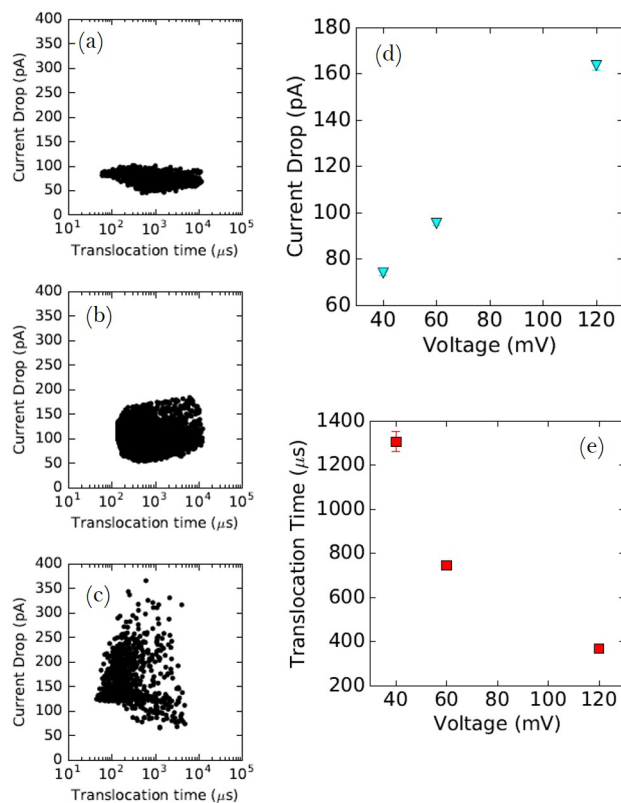
Figure 4.2: Scatter plot of anaylsed translocation data at (a) 40 mV. (b) 60 mV. (c) 120 mV. Each dot represents an event. (d) Average current drop vs Voltage. (e) Average translocation time vs Voltage.

then was processed in the Matlab based routine DNA7. More details on experimental protocols and data analysis are included in Chapter 2. To generate these scatterplots several limits were established on the x-parameter, translocation time and y-parameter, current drop. For translocation time, events smaller than 70 μs were not included for further analysis. This threshold was established as the sampling frequency used to collect the data was 250 kHz, the rise time from the sampling frequency would be $\frac{1}{250kHZ} \approx 33\mu s$, and the time threshold was twice the minimum rise time. Events larger than 10000 μs [10ms] were not included as they would indicate blockages caused by translocating nanoparticles. Current drop events with an amplitude less than 30 pA were not included as they would represent the 2 times the rms noise in the system and events with an amplitude greater than 500 pA were not included for this analysis.

Scatter plots yield the value of current drop and translocation time for every event defined by the limits set by the user. The average current drop and the average translocation time were calculated by estimating the average value of the given sample using Matlab. From Fig 4.2(d), we can see that the average current drop increases with the increase in applied voltage. This can be interpreted in the following way; the electrical equivalent of a nanopore is a resistor and at higher voltage the resistor yields a higher current. Nanoparticle translocations are considered as a change in that resistance or current value. The nanopore yields a higher current at greater voltage; therefore the average current drop caused by a translocating nanoparticle should be higher. This behavior is clearly represented by the plot in Fig 4.2(d) as the average current drop values for increasing voltage were as follows (164 pA; 120 mV), (96 pA; 60 mV), (74 pA; 40 mV).

Fig 4.2(e) is a plot representing the behavior of average translocation time vs applied voltage. The translocation time taken by the nanoparticle to pass through the pore depends on its drift velocity, charge and forces experienced by it in the nanopore environment. The expected behavior that the nanoparticles are driven at a faster rate through the pore with applied voltage indicates that the average translocation time should decrease as the applied
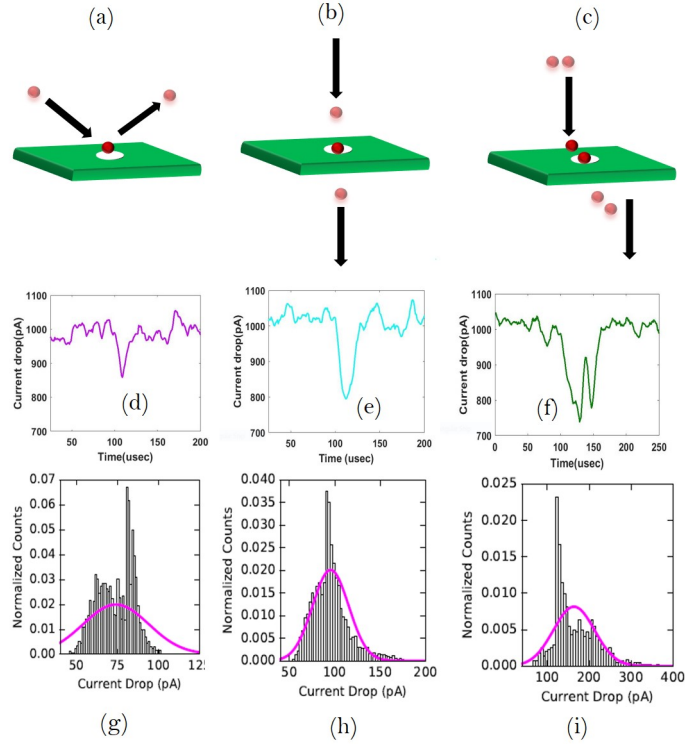
Figure 4.3: Schematic illustration of type of events generated by the nanoparticles when passing through the nanopore. (a) Collision type or fly away event. (b) One single particle entering and leaving the nanopore. (c) A longer event caused by more than one particle entering and leaving the pore. Illustration of actual experimental data recorded at 120 mV with iron nanoparticles. (d) Collision type event with observed (I, t_d). (e) Single nanoparticle event with observed (I, t_d). (f) An event caused by more than one nanoparticle passing / interacting with the nanopore with observed (I, t_d). Current drop distributions of nanoparticle translocation events detected at different voltages. (g) 40 mV. (h) 60 mV. (i) 120 mV.

voltage increases. This is clearly observed in Fig 4.2(e) as the average translocation time is reduced with an increase in voltage and the values are as follows (483 μs; 120 mV), (745 μs; 60 mV), (1302 μs; 40 mV).

Current drop distributions

Fig 4.3 consists of nine subplots and represents the broad classification of type of events observed when iron nanoparticle interacts with the nanopore [11, 21, 40], their schematic representation and the current drop histograms of iron nanoparticle at 40 mV, 60 mV,120 mV. Fig 4.3(a)-(c) shows the schematic representation of the type of interaction between the

nanoparticle and nanopore. Fig 4.3(d)-(f) are a schematic illustration of events each corresponding to the type of interaction directly above it. Fig 4.3(g)-(i) are the current drop histograms generated from the y-axis parameter current drop of the scatterplot shown in Fig 4.2. Each current drop histogram is for a specific voltage. From Fig 4.3(a)-(c), we can broadly classify the interaction of the nanoparticle with the nanopore into three categories.

1. The nanoparticle has a collision with the nanopore surface giving rise to a collision type or a fly away event. In this case, the nanoparticle does not enter the nanopore and translocate to successfully come out on the other side but just collides with the surface of the pore and flys away. This type of event would cause an event with a small current drop and a short event duration, as it is blocking only a few Cl^- ions from the surface of the nanopore. Such type of event is represented in Fig 4.3(d), which is directly below the schematic. This event was part of the processed data recorded at 120 mV.

2. The nanoparticle enters the nanopore and exits on the other side, giving rise to a traditional translocation type event. This event is caused by a single nanoparticle inside the nanopore. This type of event is the foundation for the resistive pulse technique. A single nanoparticle event is shown in Fig 4.3(e) directly below this schematic. This event is similar to 4.3(d), was part of the processed data recorded at 120 mV.

3. More than one nanoparticle is entering into the pore environment near its sensing zone. This type of event can be generalized as a multi particle event which gives rises to an event with greater current amplitude and duration. This type of event does not result in clogging of the pore. It may be preceded or followed by a collision or translocation type of event. A multi particle event is shown directly below in Fig 4.3(f). The amplitude and shape of each event is different, indicating a specific particle-pore interaction. The fly away event in Fig. 4.3(d) has a smaller amplitude of 100 pA and the bottom of the event shows a single level. The single translocation in Fig 4.3(e) has

a larger amplitude of 200 pA than the fly away event in Fig. 4.3(c). It also reveals a single level but with more broader base. The multi-level event in Fig. 4.3(f) has an even larger amplitude of 250 pA clearly showing two distinct drops one followed by another very closely represents a two-particle translocation event. Events with more than two levels also have been observed that are not shown here.

There are additional types of interactions that result in the temporary clogging of the nanopore when a huge blockage is observed suddenly while recording events. This can be reversed by changing the polarity of the applied voltage. Permanent clogging of the nanopore [11, 21] occurs when multiple nanoparticles gather around the pore surface, not facilitating translocation. This results in a completely clogged nanopore, mostly irreversible after which the nanopore translocation experiment is concluded.

The current drop distributions are shown in Fig 4.3(g)-(i). These distributions are generated from the current drop values for each event processed at three different voltages. All the three distributions have been fitted with a Gaussian pdf to estimate the average value of the current drop from the mean of the fit. It is clear that these distributions are multimodal and one way of interpreting these distributions would be as by the distribution of peaks and assigning each peak to be caused by a specific pore-particle interaction discussed above. At 40 mV, clearly two modes are visible at 65 pA and 85 pA. The first mode corresponds to collision type events and the second mode to a single particle translocation type. At 60 mV, the distribution presents three modes; the first one can be seen as a shoulder due to collision type events, the second mode due to single particle translocation events. This is followed by a third mode in the form of a tail due to multi particle events. These three modes can be observed at approximately 75 pA, 100 pA and 125 pA. At 120 mV, we see a multimodal distribution with a tail at longer current drops. The first mode in the shoulder can be attributed to a collision type events, followed by the second mode caused by single particle translocation events, followed by a long tail of multi particle events. These three modes can be observed at approximately 100 pA, 150 pA and 200 pA.

Event duration distributions

Fig 4.4 consists of four subplots that describe the event duration histograms, the probability distribution fits and the parameters derived from the PDF as a function of voltage. Fig 4.4(a-c) consist of event duration histograms at 40 mV, 60 mV and 120 mV respectively. The event duration for each event are processed from the initial data and plotted on the x-axis of the scatter plot in Fig 4.2. These histograms have been fitted with a 1D drift-diffusion model. Fig 4.4(d) consist of the parameters derived from the fit of the 1D drift diffusion model to the Event duration histograms. These two parameters are drift velocity and diffusion coefficient. Drift velocity is plotted as a function of applied voltage in Fig 4.4(d) and it exhibits a linear relationship with the applied voltage.

The event duration histograms plotted at three different voltages are fitted with the 1D drift diffusion model. The PDF is an inverse Gaussian resulting in the probability distribution of the given data with two parameters extracted from the fit; the mean and the sharpness of the peak. When the PDF is compared to the $1D$ drift diffusion probability function, the diffusion coefficient can be derived by knowing the sharpness of the peak and the drift velocity is derived from the mean of the distribution.

$$f(x|\mu, \lambda) = \left(\frac{\lambda}{2\pi t^2}\right)^{1/2} \exp\left(-\frac{\lambda(x-\mu)^2}{2\mu^2 x}\right) \tag{4.1}$$

Where λ : sharpness and μ : mean of the distribution. The drift velocity as a function of applied voltage shows a linearly increasing trend. This is consistent with the predicted behavior that the nanoparticles are moving with an increasing velocity through the pore as more potential is applied across the pore [29, 98]. The diffusion coefficient is not shown here, but as a function of applied voltage shows a linearly increasing trend. Although it is expected to be constant for different values of voltage as the bulk ion concentration remains the same. This may be affected by surface charge fluctuations. This value presented here is an estimation derived from an inverse Gaussian fit to the data, more evidence is needed
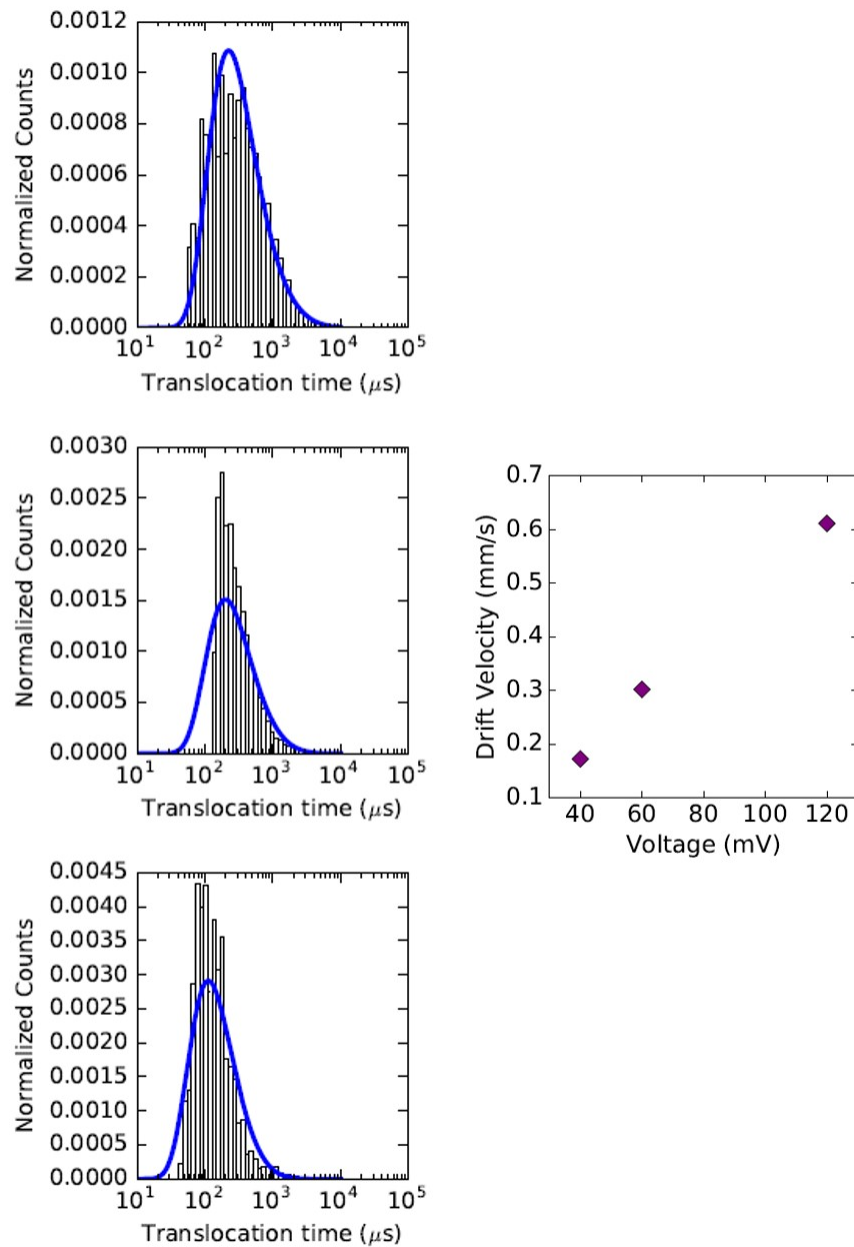
Figure 4.4: Event duration histograms for analysed events at three different voltages (a) 40 mV. (b) 60 mV. (c) 120 mV. These histograms also show the probability distribution fits from which the drift velocity and diffusion coefficient are extracted. (d) Drift velocity vs Voltage.

Manufacturers diameter (in DI Water)	25 ± 2 nm
DLS estimated diameter (in electrolyte)	54 ± 10 nm
Nanopore estimated average diameter	59.6 ± 4.7 nm

Table 4.1: Size estimation of iron nanoparticles

to verify the diffusion coefficient by using alternate electro-optical sensing experiments with this pore geometry and nanoparticle [98].

Size estimation of iron nanoparticles
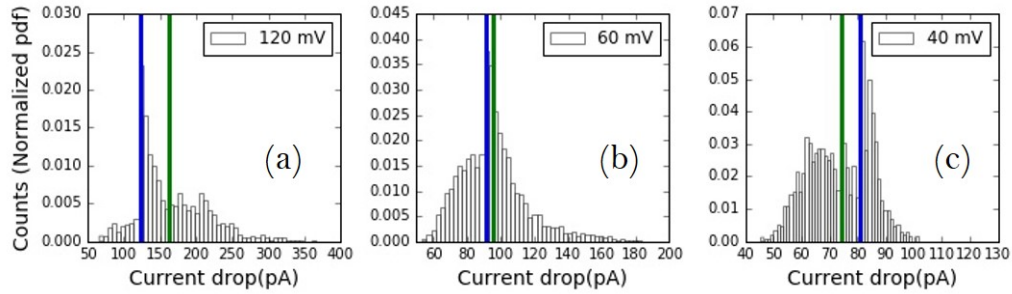
Figure 4.5: Current drop histograms at different voltages (a) 120 mV. (b) 60 mV. (c) 40 mV. The mean and mode of the distributions are indicated on them. The mean is represented by a green bar and the mode is represented by a blue bar in each distribution.

In this section, we conclude the study of iron nanoparticle translocation using solid state nanopores by discussing the estimation of nanoparticle size from current drop distributions. Fig 4.5(a-c) shows the current drop distributions of nanoparticle events collected and analysed at three different voltages; 120 mV, 60 mV and 40 mV. The mean and mode of each distribution is represented using a different color and is shown in each distribution.

Since each distribution appears to be a combination of different types of events, namely collison type, single particle translocation type, and multiple particle translocation type. The mean value represents of the distribution is taken to estimate the size of the nanoparticle passing through the nanopore. In some nanoparticle studies [41, 98], the mode of the distribution has been used as it is the most probable value. The DLS measurement of the nanoparticle yielded an average value of 54 ± 10 nm with a poly dispersity index of 0.30.

79

The size estimated from the mean of current distributions is as follows: (70 nm; 120 mV), (59 nm; 60 mV) and (54 nm; 40 mV). The size estimated from using the mode of the current distribution is (65 nm; 120 mV), (58 nm; 60 mV) and (56 nm; 40 mV). We estimated the size of the Iron nanoparticles with $-COOH$ group using the semi empirical model from [11]. The nanoparticle diameter is estimated using the following relation that connects the pore geometry (L,D) to the nanoparticle geometry (d) using the concepts of resistive pulse technique and the contribution of access resistance of the pore [43].

$$\frac{\delta I}{I_0} = \frac{d^3}{(L + 0.8D)D^2} \tag{4.2}$$

In equation (4.2), the $\frac{\delta I}{I_0}$ is the relative change in the current that can be extracted for current drop histograms from the experimental data. This equation is valid for nanoparticles smaller than the effective length of the nanopore. The diameter D of the nanopore is taken from the TEM measurements and the effective length l_{eff} or L is calculated from I-V measurements during the experiment. Comparing the size estimation and the DLS measurement, we see that they are not exact, but the nanopore measurements are still within 1σ of the DLS measurement. Another significant factor is the model used to estimate the size distribution assumes that the pore has no surface charge and does not contribute to translocation kinetics. This however cannot be ignored and as discussed in Section(3.3), the surface charge and zeta potential of the pore are dependent on the electrolyte molar concentration and pH of the electrolyte. The interaction of the pore with the particle gives rise to different types of events instead of just having the single type translocation events. These different types of events cannot be ignored as they give a complete picture in understanding the interaction. Also, the polydispersity index as measured by DLS suggests that this nanoparticle has high polydispersity and hence, expecting a definite value from size measurements might be ignoring the polydispersity.

4.4 Results & Discussion : Polystyrene nanoparticles $-NH_2$ surface group

Motivation

Polystyrene nanoparticles are considered good model particles that resemble viruses as they can be easily introduced into a cell environment to study the interaction with a biological system [99]. Polystyrene nanoparticles are a popular choice due to their properties such as stability and biocompatibilty. These nanoparticles are commercially available in a wide range of sizes (30-1000 nm) at the nanometer scale. They can be easily functionalized with a surface charge group, they are homogenous, usually with a low poly dispersity index, and they form stable colloids. These particles have applicability in fields such as optics and photonics , self- assembled nanostructures, and biosensors [100].

In the field of resistive pulse technology, polystyrene nanoparticles have been widely used. In one of the significant studies to impact this field, Deblois & Bean et.al, [25] used latex nanoparticles to generate the corresponding data for the suggested theoretical model about counting and sizing of nanoparticles. This work, published in 1970, later inspired a number of studies in this field and with the advancement of nanotechnology resistive pulse technology was studied in channels or pores at the dimensions of several hundreds of nanometers [10, 12, 14, 19, 21, 22, 37] using polystyrene nanoparticles of similar dimensions. In recent years, researchers in this field have been able to study polystyrene nanoparticles under 100 nm using nanopores fabricated by techniques such as Focused ion beam milling, TEM drilling and E-beam lithography [72]. Apart from nanoparticle detection, their translocation dynamics reveals information about the pore geometry [101]. Negatively charged polystyrene $-COOH$ nanoparticle is a preferred particle for nanopore experiments [38, 41]. Two studies [38, 63] have reported that chemically modifying the nanopore surface using APTES has resulted in an increased detection rate using polystyrene $-COOH$ nanoparticles. This chemical modification results in a net positive surface charge for the nanopore. In studies conducted by our group presented in Chapter 3, we have observed that detecting 33 nm
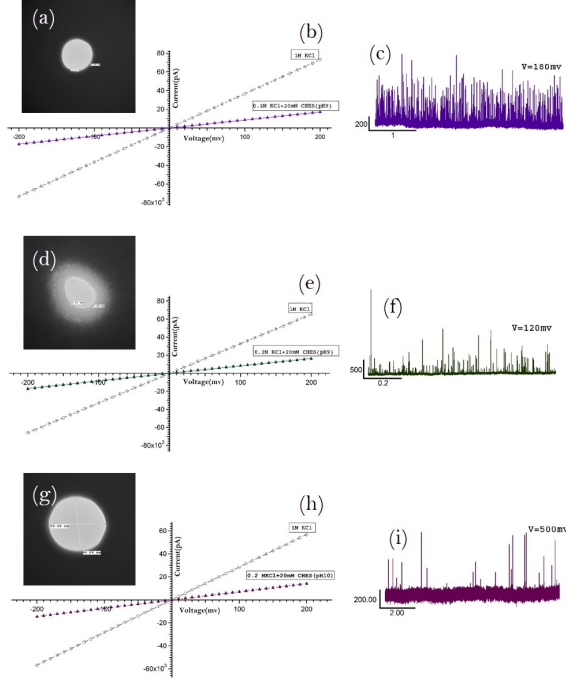
Figure 4.6: (a) TEM image of a 99 nm diameter nanopore made by FIB milling. (b) I-V curves for the nanopore in (a) at two different salt concentrations 1 M KCl and 0.2 M KCl + 20 mM CHES at pH 9. (c) An event trace recorded at -180 mV showing PS$-NH_2$ translocations. (d) TEM image of a 80 nm diameter nanopore made by IBS method. (e) I-V curves for the nanopore in (d) at two different salt concentrations 1 M KCl and 0.2 M KCl + 20 mM CHES at pH 9. (f) An event trace recorded at -120 mV showing PS$-NH_2$ translocations. (g) TEM image of a 97 nm diameter nanopore made by FIB milling. (h) I-V curves for the nanopore in (g) at two different salt concentrations 1 M KCl and 0.2 M KCl + 20 mM CHES at pH 10. (i) An event trace recorded at -500 mV showing PS$-NH_2$ translocations.

polystyrene $-COOH$ nanoparticles using 40-70 nm IBS nanopores has not resulted in predicted voltage dependent translocation behavior. This led us to consider studying a slightly bigger, positively charged polystyrene$-NH_2$ with the 100 nm FIB holes available to us.

In this section, we present the translocation dynamics observed in 100 nm silicon nitride nanopores using 53 nm positively charged polystyrene nanoparticles with $-NH_2$ surface charge group.

Determining the nanopore geometry

Three FIB nanopore results are presented in this work and TEM images of these FIB's are shown in Fig 4.6(a), (d), (g). From now on they will be referred to as FIB 1, FIB 2 and FIB 3.

Figure 4.6 presents information about each FIB used in this experiment to study $PS-NH_2$ translocations. This includes HR-TEM images shown in Fig. 4.6(a), (d) and (g) taken using JEOL-JEM 1011 at a magnification of 500 KX. I-V curves for each nanopore are shown in Fig. 4.6(b), (e) and (h) and these I-V measurements were recorded with varying voltage from -200 mV to +200 mV using pCLAMP 9. These I-V measurements were also conducted for two different electrolyte concentrations of 1 M KCl and 0.2 M KCl + 20 mM CHES. Also shown in Fig. 4.6(c), (f), (i) are illustrations of event traces recorded during the translocation experiment by adding $PS-NH_2$ nanoparticle suspension in 0.2 M KCl + 20 mM CHES + 0.01% $\left(\frac{V}{V}\right)$ Triton X-100. These results were recorded at voltages of -180 mV, -120 mV and -500 mV. The translocation experiments conducted for pores shown in Fig. 4.6(a) and (d) were at electrolyte pH 9 and for the nanopore shown in Fig. 4.6(e) at electrolyte pH 10.

The dimensions of each nanopore were measured using TEM. The average diameter calculated for each nanopore used were 99 nm, 80 nm and 97 nm respectively. All the nanopores were pre-wetted and p-cleaned before the translocation experiment. All the pore conduction protocols were recorded to ensure that the nanopore showed the appropriate conductance measurements with 1 M KCl. 20 nm filtered DI water rinse was performed several times through the inlets and outlets before adding 0.2 M KCl + 20 mM CHES to the nanopore. All the pore conduction protocols were repeated with 0.2 M KCl + 20 mM CHES and the nanopore showed the expected conductance measurements with this electrolyte. The effective length l_{eff} of the nanopore was calculated from the slope of the I-V curve. We were able to record events at higher voltages than usual with FIB 3 due to lower initial conductance values shown by the pore. FIB 2 used in this study was a 80 nm diameter IBS scuplted nanopore but once wet it showed open pore current and conductance measurements

Figure 4.7: (a) Scatter plot for analysed translocation events for FIB 1. This plot consists of all the processed events that were recorded at three different voltages -60 mV, -120 mV and -180 mV. (b) Scatter plot for analysed translocation events for FIB 2. This plot consists of all the processed events that were recorded at two different voltages -60 mV, -120 mV. Both these experiments were conducted with 0.2 M KCl + 20 mM CHES at pH 9.

similar to that of an FIB with 90 nm diameter, so it was estimated as an FIB for all further calculations.

Voltage dependent translocation behavior

All three of the translocation experiments with FIB 1, FIB 2 and FIB 3 showed voltage dependent translocation behavior. Events were recorded for at least three different voltages using PS$-NH_2$ in all three experiments. Fig. 4.7(a-b) consists of two scatter plots showing processed event data, where each circle in the scatter plot represents an event. These events are characterized by their current drop (pA) and event duration (μs). The two scatter plots shown in Fig. 4.7(a) and (b) are for FIB 1 and FIB 2. The third scatter plot shown in Fig 4.8(c) is for FIB 3. Each scatter plot consists of processed events recorded at different
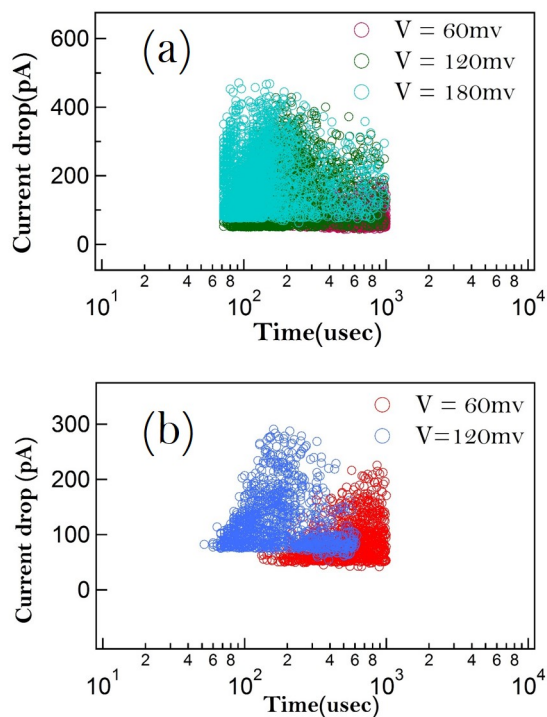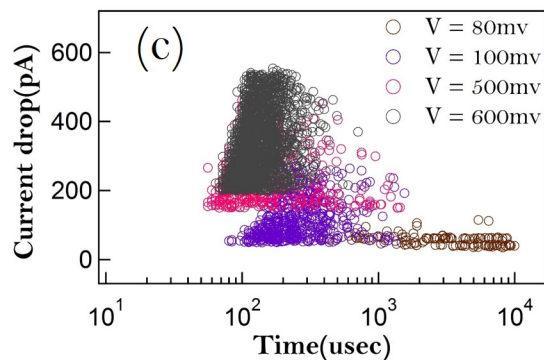
Figure 4.8: (c) Scatter plot for analysed translocation events for FIB 3. This plot consists of all the processed events that were recorded at four different voltages −80 mV, −100 mV, −500 mV and −600 mV. This experiments was conducted with 0.2 M KCl + 20 mM CHES at pH 10.

voltages. The minimum and maximum limits on event duration were set to 70 μs and 1000 μs and for current drop were set to 45 pA and 600 pA and these parameters were varied depending on the voltage. Any data points out of these limits were not included for this data.

The scatter plots shown in Fig 4.7(a) were generated from events recorded at three different voltages -60 mV, -120 mV and -180 mV using a 99 nm average diameter nanopore and 53 nm PS$-NH_2$ suspended in 0.2 M KCl + 20 mM CHES + 0.01% $\left(\frac{V}{V}\right)$ Triton X-100 at pH 9. Events recorded at -60 mV are overlapped by events at higher voltages in the scatter plot. These translocation experiments were conducted using 0.2 M KCl+ 20 mM CHES at pH 9 as the electrolyte.

Similarly for Fig. 4.7(b), the events were recorded using a 80 nm IBS nanopore that once wet resembled FIB measurements in open pore current and conductance at two different voltages: -60 mV and -120 mV. The experimental conditions were the same as those stated for FIB 1.

The scatter plot shown in Fig. 4.8(c) presents events recorded at four different voltages: -80 mV, -100 mV, -500 mV and -600 mV. FIB 3 had a slightly lower conductance compared to the other two FIB's presented here. Usually voltages higher than -200 mV were avoided
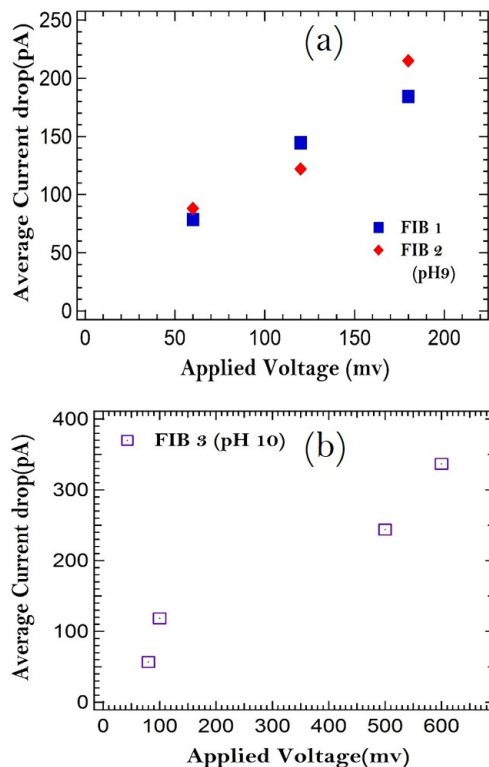
Figure 4.9: (a) Average current drop (pA) vs Applied voltage (mV) for events that were recorded at three different voltages −60 mV, −120 mV and −180 mV for FIB 1 and for FIB 2. (b) Average current drop (pA) vs Applied voltage (mV) for events that were recorded at four different voltages −80 mV, −100 mV, −500 mV and −600 mV for FIB 3.

for event collection as it would result in temporary clogging of the nanopore followed by an increase in rms noise of the pore. Within minutes of this behavior the nanopore would permanently clog. For this pore, we were able to record events at higher voltages -500 mV and -600 mV. This can be attributed to lower initial conductance of the pore and taking measurements at pH 10 electrolyte which increases the negative surface charge of the pore.

In all of the experiments, the number of events increased with an increase in voltage, supporting the idea that more nanoparticles were translocated through the pore as the voltage across it was increased.

Current drop distributions

Fig. 4.9 consisting of two subplots 4.9(a) and 4.9(b) represents the average current drop produced by the nanoparticles while interacting with the pores. These plots are divided into subplots on the basis of electrolyte pH. Fig. 4.9(a) shows the average current drop for FIB 1 and FIB 2 at three different voltages -60 mV, -120 mV and -180 mV respectively. Fig. 4.9(b) shows the average current drop for FIB 3 at four different voltages -80 mV, -100 mV, -500 mV, -600 mV.

From both Fig. 4.9(a) and (b), we see that the average current drop increases as the applied voltage across the nanopore is increased. This agrees with the nanoparticle translocation behavior observed using the polystyrene with $-COOH$ nanoparticles in various nanopore systems [72, 92, 98]. We can extend the same behavior to our positively charged 53 nm polystyrene with $-NH_2$ nanoparticles. We know from the principle of resistive pulse technique that this increase in current drop is attributed to an increase in resistance as more voltage is applied across the pore. The average current drops for FIB 1 were estimated to be 78.6 pA, 144.5 pA, and 184.3 pA and the average current drops for FIB 2 were estimated to be 88.2 pA, 122 pA, and 215 pA. For both the FIB's these events were recorded at -60 mV, -120 mV and -180 mV using 0.2 M KCl+ 20 mM CHES at pH 9. From these average values, we observe that the current drop produced by the same nanoparticle in a similar diameter nanopore, under identical experimental conditions showing similar conductance values is similar. These similar values of average current drop restate the importance of conductance and pore geometry of the nanopore.

In case of FIB 3, the estimated average current drops were 56.7 pA, 118.5 pA, 243.8 pA, 336.6 pA for the events recorded at -80 mV, -100 mV, -500 mV, -600 mV using 0.2 M KCl+ 20 mM CHES at pH 10. Comparing the average values in Fig. 4.9(a) and (b), we see that the average current drop values are lower for FIB 3 and this is due to lower initial conductance values that allowed us to observe events at higher voltages instead of clogging. This re-emphasizes the fact that the pore geometry dominates the translocation behavior.

Different type of events that arise due to various interactions of the nanoparticle with nanopore also have a significant contribution towards average current drop. These different types of events are mainly classified as collision type, single particle events and multi particle events. They are clearly observed in each and every event trace collected at different voltages in all the three FIB's. This suggests that the particle can participate in any type of interaction and still contribute to an event. The average current drop for each voltage was estimated by computing the mean of the current drop distribution generated from the scatter plot of the processed event data. The current drop distribution histograms are not included here.

Event duration distributions

After looking at the current drop produced by the nanoparticle due to various types of interactions with the nanopore, we look at the other parameter that describes the translocation behavior- the average translocation time. The event duration histograms are generated from the processed event data represented in the scatter plots shown in Fig. 4.7 and Fig. 4.8. the event duration histograms are not shown here. These histograms were then fit using a probability distribution function representing an inverse-Gaussian distribution, because the event duration histograms usually have a narrrow peak followed by a long tail. Fitting an inverse-Gaussian distribution also helps us to determine the mean event duration (μ) and the shape factor (λ) of the distribution. These two parameters can be related to the drift velocity (v_d) and the diffusion coefficient (D) using the 1D-drift diffusion model, given that the effective length (l_{eff}) of the nanopore is known.

Fig. 4.10 consists of two plots that describe the behavior of the average event duration as a function of applied voltage. Fig. 4.10(a) shows the average event duration values for FIB 1 and FIB 2. The events were recorded at three different voltages: -60 mV, -120 mV and -180 mV. The average event duration for -180 mV for FIB2 was excluded from here due to the blockages in the trace affected the computed value of average event duration. Fig. 10(b) shows the average event duration values for FIB 3. The events were recorded at four different

Figure 4.10: (a) Average event duration(usec) vs Applied voltage (mV) for events that were recorded at three different voltages −60 mV, −120 mV and −180 mV for FIB 1 and at two different voltages −60 mV, −120 mV for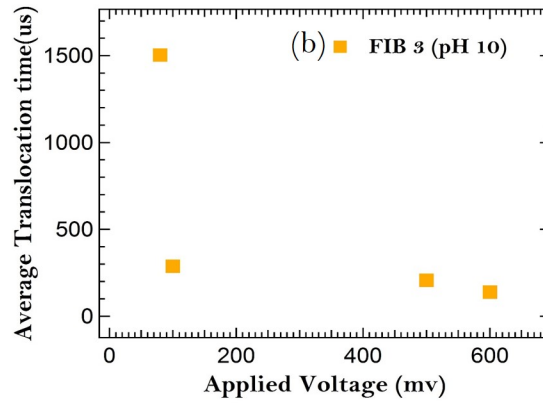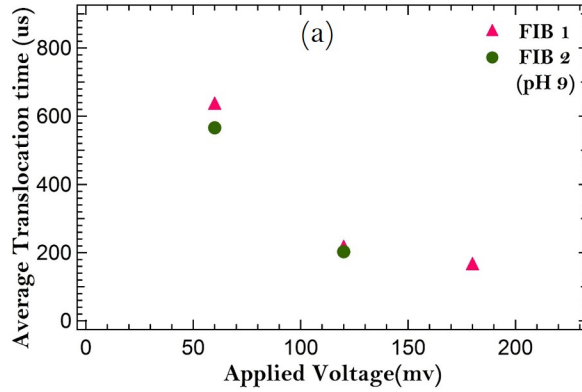 FIB 2. (b) Average event duration (usec) vs Applied voltage (mV) for events that were recorded at four different voltages −80 mV, −100 mV, −500 mV and −600 mV for FIB 3.
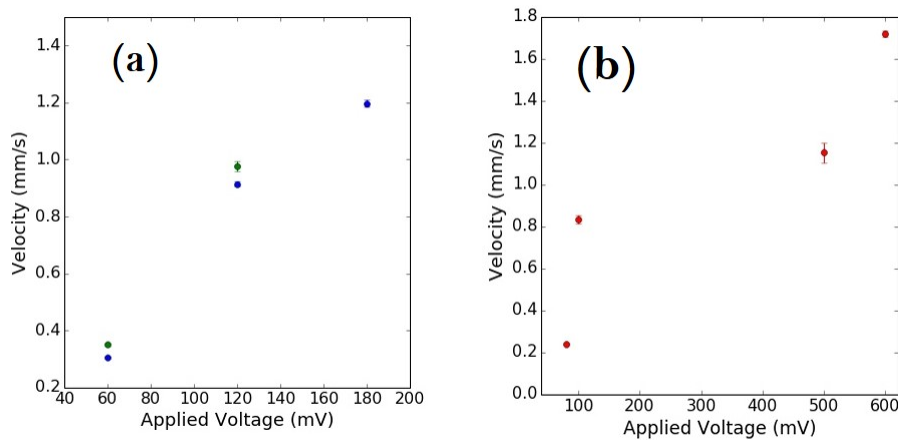

Figure 4.11: Drift Velocity estimated from inverse Gaussian PDF using 1D- Drift diffusion model on event duration histograms.(a) Velocity vs Voltage for FIB1 and FIB2. (b) Velocity vs Voltage for FIB3.

voltages: -80 mV, -100 mV,-500 mV and -600 mV. All the average values were computed from the inverse-Gaussian PDF and represent the parameter mean (μ)of the distribution. From both the plots we can see that the average event duration decreases as the applied voltage increases. This is in agreement with the translocation behavior of polystyrene nanoparticles with $-COOH$ group reported by [22, 33, 41, 72]. This behavior also supports the notion that the nanoparticles are driven at a faster rate due to the increased potential.

Another parameter that supports this notion is the drift velocity of the nanoparticle. The drift velocity is extracted by applying 1D-drift diffusion model and the mean translocation time μ of the PDF. As the effective length l_{eff} of the nanopore is assumed to remain same throughout the experiment, the drift velocity varies inversely as the mean of the PDF fit to each event duration histogram. This results in drift velocity having an increasing trend with the applied voltage. Drift velocity values extracted from each event duration histogram are plotted as a function of voltage in Fig. 4.11(a) and (b). Fig. 11(a) consists the drift velocity measurements for FIB 1 and FIB 2, whereas Fig. 4.11(c) represents the drift velocity measurements for FIB 3. We report values ranging from 200 $\frac{mm}{s}$ to 18000 $\frac{mm}{s}$ for applied voltages in the range of -60 mV to -600 mV. These values are comparable to the published values of drift velocity computed in PDMS nanochannels with flouroscent polystrene nanoparticles using the 1D-drift diffusion model [29, 98]. The velocity values observed by us are a bit on the higher side to the reference. This can be explained due to the material and charge on the nanopore used. We conducted these experiments using negatively charged silicon nitride whereas the reference used a neutrally charged PDMS nanochannel. Electo-osmotic effects can influence the rate at which a nanoparticle is translocating through the pore for charged surfaces.

The diffusion coefficient extracted from the PDF of the event duration histogram as a function of applied voltage is not shown here. The diffusion coefficient computed values are slightly higher than the bulk diffusion coefficient of the electrolyte outside the nanopore. This can be attributed to the data truncation imposed by setting limits on event duration
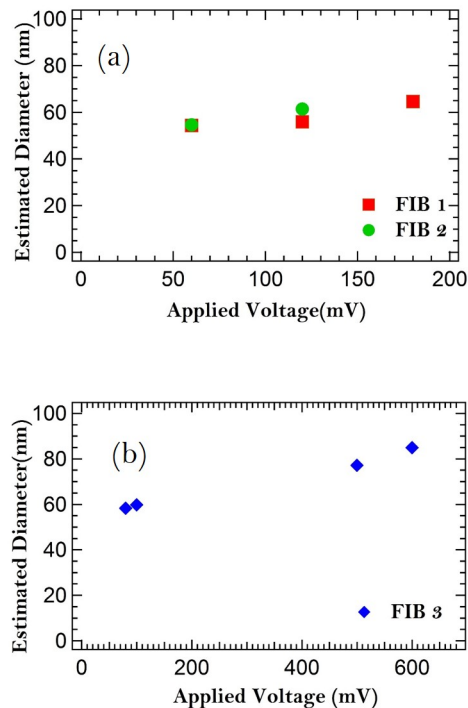
Figure 4.12: (a) Estimated nanoparticle diameter (nm) vs Applied voltage (mV) from events that were recorded at three different voltages -60 mV, -120 mV and -180 mV for FIB 1 and at two different voltages -60 mV, -120 mV for FIB 2. (b) Estimated nanoparticle diameter (nm) vs Applied voltage (mV) from events that were recorded at four different voltages -80 mV, -100 mV, -500 mV and -600 mV for FIB 3.

by ignoring shorter and longer events and also not accounting for the effect of surface charge fluctuations.

Size estimation of polystyrene$-NH_2$ nanoparticles

In section 4.3.5, we estimated the size of the Iron nanoparticles with $-COOH$ group using the semi empirical model from [11] and found that the size estimation is slightly skewed towards higher values than the estimated DLS measurement. In this section, we repeat the same procedure to estimate the size of Polystyrene-NH$_2$ nanoparticles. From DLS measurement's the estimated size of this nanoparticle in 0.2 M KCl + 20 mM CHES + 0.01% $\left(\frac{V}{V}\right)$ Triton X-100 both at pH 9 and pH 10 was found to be around 55 ± 5 nm, this value is well within the manufacturers measurement and does not suggest aggregation. The polydispersity index

91

Manufacturers diameter (in DI Water)	53 ± 10 nm
DLS estimated diameter (in electrolyte)	55 ± 5 nm
Nanopore estimated average diameter	59 ± 8.8 nm

Table 4.2: Size estimation of polystyrene nanoparticles

of this sample in this electrolyte was mostly monodisperse.

The nanoparticle diameter is estimated using the following relation that connects the pore geometry (L,D) to the nanoparticle geometry (d) using the concepts of resistive pulse technique and the contribution of access resistance of the pore[43]

$$\frac{\delta I}{I_0} = \frac{d^3}{(L + 0.8D)D^2} \tag{4.3}$$

In equation (4.2), the $\frac{\delta I}{I_0}$ is the relative change in the current that can be extracted for current drop histograms from the experimental data. This equation is valid for nanoparticles smaller than the effective length of the nanopore. The diameter D of the nanopore is taken from the TEM measurements and the effective length l_{eff} or L is calculated from I-V measurements during the experiment.

The quantity relative change in current is usually the most probable value observed in the distribution when the current drop distribution can be fit using a Gaussian PDF. In our case the distributions were ill fit when using a Gaussian PDF so instead of using the mean of the distribution, we calculated the estimated diameter using the mode of the distribution. The mode represents the peak in a distribution.

From equation 4.2, we can see that the diameter of the nanoparticle is independent of the applied voltage that dictates the relative change in current value. When the diameter of the nanoparticle is estimated using mode of the current distribution, we observed that the estimated diameter value remains the same within the standard deviation for voltages up to 200 mV. This is shown in Fig. 4.12 which consists of these two plots for estimated diameter as a function of applied voltage for all the three FIB's used in this experiment.

All of these estimated values are well within 1σ of the measured DLS values for this nanoparticle suspension. The estimated values at higher voltages are slightly deviant from the measured value but this can be attributed to a higher mode value observed due to multi-particle events.

Estimation of effective charge of the nanoparticle

To estimate the effective charge on the nanoparticle, the inter-event time was calculated using Clampex and the event frequency for each voltage was obtained. This was done for translocation data obtained from FIB 3. Event frequency was plotted as a function of applied voltage as shown in Fig 4.13 and an exponential fit was done to estimate the effective charge on the nanoparticle [40, 102]

The blockade rate (R) is described by Van't Hoff- Arrhenius relation

$$R = R_0 \exp\left(V/V_0\right) \tag{4.4}$$

Where $R \propto \kappa f$ and $\kappa : probability factor$ Re-writing the above equation in terms of frequency,

$$f = f_0 \exp\left(V/V_0\right) \tag{4.5}$$

Here f_0: frequency of events at zero voltage due to diffusion when they over come the activation energy barrier and V_0: barrier reduction factor acting on the effective charge of the particle.

$$\log f = \log f_0 + V\left(\frac{1}{V_0}\right) \tag{4.6}$$

where

$$f_0 = \nu \exp\left(-\frac{U}{kT}\right) \tag{4.7}$$

and
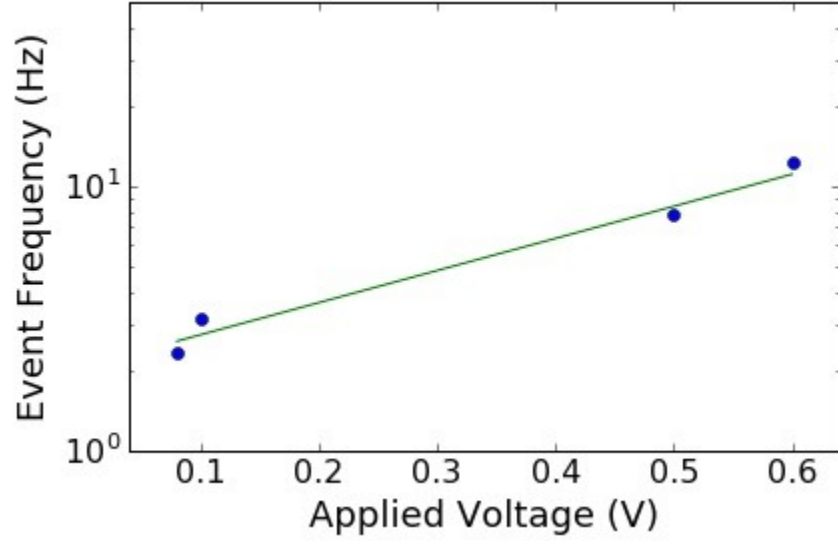
Figure 4.13: Event frequency(Hz) vs applied voltage(V) for events collected using FIB 3. The green line is an exponential fit using $f = \exp\left(\frac{V}{V_0}\right)$.

$$V_0 = \frac{kT}{ze} \tag{4.8}$$

so

$$z = \frac{kT}{V_0 z} = \frac{mkT}{e} \tag{4.9}$$

From the fit we deduce that $f_0 = 0.73$ Hz and $V_0 = 352$ mV and the effective charge on the colloid is found to be 0.07e, which is an estimation obtained from the equations above.

Chapter 5

Conclusion

Solid state nanopores are widely used to study highly charged long biomolecules like DNA and protein. Nanopores fabricated using the ion beam sculpting method have been extensively used to study ssDNA, dsDNA and different kinds of protein molecules. Using nanopore as a sensor, several physical and chemical properties of single molecules can be characterized. In this dissertation, we use the ion beam sculpted nanopores to study spherically charged nanoparticles. In a similar fashion to studying DNA molecules, we aim to look at the physical and chemical properties of spherically charged nanoparticles. Spherically charged nanoparticles are not highly charged or long molecules like DNA, so to use the same sensor that is used to study DNA molecules is challenging and presents us with different event data.

In this work, I characterized two different type of spherical nanoparticles with different surface charge and different polydispersity index using nanopores. One is an iron oxide nanoparticle with -COOH surface group and the other is polystyrene nanoparticle with -NH_2 surface group. Both these particles are under 60 nm in diameter and nanopores used in this study are around 100 nm in diameter. Looking at the event data and particle- pore interaction provides insight into type of events that occur when a particle interacts with the pore. The size of the nanoparticle is characterized using the theory of the resistive pulse technique from the observed event data. This size is verified by an ensemble technique like dynamic light scattering. The event data using a nanopore provide a single particle readout as its electrical signature and this makes nanopores a unique sensor to study nanoparticles.

Also, using the same silicon nitride membrane, I am able to study the events produced by both positively and negatively charged nanoparticles. This was done without any surface modifications to alter the charge of the membrane. This also included verifying some important considerations about the pore to particle ratio and suitable electrolyte concentration to support expected event behavior.

Follow up investigations into to the event dynamics of nanoparticles could include look-

ing at modifying the nanopore surface, as well as looking at the differences in behavior of nanoparticles in monovalent and divalent electrolytes.

Bibliography

[1] G. Binnig and H. Rohrer. Scanning tunneling microscopy. *Surface Science*, 126(1-3):236–244, mar 1983.

[2] G. Binnig, C. F. Quate, and Ch. Gerber. Atomic force microscope. *Physical Review Letters*, 56(9):930–933, mar 1986.

[3] A. J. Storm, J. H. Chen, X. S. Ling, H. W. Zandbergen, and C. Dekker. Fabrication of solid-state nanopores with single-nanometre precision. *Nature Materials*, 2(8):537–540, jul 2003.

[4] Jiali Li, Derek Stein, Ciaran McMullan, Daniel Branton, Michael J. Aziz, and Jene A. Golovchenko. Ion-beam sculpting at nanometre length scales. *Nature*, 412(6843):166–169, jul 2001.

[5] A. Meller, L. Nivon, E. Brandin, J. Golovchenko, and D. Branton. Rapid nanopore discrimination between single polynucleotide molecules. *Proceedings of the National Academy of Sciences*, 97(3):1079–1084, feb 2000.

[6] Ruoshan Wei, Volker Gatterdam, Ralph Wieneke, Robert Tampé, and Ulrich Rant. Stochastic sensing of proteins with receptor-modified solid-state nanopores. *Nature Nanotechnology*, 7(4):257–263, mar 2012.

[7] David J. Niedzwiecki, Raghuvaran Iyer, Philip N. Borer, and Liviu Movileanu. Sampling a biomarker of the human immunodeficiency virus across a synthetic nanopore. *ACS Nano*, 7(4):3341–3350, apr 2013.

[8] E Berkane, F Orlik, A Charbit, C Danelon, D Fournier, R Benz, and M Winterhalter. *Journal of Nanobiotechnology*, 3(1):3, 2005.

[9] Jiali Li, Marc Gershow, Derek Stein, Eric Brandin, and J. A. Golovchenko. DNA molecules and configurations in a solid-state nanopore microscope. *Nature Materials*, 2(9):611–615, aug 2003.

[10] Takashi Ito, Li Sun, and Richard M. Crooks. Simultaneous determination of the size and surface charge of individual nanoparticles using a carbon nanotube-based coulter counter. *Analytical Chemistry*, 75(10):2399–2406, may 2003.

[11] Matthew Davenport, Ken Healy, Matthew Pevarnik, Nick Teslich, Stefano Cabrini, Alan P. Morrison, Zuzanna S. Siwy, and Sonia E. Létant. The role of pore geometry in single nanoparticle detection. *ACS Nano*, 6(9):8366–8380, sep 2012.

[12] Makusu Tsutsui, Sadato Hongo, Yuhui He, Masateru Taniguchi, Nobuhiro Gemma, and Tomoji Kawai. Single-nanoparticle detection using a low-aspect-ratio pore. *ACS Nano*, 6(4):3499–3505, apr 2012.

[13] Daniel Fologea, Marc Gershow, Bradley Ledden, David S. McNabb, Jene A. Golovchenko, and Jiali Li. Detecting single stranded DNA with a solid state nanopore. *Nano Letters*, 5(10):1905–1909, oct 2005.

[14] Takashi Ito, Li Sun, Michael A. Bevan, and Richard M. Crooks. Comparison of nanoparticle size and electrophoretic mobility measurements using a carbon-nanotube-based coulter counter, dynamic light scattering, transmission electron microscopy, and phase analysis light scattering. *Langmuir*, 20(16):6940–6945, aug 2004.

[15] Mirna Mihovilovic, Nicholas Hagerty, and Derek Stein. Statistics of DNA capture by a solid-state nanopore. *Physical Review Letters*, 110(2), jan 2013.

[16] Erik C. Yusko, Jay M. Johnson, Sheereen Majd, Panchika Prangkio, Ryan C. Rollings, Jiali Li, Jerry Yang, and Michael Mayer. Controlling protein translocation through nanopores with bio-inspired fluid walls. *Nature Nanotechnology*, 6(4):253–260, feb 2011.

[17] Calin Plesa, Stefan W. Kowalczyk, Ruben Zinsmeester, Alexander Y. Grosberg, Yitzhak Rabin, and Cees Dekker. Fast translocation of proteins through solid state nanopores. *Nano Letters*, 13(2):658–663, feb 2013.

[18] Kimberly E. Venta, Mehdi B. Zanjani, Xingchen Ye, Gopinath Danda, Christopher B. Murray, Jennifer R. Lukes, and Marija Drndić. Gold nanorod translocations and charge measurement through solid-state nanopores. *Nano Letters*, 14(9):5358–5364, sep 2014.

[19] Makusu Tsutsui, Yoichi Maeda, Yuhui He, Sadato Hongo, Sou Ryuzaki, Satoyuki Kawano, Tomoji Kawai, and Masateru Taniguchi. Trapping and identifying single-nanoparticles using a low-aspect-ratio nanopore. *Applied Physics Letters*, 103(1):013108, jul 2013.

[20] Kimberly Venta, Meni Wanunu, and Marija Drndić. Electrically controlled nanoparticle synthesis inside nanopores. *Nano Letters*, 13(2):423–429, feb 2013.

[21] Akihide Arima, Makusu Tsutsui, and Masateru Taniguchi. Discrimination of equisized nanoparticles by surface charge state using low-aspect-ratio pore sensors. *Applied Physics Letters*, 104(16):163112, apr 2014.

[22] O. A. Saleh and L. L. Sohn. Quantitative sensing of nanoscale colloids using a microchip coulter counter. *Review of Scientific Instruments*, 72(12):4449–4451, dec 2001.

[23] Wallace h. coulter. means for counting particles suspended in a fluid, october 1953. u.s. classification: 324/71.1., 1953.

[24] George T. Roberts and Saad B. EL Badawi. Red blood cell distribution width index in some hematologic diseases. *American Journal of Clinical Pathology*, 83(2):222–226, feb 1985.

[25] R. W. DeBlois and C. P. Bean. Counting and sizing of submicron particles by the resistive pulse technique. *Review of Scientific Instruments*, 41(7):909–916, jul 1970.

[26] M GRAHAM. The coulter principle: foundation of an industry. *Journal of the Association for Laboratory Automation*, 8(6):72–81, dec 2003.

[27] R. M. ROWAN, C. FRASER, J. H. GRAY, and G. A. MDONALD. The coulter counter model s plus- the shape of things to come. *Clinical & Laboratory Haematology*, 1(1):29–40, jun 2008.

[28] Grégory F. Schneider, Qiang Xu, Susanne Hage, Stephanie Luik, Johannes N. H. Spoor, Sairam Malladi, Henny Zandbergen, and Cees Dekker. Tailoring the hydrophobicity of graphene for its use as nanopores for DNA translocation. *Nature Communications*, 4, oct 2013.

[29] Joseph Larkin, Robert Y. Henley, Murugappan Muthukumar, Jacob K. Rosenstein, and Meni Wanunu. High-bandwidth protein analysis using solid-state nanopores. *Biophysical Journal*, 106(3):696–704, feb 2014.

[30] Masateru Taniguchi. Selective multidetection using nanopores. *Analytical Chemistry*, 87(1):188–199, jan 2015.

[31] Daniel Branton, David W Deamer, Andre Marziali, Hagan Bayley, Steven A Benner, Thomas Butler, Massimiliano Di Ventra, Slaven Garaj, Andrew Hibbs, Xiaohua Huang, Stevan B Jovanovich, Predrag S Krstic, Stuart Lindsay, Xinsheng Sean Ling, Carlos H Mastrangelo, Amit Meller, John S Oliver, Yuriy V Pershin, J Michael Ramsey, Robert Riehn, Gautam V Soni, Vincent Tabard-Cossa, Meni Wanunu, Matthew Wiggin, and Jeffery A Schloss. The potential and challenges of nanopore sequencing. *Nature Biotechnology*, 26(10):1146–1153, oct 2008.

[32] Minsoung Rhee and Mark A. Burns. Nanopore sequencing technology: nanopore preparations. *Trends in Biotechnology*, 25(4):174–181, apr 2007.

[33] Jinglin Kong, Hongwen Wu, Liping Liu, Xiao Xie, Lingzhi Wu, Xiaofeng Ye, and Quanjun Liu. Silicon nitride nanopores for nanoparticle sensing. *Journal of Nanoscience and Nanotechnology*, 13(6):4010–4016, jun 2013.

[34] J.C.Maxwell. *A treatise on Electricity & Magnetism, Vol 1, 3rd edition*. Oxford, 1904.

[35] R W DeBlois and R K Wesley. Sizes and concentrations of several type c oncornaviruses and bacteriophage t2 by the resistive-pulse technique. *J. Virol. August 1977 vol. 23 no. 2 227-233*, 1977.

[36] Ronald R. Henriquez, Takashi Ito, Li Sun, and Richard M. Crooks. The resurgence of coulter counting for analyzing nanoscale objects. *The Analyst*, 129(6):478, 2004.

[37] L Petrossian, S J Wilk, P Joshi, S M Goodnick, and T J Thornton. Demonstration of coulter counting through a cylindrical solid state nanopore. *Journal of Physics: Conference Series*, 109:012028, mar 2008.

[38] Anmiv S Prabhu, Talukder Zaki N Jubery, Kevin J Freedman, Rafael Mulero, Prashanta Dutta, and Min Jun Kim. Chemically modified solid state nanopores for high throughput nanoparticle separation. *Journal of Physics: Condensed Matter*, 22(45):454107, oct 2010.

[39] Reiyu Chein and Prashanta Dutta. Effect of charged membrane on the particle motion through a nanopore. *Colloids and Surfaces A: Physicochemical and Engineering Aspects*, 341(1-3):1–12, jun 2009.

[40] L. Bacri, A. G. Oukhaled, B. Schiedt, G. Patriarche, E. Bourhis, J. Gierak, J. Pelta, and L. Auvray. Dynamics of colloids in single solid-state nanopores. *The Journal of Physical Chemistry B*, 115(12):2890–2898, mar 2011.

[41] Wen-Jie Lan, Deric A. Holden, Bo Zhang, and Henry S. White. Nanoparticle transport in conical-shaped nanopores. *Analytical Chemistry*, 83(10):3840–3847, may 2011.

[42] Wen-Jie Lan, Deric A. Holden, Jin Liu, and Henry S. White. Pressure-driven nanoparticle transport across glass membranes containing a conical-shaped nanopore. *The Journal of Physical Chemistry C*, 115(38):18445–18452, sep 2011.

[43] Joshua B. Edel and Tim Albrecht. *Engineered Nanopores for Bioanalytical Applications*. WILLIAM ANDREW PUB, 2013.

[44] J. E. Hall. Access resistance of a small circular pore. *The Journal of General Physiology*, 66(4):531–532, oct 1975.

[45] Hans-Jrgen Butt, Karlheinz Graf, and Michael Kappl. *Physics and Chemistry of Interfaces*. Wiley-VCH, 2006.

[46] Jacob H. Masliyah and Subir Bhattacharjee. *Electrokinetic and Colloid Transport Phenomena*. John Wiley & Sons, 2006.

[47] Robert J. Hunter. *Foundations of Colloid Science*. Oxford University Press, 2001.

[48] Darby Kozak, Will Anderson, Robert Vogel, and Matt Trau. Advances in resistive pulse sensors: Devices bridging the void between molecular and microscopic detection. *Nano Today*, 6(5):531–545, oct 2011.

[49] Jean-Luc Fraikin, Tambet Teesalu, Christopher M. McKenney, Erkki Ruoslahti, and Andrew N. Cleland. A high-throughput label-free nanoparticle analyser. *Nature Nanotechnology*, 6(5):308–313, mar 2011.

[50] Ronald R. Henriquez Takashi Ito, Li Sun and Richard M. Crooks. A carbon nanotube-based coulter nanoparticle counter. Web, October 2004.

[51] James Hurley. Sizing particles with a coulter counter. *Biophysical Journal*, 10(1):74–79, jan 1970.

[52] D. C. Golibersuch. Observation of aspherical particle rotation in poiseuille flow via the resistance pulse technique. II. application to fused sphere dumbbells. *Journal of Applied Physics*, 44(6):2580–2584, jun 1973.

[53] G. Seth Roberts, Darby Kozak, Will Anderson, Murray F. Broom, Robert Vogel, and Matt Trau. Tunable nano/micropores for particle detection and discrimination:

Scanning ion occlusion spectroscopy. *Small*, 6(23):2653–2658, oct 2010.

[54] Erik C. Yusko, Brandon R. Bruhn, Olivia M. Eggenberger, Jared Houghtaling, Ryan C. Rollings, Nathan C. Walsh, Santoshi Nandivada, Mariya Pindrus, Adam R. Hall, David Sept, Jiali Li, Devendra S. Kalonia, and Michael Mayer. Real-time shape approximation and fingerprinting of single proteins using a nanopore. *Nature Nanotechnology*, dec 2016.

[55] Daniel Fologea, Eric Brandin, James Uplinger, Daniel Branton, and Jiali Li. DNA conformation and base number simultaneously determined in a nanopore. *ELEC-TROPHORESIS*, 28(18):3186–3192, sep 2007.

[56] Daniel Fologea, James Uplinger, Brian Thomas, David S. McNabb, and Jiali Li. Slowing DNA translocation in a solid-state nanopore. *Nano Letters*, 5(9):1734–1737, sep 2005.

[57] James Uplinger, Brian Thomas, Ryan Rollings, Daniel Fologea, David McNabb, and Jiali Li. K , na , and mg 2 on DNA translocation in silicon nitride nanopores. *ELECTROPHORESIS*, 33(23):3448–3457, nov 2012.

[58] Daniel Fologea, Bradley Ledden, David S. McNabb, and Jiali Li. Electrical characterization of protein molecules by a solid-state nanopore. *Applied Physics Letters*, 91(5):053901, jul 2007.

[59] David S. Talaga and Jiali Li. Single-molecule protein unfolding in solid state nanopores. *Journal of the American Chemical Society*, 131(26):9287–9297, jul 2009.

[60] Furat Sawafta, Autumn Carlsen, and Adam Hall. Membrane thickness dependence of nanopore formation with a focused helium ion beam. *Sensors*, 14(5):8150–8161, may 2014.

[61] 1984 Graef, Edward William. Reducing the thickness of silicon nitride nanopores. Master's thesis, University of Arkansas, 2010.

[62] Meni Wanunu, Tali Dadosh, Vishva Ray, Jingmin Jin, Larry McReynolds, and Marija Drndić. Rapid electronic detection of probe-specific microRNAs using thin nanopore sensors. *Nature Nanotechnology*, 5(11):807–814, oct 2010.

[63] Shengwei Tan, Lei Wang, Hang Liu, Hongwen Wu, and Quanjun Liu. Single nanoparticle translocation through chemically modified solid nanopore. *Nanoscale Research Letters*, 11(1), feb 2016.

[64] Cees Dekker. Solid-state nanopores. *Nature Nanotechnology*, 2(4):209–215, mar 2007.

[65] Derek Martin Stein. *Ion Beam Sculp ting Molecular Scale Devices*. PhD thesis, Division of Engineering and Applied Sciences, Harvard University, 2002.

[66] W. van Gelder and V. E. Hauser. The etching of silicon nitride in phosphoric acid with silicon dioxide as a mask. *Journal of The Electrochemical Society*, 114(8):869, 1967.

[67] J. Lee, Z. Yang, W. Zhou, S. J. Pennycook, S. T. Pantelides, and M. F. Chisholm. Stabilization of graphene nanopore. *Proceedings of the National Academy of Sciences*, 111(21):7522–7526, may 2014.

[68] Chris A. Merchant and Marija Drndić. Graphene nanopore devices for DNA sensing. In *Methods in Molecular Biology*, pages 211–226. Springer Nature, 2012.

[69] Christopher A. Merchant, Ken Healy, Meni Wanunu, Vishva Ray, Neil Peterman, John Bartel, Michael D. Fischbein, Kimberly Venta, Zhengtang Luo, A. T. Charlie Johnson, and Marija Drndic
. DNA translocation through graphene nanopores. *Nano Letters*, 10(8):2915–2921, aug 2010.

[70] Aleksandra Radenovic. Molybdenum disulfide nanopores: Why 3 atoms are better than one? *Biophysical Journal*, 108(2):489a, jan 2015.

[71] Ke Liu, Jiandong Feng, Andras Kis, and Aleksandra Radenovic. Atomically thin molybdenum disulfide nanopores with high sensitivity for DNA translocation. *ACS Nano*, 8(3):2504–2511, mar 2014.

[72] Shuo Liu, Thomas D. Yuzvinsky, and Holger Schmidt. Effect of fabrication-dependent shape and composition of solid-state nanopores on single nanoparticle detection. *ACS Nano*, 7(6):5621–5627, jun 2013.

[73] Jijin Yang, David C Ferranti, Lewis A Stern, Colin A Sanford, Jason Huang, Zheng Ren, Lu-Chang Qin, and Adam R Hall. Rapid and precise scanning helium ion microscope milling of solid-state nanopores for biomolecule detection. *Nanotechnology*, 22(28):285310, jun 2011.

[74] Eric Beamish, Harold Kwok, Vincent Tabard-Cossa, and Michel Godin. Precise control of the size and noise of solid-state nanopores using high electric fields. *Nanotechnology*, 23(40):405301, sep 2012.

[75] Bradley Thomas Ledden. Fabrication of solid states nanopores using feedback controlled ion beam sculpting techniques. master's thesis. Master's thesis, University of Arkansas, 2004.

[76] Derek Stein, Jiali Li, and Jene A. Golovchenko. Ion-beam sculpting time scales. *Physical Review Letters*, 89(27), dec 2002.

[77] Qun Cai, Brad Ledden, Eric Krueger, Jene A. Golovchenko, and Jiali Li. Nanopore sculpting with noble gas ions. *Journal of Applied Physics*, 100(2):024914, jul 2006.

[78] Ryan Rollings, Edward Graef, Nathan Walsh, Santoshi Nandivada, Mourad Benamara, and Jiali Li. The effects of geometry and stability of solid-state nanopores on detecting single DNA molecules. *Nanotechnology*, 26(4):044001, jan 2015.

[79] Aaron T. Kuan and Jene A. Golovchenko. Nanometer-thin solid-state nanopores by

cold ion beam sculpting. *Applied Physics Letters*, 100(21):213104, may 2012.

[80] Ryan C. Rollings, David S. McNabb, and Jiali Li. DNA characterization with ion beam-sculpted silicon nitride nanopores. In *Nanopore -Based Technology*, pages 79–97. Springer Nature, 2012.

[81] Bradley Thomas Ledden. *Sensing Native and Unfolded Single Protein Molecules with Solid-State Nanopores*. PhD thesis, University of Arkansas, 2011.

[82] James Robert Uplinger. *Kinetics of DNA Translocation in a Solid-State Nanopore*. PhD thesis, University of Arkansas, 2007.

[83] Ryan Connor Rollings. *The geometry and sensitivity of ion-beam sculpted nanopores for single molecule DNA analysis*. PhD thesis, University of Arkansas, 2013.

[84] Kathryn G. Klemic, James F. Klemic, Mark A. Reed, and Fred J. Sigworth. Micro-molded PDMS planar electrode allows patch clamp electrical recordings from cells. *Biosensors and Bioelectronics*, 17(6-7):597–604, jun 2002.

[85] R. M. M. Smeets, U. F. Keyser, M. Y. Wu, N. H. Dekker, and C. Dekker. Nanobubbles in solid-state nanopores. *Physical Review Letters*, 97(8), aug 2006.

[86] Gaurav Goyal, Kevin J. Freedman, and Min Jun Kim. Gold nanoparticle translocation dynamics and electrical detection of single particle diffusion using solid-state nanopores. *Analytical Chemistry*, 85(17):8180–8187, sep 2013.

[87] Changbae Hyun, Ryan Rollings, and Jiali Li. Probing access resistance of solid-state nanopores with a scanning-probe microscope tip. *Small*, 8(3):385–392, dec 2011.

[88] Bertil Hille. *Ion Channels of Excitable Membranes*. Sinauer Associates Inc.,U.S., 2001.

[89] Marcel Aguilella-Arzo, Vicente M. Aguilella, and R. S. Eisenberg. Computing numerically the access resistance of a pore. *European Biophysics Journal*, 34(4):314–322, mar 2005.

[90] Ralph M. M. Smeets, Ulrich F. Keyser, Diego Krapf, Meng-Yue Wu, Nynke H. Dekker, and Cees Dekker. Salt dependence of ion transport and DNA translocation through solid-state nanopores. *Nano Letters*, 6(1):89–95, jan 2006.

[91] David P. Hoogerheide, Slaven Garaj, and Jene A. Golovchenko. Probing surface charge fluctuations with solid-state nanopores. *Physical Review Letters*, 102(25), jun 2009.

[92] Leo Petrossian. *Cylindrical Solid State Nanopores*. PhD thesis, University of Arizona, 2007.

[93] Matthew W.Davenport. *Synthetic Nanopores: Biological Analogues and Nanofluidic Devices*. PhD thesis, Univeristy of California, Irivine, 2013.

[94] Matthias Firnkes, Daniel Pedone, Jelena Knezevic, Markus Doblinger, and Ul-

rich Rant. Electrically facilitated translocations of proteins through silicon nitride nanopores: Conjoint and competitive action of diffusion, electrophoresis, and electroosmosis. *Nano Letters*, 10(6):2162–2167, jun 2010.

[95] Long Luo, Sean R. German, Wen-Jie Lan, Deric A. Holden, Tony L. Mega, and Henry S. White. Resistive-pulse analysis of nanoparticles. *Annual Review of Analytical Chemistry*, 7(1):513–535, jun 2014.

[96] Yixian Wang, Kaan Kececi, Michael V. Mirkin, Vigneshwaran Mani, Naimish Sardesai, and James F. Rusling. Resistive-pulse measurements with nanopipettes: detection of au nanoparticles and nanoparticle-bound anti-peanut IgY. *Chem. Sci.*, 4(2):655–663, 2013.

[97] Esther Amstad, Marcus Textor, and Erik Reimhult. Stabilization and functionalization of iron oxide nanoparticles for biomedical applications. *Nanoscale*, 3(7):2819, 2011.

[98] Elena Angeli, Andrea Volpe, Paola Fanzio, Luca Repetto, Giuseppe Firpo, Patrizia Guida, Roberto Lo Savio, Meni Wanunu, and Ugo Valbusa. Simultaneous electrooptical tracking for nanoparticle recognition and counting. *Nano Letters*, 15(9):5696–5701, sep 2015.

[99] Cornelia Loos, Tatiana Syrovets, Anna Musyanovych, Volker Mailnder, Katharina Landfester, G Ulrich Nienhaus, and Thomas Simmet. Functionalized polystyrene nanoparticles as a platform for studying bio–nano interactions. *Beilstein Journal of Nanotechnology*, 5:2403–2412, dec 2014.

[100] Vincent M. Rotello, Andrew K. Boal, Faysal Ilhan, Jason E. DeRouchey, Thomas Thurn-Albrecht, and Thomas P. Russell. *Nature*, 404(6779):746–748, apr 2000.

[101] Matthew Pevarnik, Ken Healy, Maria Eugenia Toimil-Molares, Alan Morrison, Sonia E. Létant, and Zuzanna S. Siwy. Polystyrene particles reveal pore substructure as they translocate. *ACS Nano*, 6(8):7295–7302, aug 2012.

[102] Sarah E. Henrickson, Martin Misakian, Baldwin Robertson, and John J. Kasianowicz. Driven DNA transport into an asymmetric nanometer-scale pore. *Physical Review Letters*, 85(14):3057–3060, oct 2000.